Modeling the Dynamic Characteristics of Slack Wire Cables in STOCKBRIDGE Dampers

Vom Fachbereich Mechanik
der Technischen Universität Darmstadt
zur Erlangung des Grades eines
Doktor-Ingenieurs (Dr.-Ing.)
genehmigte

Dissertation

von

Dipl.-Ing. Daniel Sauter

aus Konstanz

Referent:	Prof. Dr. Peter Hagedorn
Korreferent:	Prof. Dr. Dieter Ottl
Tag der Einreichung:	07. Juni 2003
Tag der mündlichen Prüfung:	05. Dezember 2003

Darmstadt 2003

D 17

Vorwort

Die vorliegende Arbeit entstand während meiner Tätigkeit als wissenschaftlicher Mitarbeiter bei Prof. Dr. Peter Hagedorn in der Arbeitsgruppe Dynamik des Fachbereichs Mechanik der Technischen Universität Darmstadt.

Für die Anregung zu dieser Arbeit und deren großzügige Förderung bin ich Herrn Professor Hagedorn besonderem Dank verpflichtet. Mein weiterer Dank gilt Herrn Professor Dieter Ottl für die bereitwillige Übernahme des Korreferats und sein großes Interesse an der Arbeit.

Besonders nachdrücklich bedanke ich mich bei meinen Ex-Kolleginnen und Kollegen, Jutta Braun, Renate Schreiber, Stefanie Gutschmidt, Thira Jearsiripongkul, Sandeep Parashar, Himanshu Verma, Xian-Tong Zhang, Peter Gibson, Goutam Chakraborty, Tobias Vomstein, Kai Wolf, Thomas Sattel, Marcus Berg, Georg Wegener, Hartmut Bach, Norbert Skricka, Roland Platz, Malte Seidler, Uli Ehehalt, Minh Nam Nguyen, Joachim Schmidt, Ulrich Gutzer, Thomas Hadulla, Karl-Josef Hoffmann, Dirk Laier, Utz von Wagner, Christoph Reuter sowie den Herren Professoren Richard Markert und Wolfgang Seemann für Ihre fachliche und außerfachliche Inspiration und stetige Hilfsbereitschaft.

Der experimentelle Teil dieser Arbeit wurde zu einem beträchtlichen Teil in Zusammenarbeit mit der Firma RIBE Electrical Fittings GmbH & Co. KG durchgeführt. Hierbei möchte ich mich besonders für die Mithilfe und die Impulse der Herren Gerhard Biedenbach und Hans-Jörg Krispin bedanken.

Darmstadt, im Dezember 2003

Daniel Sauter

Contents

Chapter 1

Introduction

The main purpose of wire cables is the transfer of forces in the axial direction of the cable. Due to this axial force wire cables are taut in general. Damping due to internal friction in taut wire cables undergoing bending vibrations is negligible in many cases. Slack cables, however, exhibit significant flexural hysteresis resulting from inter-strand friction. This type of static hysteresis is utilized in various applications where wire cables are used in damping of mechanical vibrations. Such kind of dampers are low-priced, easy to manufacture, maintenance-free, and their function is insensitive to weather as well as to the temperature. One of very few disadvantages may sometimes be the construction volume. Unfortunately dimensioning the slack cables is quite elaborate which is also due to the lack of knowledge about their mechanical behavior. A typical example are wire rope dampers (Figure 1.1) which are used e.g. for simultaneous shock and vibration protection of sensitive electronic devices in industrial and defense applications. STOCKBRIDGE *dampers* [32] in overhead transmission lines which are used in damping wind-excited oscillations due to vortex shedding are another example (see Figure 1.2). A STOCKBRIDGE damper (Figure 1.3) consists of a wire cable (*damper cable*), two rigid bodies ("*inertial masses*"), and a clamp for mounting the damper to the conductor. In these dampers, mechanical energy is dissipated in the damper cables (Figure 1.4).

The damping mechanism in slack wire cables is due to statical hysteresis resulting from COULOMB (dry) friction between the individual wires of the cable (*inter-strand friction*) undergoing bending deformation. Unlike most other wire cables (e.g. conductors in overhead transmission lines) damper cables are not subjected to axial loads. Thus they exhibit a bending behavior different from that of taut cables.

Damper cables of STOCKBRIDGE dampers consist quite often of a core wire and one

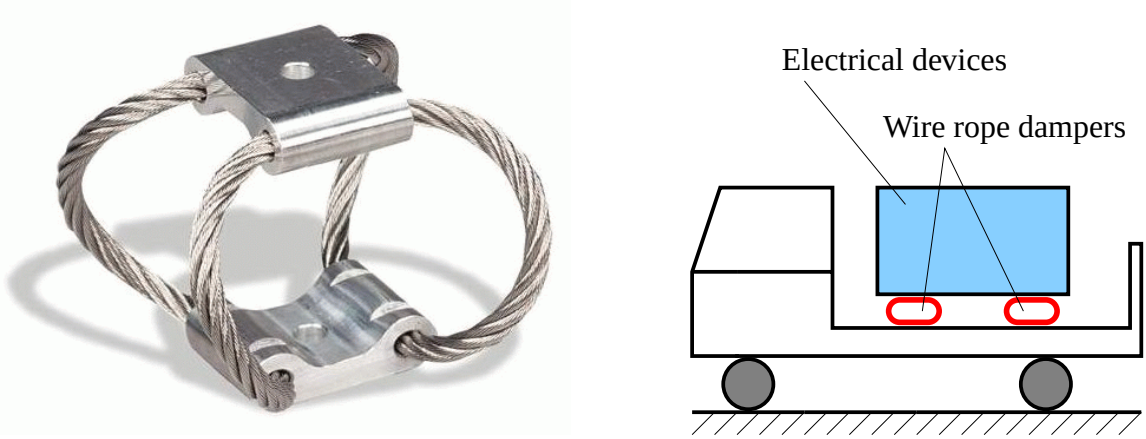

(a) Wire rope damper (ENIDINE Inc.)

(b) Example of application

Figure 1.1: Wire rope damper with an example of application

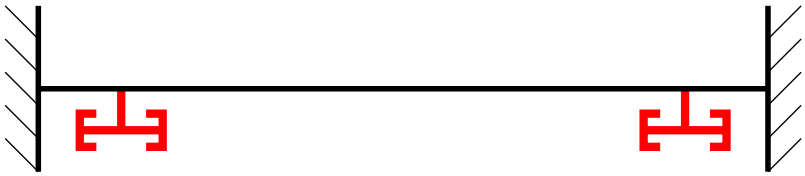

Figure 1.2: Tensioned Cable with STOCKBRIDGE dampers attached (schematic)

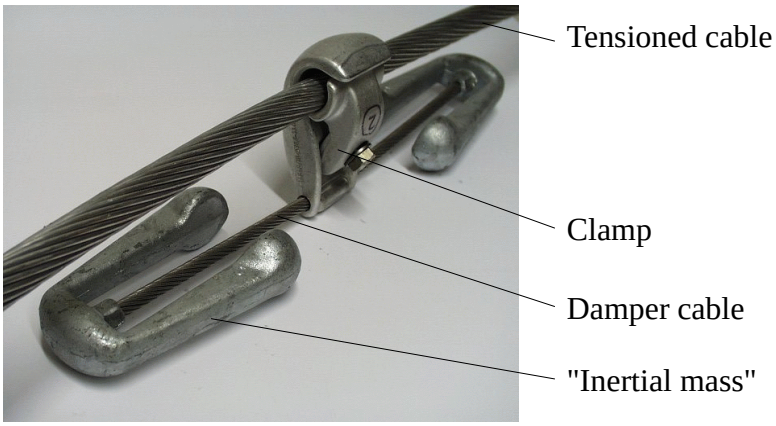

Figure 1.3: STOCKBRIDGE damper (RIBE Electrical Fittings GmbH & Co. KG)

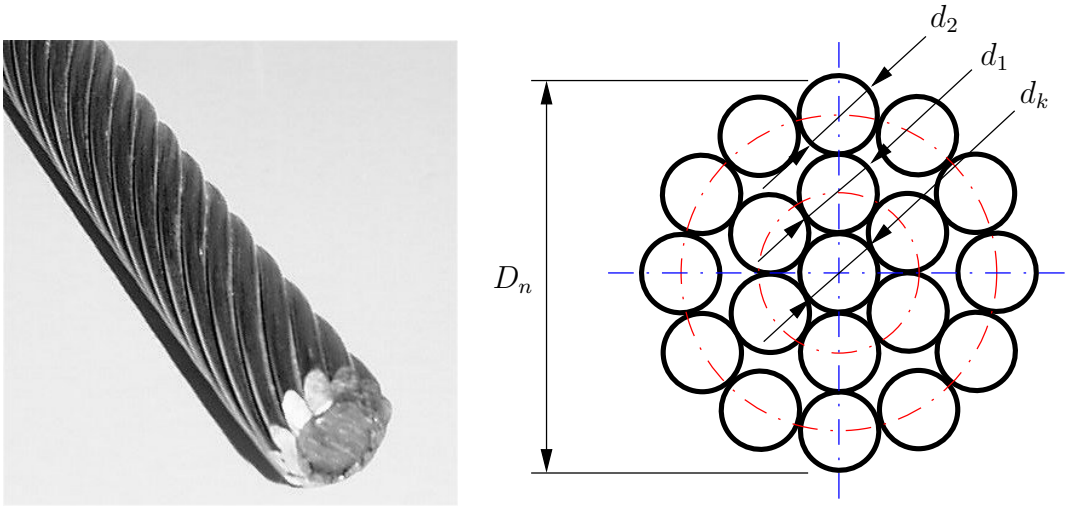

(a) Damper cable (b) Cross section

Figure 1.4: Damper cable of a STOCKBRIDGE damper

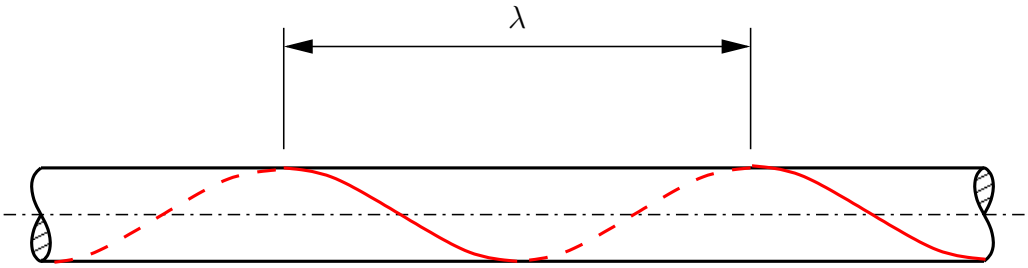

Figure 1.5: Lay length λ (wire wound around a rigid cylinder)

or two layers of wire wound around. Figure 1.4 shows a typical two-layered wire cable. Besides the wire diameters d_k, d_1, d_2 (see Figure 1.4b) the lay lengths λ_1, λ_2 of the layers (see Figure 1.5) are the remaining parameters needed in order to describe the geometry of a cable.

The damper cables pieces are cut off from long cable rolls, and the damper clamp as well as the inertial masses are pressed to the cable. For every type of STOCKBRIDGE damper frequency response experiments are normally carried out in order to determine the design parameters such as the length of the damper cable. This means that in the current design process the properties of the cables are not considered directly. One reason for this is the lack of a good description of the mechanical properties of the vibrating slack wire cables. With a good knowledge of these properties, different types of dampers (e.g. with

different cables length) with predetermined impedances could be conveniently designed.

Several dynamical models for STOCKBRIDGE dampers can be found in the literature [22, 12, 14] where also the principle of operation is described in more detail. The distributed energy dissipation due to inter-strand friction has however not been described in detail. Therefore important features, such as changes in the dynamic behavior with varying vibration amplitudes, could so far not be described in a satisfying manner.

In order to accurately model the mechanical behavior of the STOCKBRIDGE damper a good model for the slack wire cable is needed. A multitude of models for wire cables can be found in literature in which the wire structure of the cable is reproduced in detail in order to derive the mechanical properties from the geometry. Depending on the accuracy of such a model, difficult mathematical expressions are obtained. It is easy to imagine that a practical description of the interaction of multiple wires requires substantial simplifications. A number of computations can be found in [5], the approach in the case of small tension forces as well as a detailed literature survey in [28]. Regardless of the accuracy of the model also the tribological characteristics have to be obtained from experiments.

Most wire cables models consider the behavior of cables taut in the axial direction. The bending of single layered cables over a pulley has been considered by WINDSPERGER [34]. Insight into the local behavior of cables was gained by PAPAILOU [27] who measured the changes in the bending stiffness of cables undergoing bending. GUTZER [7] showed that it is possible to model the damping in taut wire cables using one-dimensional continua modeled by means of JENKIN elements. Such an approach reduces the complexity of the model remarkably and makes the calculation of dynamical properties possible. In Chapter 3 we use a similar approach, modeling the damper cables as one-dimensional continua.

A damper cable undergoing alternating bending exhibits *statical hysteresis*. Here the term *hysteresis* implies that the relation between the curvature κ and the bending moment M is not unique. *Statical* means that the force does not depend on the absolute value of $\dot{\kappa}$ but only on its sign, where the dot denotes the time derivative. For any given motion $\kappa(t)$ the bending moment $M(t)$ depends not only on the actual value of $\kappa(t)$ but also on sign$(\dot{\kappa})$; more generally, the moment $M(t)$ depends on the history of the deformation. It is well known that elastic springs in conjunction with dry friction lead to static hysteresis, which can be described by different mathematical models. Since the hysteresis has its origin in the COULOMB friction between the wires, a phenomenological model such as the MASING model is convenient. In such a model several JENKIN elements arranged in parallel, consisting of linear springs and COULOMB friction elements. The damper cable

is a continuous system and damping takes place throughout the whole length of the cable, so that *distributed* JENKIN elements are used.

In the literature only scarce information is found about dynamical models for the bending of slack wire cables including the damping and hysteresis. It was shown by KOLSCH [17] that wire cables are systems with statical hysteresis and that the global behavior of damper cables can be described by a MASING model. PLAGGE [29] demonstrated, that a local MASING model can be used for damper cables. He assumed that the parameters (obtained from a *global* experiment) are constant throughout the whole cable. Applying such an approach to the STOCKBRIDGE damper however does not yield accurate results.

Therefore, in this work the *local* bending behavior of a slack wire cable will be examined experimentally beforehand in Chapter 2. The *global* behavior of a damper cable for different vibration modes can be inferred therefrom. An experiment was developed for the determination of the local *moment-curvature relation* in a damper cable. To this end, a thin instrumented steel strip was attached to the cable. In the experiments also different bending shapes were taken into account.

In order to check the feasibility of the model, some preliminary experiments were carried out (see Section 2.4). The damper cables are cut off from long cables and the sensitivity of the cable properties with respect to the position along the cable was also checked.

The identification of the model parameters from the experimentally obtained data was done numerically in the time domain (see Section 3.5). A single distributed JENKIN element is used in our model and this considerably simplified the description of the phenomena in a wire cable undergoing bending.

In a perfectly homogeneous wire cable the model parameters would be independent of the position along the cable as well as of the bending mode. For the damper cables under consideration this is unfortunately not the case. Therefore, the local MASING model in the present form is not sufficiently detailed for a precise description of the local behavior of slack cables without axial load. As a consequence a modified model is proposed in Section 3.7 in which the transverse force acting on the wire cable is also included.

In Chapter 4 such a model is used for the damper cables of a STOCKBRIDGE damper. The equations of motion of a STOCKBRIDGE damper are then formulated and spatial discretization of the damper cable leads to a system of nonlinear ordinary differential equations. In order to test this dynamical model of a STOCKBRIDGE damper we compute impedance curves and compare them to experimental results.

The computation of the response of non-linear systems to sinusoidal excitation is a

standard problem, see e.g. [26]. Little is known however if the nonlinear oscillators are hysteretic. For single degree-of-freedom (DOF) systems KOLSCH [17] gave several methods of solution. CAPECCHI [3] examined the periodic response and stability of hysteretic single DOF oscillators. A two DOF system was also considered by CAPECCHI [4]. In our analysis we will examine multi-degree of freedom hysteretic oscillators.

It is current industrial practice to characterize a STOCKBRIDGE damper by its frequency response. Every new type of STOCKBRIDGE damper has to be tested even though the same cable is used, which is quite time demanding. Admittedly it is circuitous to examine the whole damper, if the only unknown part is the damper cable. Further, it seems not be be necessary to examine the dynamic behavior of the damper cable at different frequencies if the mechanical behavior of the damper cable is not dynamic but quasi-statical. For industrial applications it would be useful to have a fast identification of the cable properties, not requiring the direct measurement of local properties. To this end an approach is presented in Section 4.3 for obtaining the local parameters from a global quasi-statical experiment in the time domain.

For the development of this thesis many numerical calculations were necessary. These computations were executed using the MATLAB software package [24].

Chapter 2

Experimental Investigation

2.1 Measurements of the Moment-Curvature Relation

In several publications (e.g. [28, 7]) the quasi-statical behavior of wire cables was described using the local correlation between the bending moment $M(s)$ and the curvature $\kappa(s) = \partial^2 w(s)/\partial s^2$ of the cable center line, w being the transverse displacement of a point at a distance s from the clamped end (see Figure 2.1). It was assumed that - as in an EULER-BERNOULLI beam - the curvature is essentially a function of the bending moment. The local behavior at every location of the wire cable was described by the *moment-curvature relation* $\kappa(M)$. A similar approach was also tried for the wire cable of a STOCKBRIDGE damper, but did not lead to completely satisfactory results [30]. Therefore an attempt is made here to measure and investigate the moment-curvature relation at different locations of the wire cable.

Efforts have been made in the past to measure the curvature of a wire cable, by optical, electromagnetical, or mechanical methods. PAPAILLOU used a laser device to measure

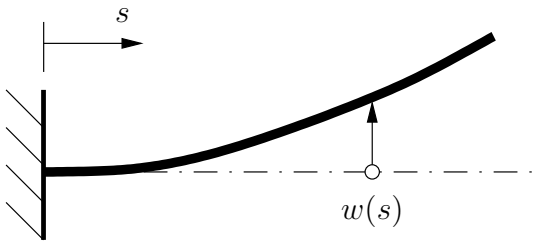

Figure 2.1: Deformation of a wire cable

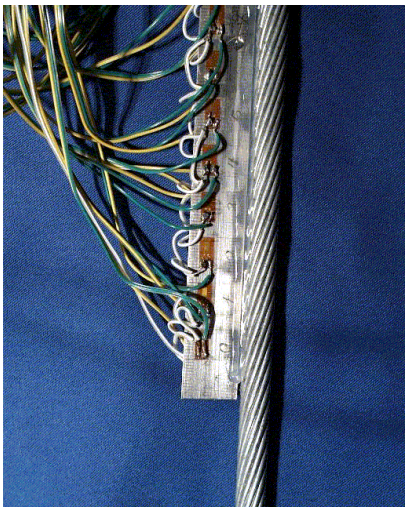

(a) Wire cable with a thin instrumented steel strip

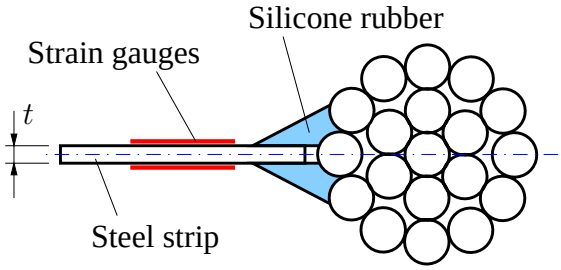

(b) Cross section

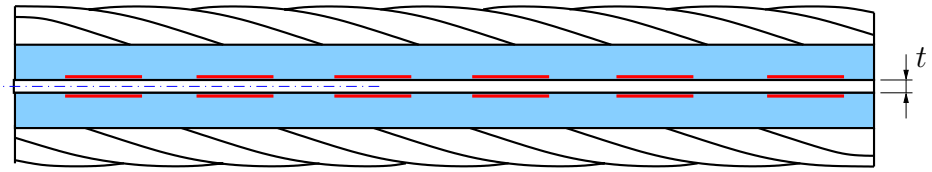

(c) Side view

Figure 2.2: Device for curvature measurement

the small displacements in the cables of overhead transmission lines [27]. In the case of large amplitudes, as in STOCKBRIDGE dampers, this is not an easy undertaking, due to the unsteady surface structure. Therefore a special device (Figure 2.2) was developed for our experimental determination of the local *moment-curvature relation* in a damper cable. To this end, a thin steel strip was attached in parallel to the cable. Instead of measuring directly the cable curvature, the local curvature of the strip is measured using *strain gauges* (half-bridge circuits) attached to the surface of the strip. The bending strains are measured via these strain gauges and the curvature $\kappa(s) = \partial^2 w(s)/\partial s^2$ can be obtained even for large amplitudes. The displacement $w(s)$ is obtained integrating the curvature. In order to get good results the neutral axis of the strip has to be oriented along that of the wire cable. This may be difficult for long wire cables.

The thin steel strip is modeled as a BERNOULLI-EULER beam. The curvature κ of the

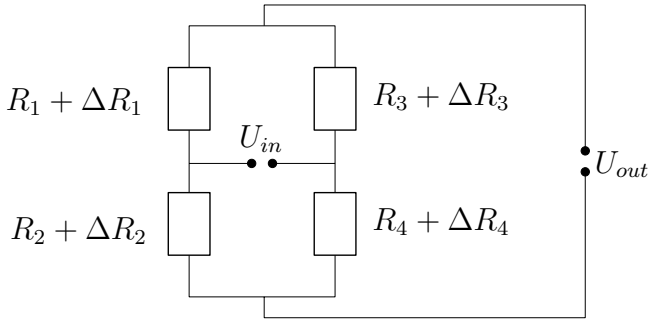

Figure 2.3: WHEATSTONE bridge (full bridge)

strip can thus be obtained from the strain ε on the surface from

$$\kappa = \frac{2}{t}\,\varepsilon\,, \tag{2.1}$$

t being the thickness of the strip.

The electric resistance R of the strain gauges changes with the strains and

$$\frac{\Delta R}{R} = K \cdot \varepsilon\,, \tag{2.2}$$

where K is the constant *gauge factor*. The value of K depends on the type of the strain gauges used.

A WHEATSTONE *bridge* as shown in Figure 2.3 is used to measure the resulting changes of resistance. Even very small changes of resistance can be precisely measured in this manner. From KIRCHHOFF's laws the ratio between the input voltage U_{in} and the output voltage U_{out} is

$$\frac{U_{out}}{U_{in}} = \frac{R_1 + \Delta R_1}{R_1 + \Delta R_1 + R_2 + \Delta R_2} - \frac{R_4 + \Delta R_4}{R_3 + \Delta R_3 + R_4 + \Delta R_4}\,, \tag{2.3}$$

where R_1 to R_4 are the resistances used in the WHEATSTONE bridge. The bridge is called *balanced* if the relation

$$\frac{R_1}{R_2} = \frac{R_4}{R_3} \tag{2.4}$$

holds. In this case the output voltage vanishes. For small changes of the resistance

$$\Delta R_i \ll R_i$$

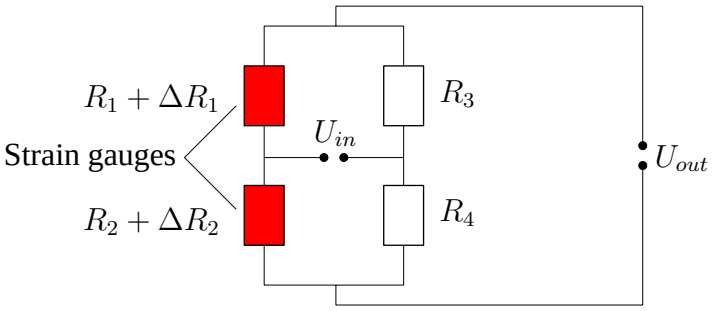

Figure 2.4: WHEATSTONE half bridge

from a balanced bridge one has approximately:

$$\frac{U_{out}}{U_{in}} = \frac{1}{4}\left(\frac{\Delta R_1}{R_1} - \frac{\Delta R_2}{R_2} + \frac{\Delta R_3}{R_3} - \frac{\Delta R_4}{R_4}\right) . \tag{2.5}$$

A *half bridge* circuit is obtained if two strain gauges only are used as shown in Figure 2.4. In this case

$$\Delta R_3 = 0, \quad \Delta R_4 = 0 \tag{2.6}$$

holds and (2.5) leads to

$$\frac{U_{out}}{U_{in}} = \frac{1}{4}\left(\frac{\Delta R_1}{R_1} - \frac{\Delta R_2}{R_2}\right) . \tag{2.7}$$

Since we use identical strain gauges (i.e. $R_1 = R_2$) one has

$$\frac{U_{out}}{U_{in}} = \frac{1}{4}\frac{\Delta R_1 - \Delta R_2}{R} . \tag{2.8}$$

Substituting (2.2) into (2.8) gives the voltage ratio as a function of the strains:

$$\frac{U_{out}}{U_{in}} = \frac{K}{4}\left(\varepsilon_1 - \varepsilon_2\right) . \tag{2.9}$$

For symmetrically attached strain gauges in a BERNOULLI-EULER beam (Figure 2.5) in bending one has

$$\varepsilon_1 = -\varepsilon_2 \tag{2.10}$$

and with $\varepsilon := \varepsilon_1$ the voltage ratio can be written as

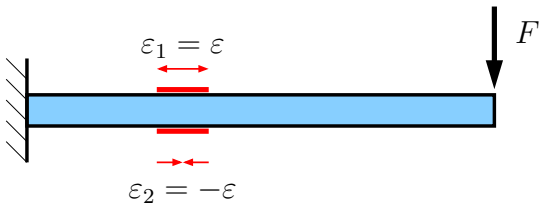

Figure 2.5: Transverse force acting on a beam with two strain gauges

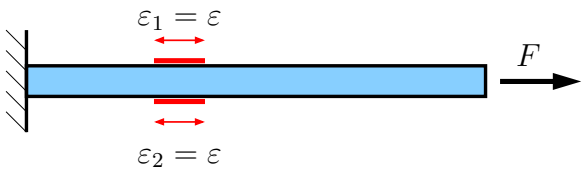

Figure 2.6: Longitudinal force acting on a beam with two strain gauges

$$\frac{U_{out}}{U_{in}} = \frac{K}{2}\,\varepsilon\,. \tag{2.11}$$

The opposite signs of the strains in (2.9) can also be used for the elimination of measurement errors. For example, a longitudinal force at the free end of the beam induces the same strains in the strain gauges, i.e. $\varepsilon_1 = \varepsilon_2$ (Figure 2.6). Thus the longitudinal force does not influence the output voltage. The same holds true for temperature strains as well: no additional strain gauges are required to compensate temperature changes.

Finally the curvature can be computed as a function of the voltage ratio. Inserting (2.1) into (2.11) and solving for the curvature yields

$$\kappa = \frac{4}{K\,t}\,\frac{U_{out}}{U_{in}}\,. \tag{2.12}$$

2.2 Two Different Types of Experiments

In some cases (e.g. Figure 1.1) a damper cable moves only in a single bending shape during operation (at different displacement amplitudes). In STOCKBRIDGE dampers the situation is more complicated. Even with the STOCKBRIDGE damper modeled as a planar linear system and neglecting the mass of the damper cable, two degrees of freedom are obtained for every arm of the damper. Two resonance frequencies with the corresponding bending shapes of the cable do then play a role. Two different types of experiments were carried out with instrumented damper cables, as shown schematically in Figure 2.7, in order to verify

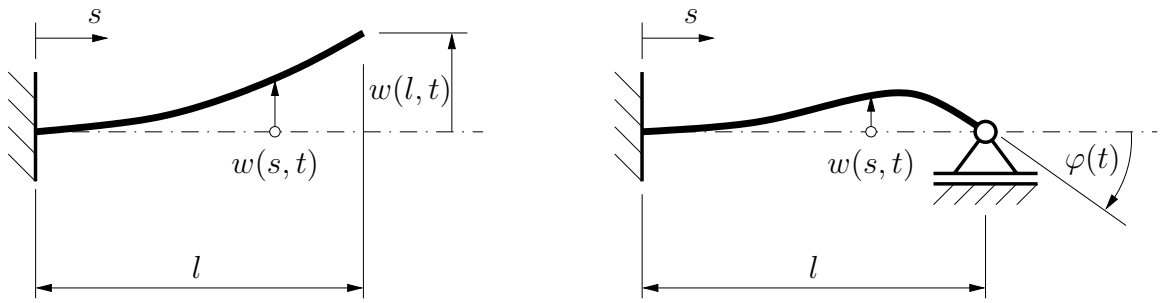

(a) Applied linear displacement of cable end point

(b) Applied rotation of cable end cross section

Figure 2.7: Two different types of experiments

that the measured local bending characteristics of the cable are really invariant with respect to the bending shape. We refer to these experiments as “experiment (a)” and “experiment (b)”, respectively. The setup for these experiments is shown in Figures 2.10, 2.11, and 2.12. The bending shapes of the damper cable in the two experiments are similar to the shapes in the first and second resonance of the STOCKBRIDGE damper, respectively.

In both cases the left end was rigidly clamped and the restraining torque $T(t)$ and the transverse force $F(t)$ were measured simultaneously at the clamp by means of a load cell (Figure 2.8). The local bending moments

$$M(s,t) = T(t) - F(t)\, s \tag{2.13}$$

could thus easily be calculated. In experiment (a) a linear cyclic displacement, $w(l,t)$, was applied at the right end which was free rotate; in experiment (b) the cable end cross section was subjected to a cyclic rotation $\varphi(t)$ (and correspondingly a torque $T(t)$ was applied).

Both experiments were carried out at low frequencies, so that inertia effects could be neglected. The right hand end cross section was clamped (in a moving clamp) in both experiments. The clamps used for both cable ends were identical. The cable data are shown in Table 2.1. The cable length was chosen to be $l = 0.3$m. This is longer than the length of damper cables of a Stockbridge damper which are typically of length $0.15\text{m} < l < 0.2\text{m}$. For $l > 0.3$m it became more and more difficult to accurately orient the steel strip.

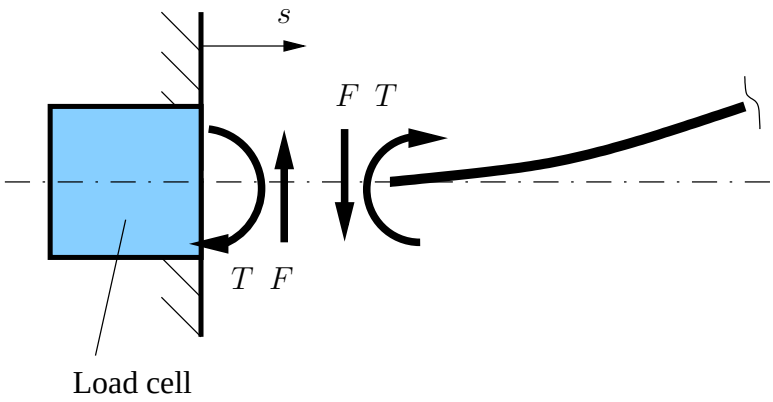

Figure 2.8: Torque $T(t)$ and the transverse force $F(t)$ measured by means of a load cell

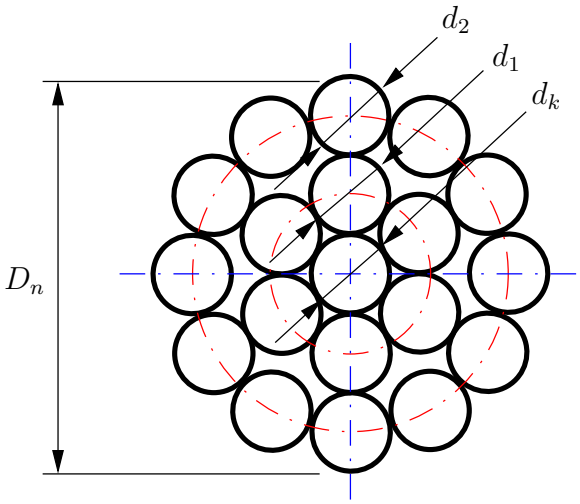

Figure 2.9: Cross section through a damper cable

	Nominal diameter D_n	10.15 mm	
Core :	Core wire diameter d_k	2.00 mm	1 wire
Layer 1:	Wire diameter d_1	2.00 mm	6 wires
	Lay length λ_1	41 mm	
Layer 2:	Wire diameter d_2	2.00 mm	12 wires
	Lay length λ_2	80 mm	
	Mass per Length μ	0.498 kg/m	

Table 2.1: Wire cable data (see Figure 2.9)

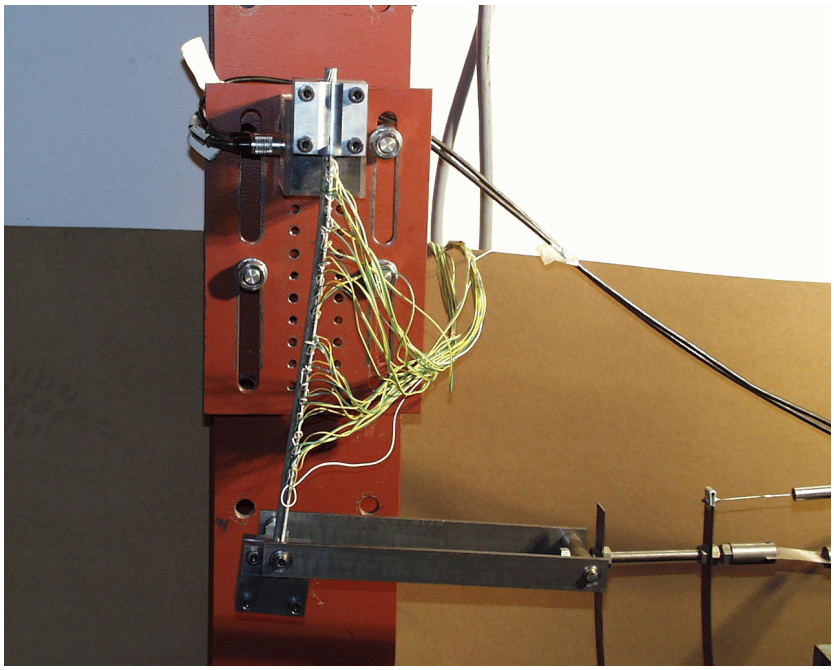

Figure 2.10: Setup for experiment (a)

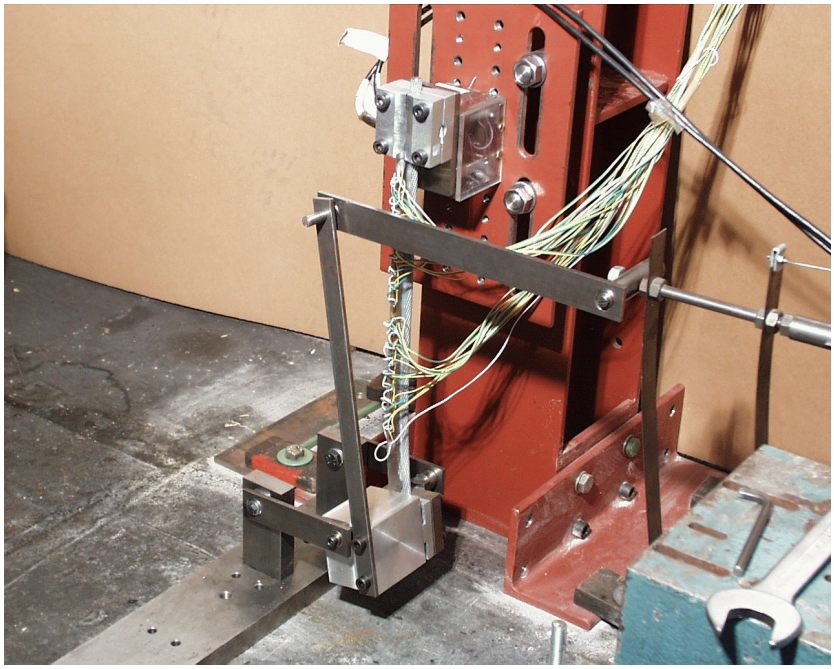

Figure 2.11: Setup for experiment (b)

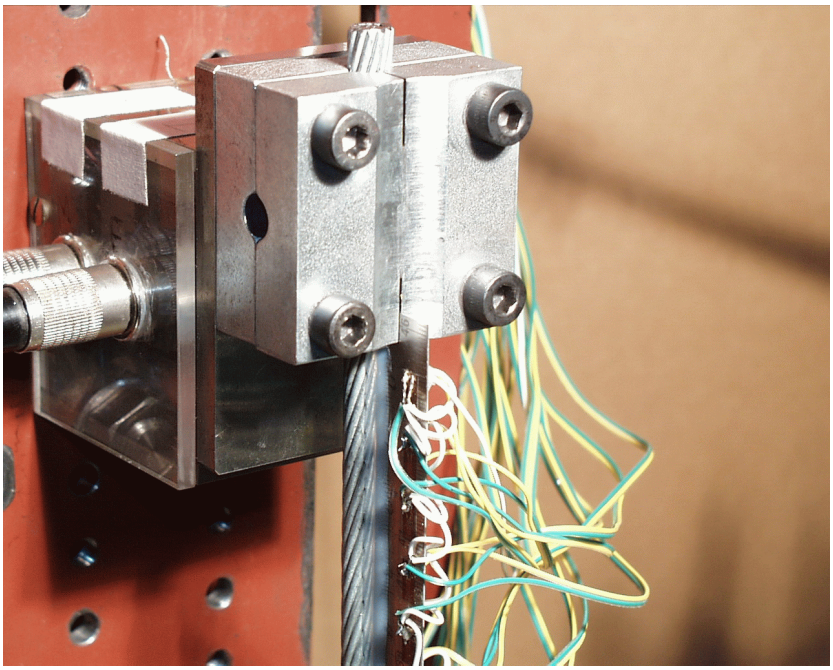

Figure 2.12: Damper cable clamped at the load cell

2.3 Experimental Data

An overview of all the experimental data for a given cable length is given in the 3D-plots (Figure 2.13). For both setups the hysteresis loops were determined from measurements at several locations along the cable for several end displacement amplitudes. Figure 2.14 shows hysteresis curves obtained at a single cable location, undergoing a cyclic bending moment and curvature at several end amplitudes. It can be seen easily that the moment-curvature relationship is not single-valued, but depends on the direction of the displacement. It was found that the velocity had no influence on the hysteresis loops, as expected. We also detected large changes of the slope, which is proportional to the bending stiffness[1]

$$EI(s,t) := \frac{\partial M(s,t)}{\partial \kappa(s,t)} \,. \tag{2.14}$$

Thus the local bending stiffness is not constant, but depends on the time history. This is typical for hysteretic systems.

In Figure 2.15 the hysteresis curves at several positions are shown for a fixed-amplitude

[1]In chapter 3 the minimum bending stiffness $ei := \min(EI)$ will be introduced. The two bending stiffnesses should not be mixed up.

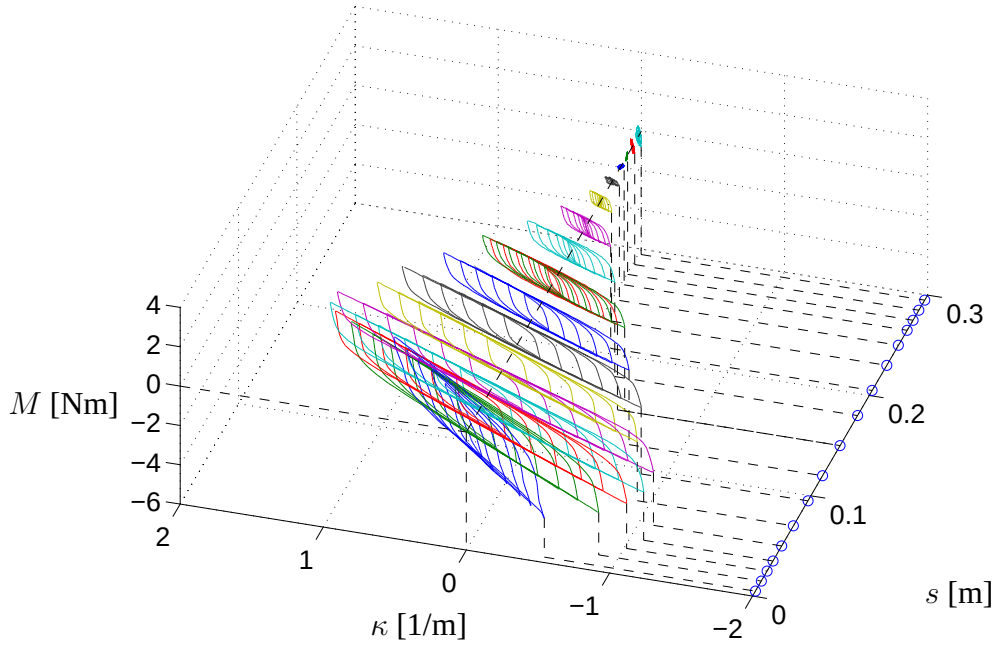

(a) Experiment a

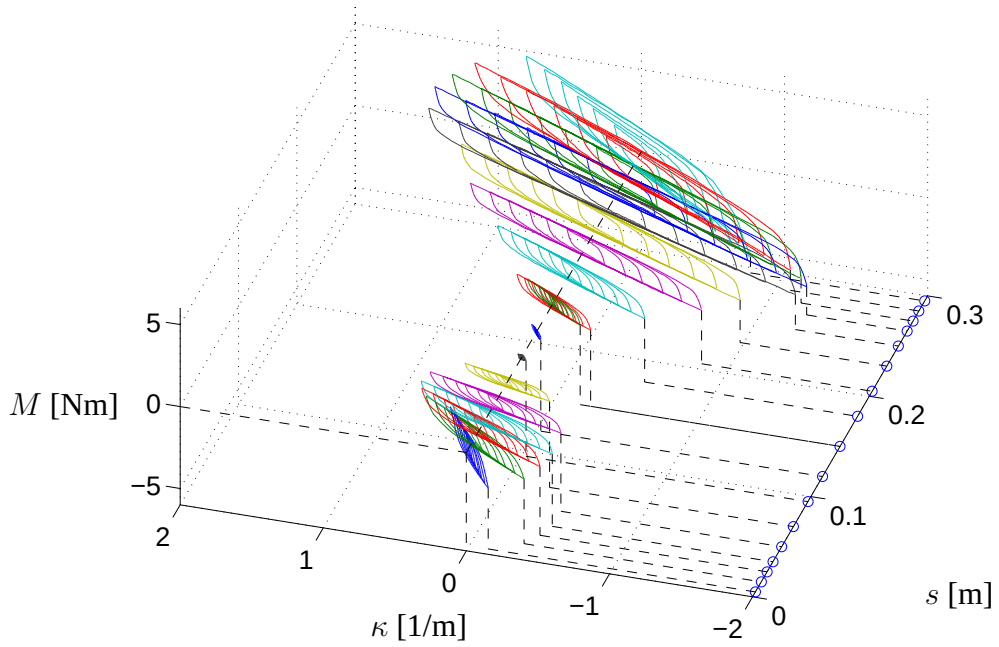

(b) Experiment b

Figure 2.13: Experimental results for different locations s and curvature amplitudes $\hat{\kappa}$

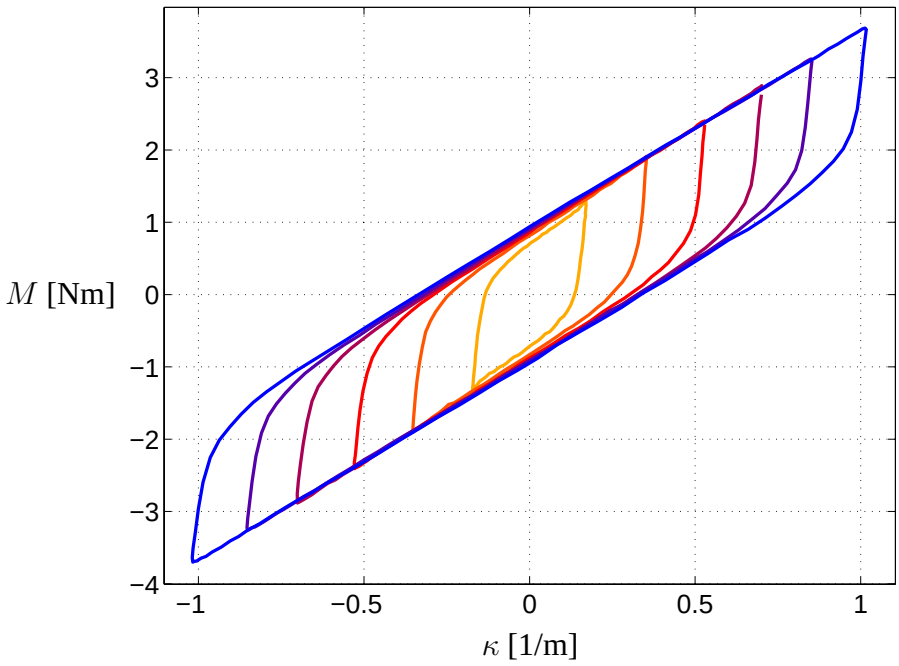

Figure 2.14: Local hysteresis cycles for different end displacement amplitudes $\hat{x}$ at the same location s (Experiment a)

displacement. Contrary to Figure 2.14 it can be seen that the shape of the hysteresis curves depends on the location along the cable. This and other related phenomena will be examined in more detail later on (see Section 3.5) and various parameters need to be identified for this purpose.

2.4 Additional Experiments

Additional experiments were done to check the homogeneity of the cable properties in a cable role as well as the influence of the clamps; they are described in this section. It is desirable to predict the mechanical behavior of a STOCKBRIDGE damper from the damper cables properties and the other design parameters. In the manufacturing process, the damper cables are cut off from long cable rolls. The aim is to build different types of STOCKBRIDGE dampers (i.e. of different cables lengths) with specified properties once the characteristics of a cable roll have been determined. Presently, separate frequency response experiments have to be executed for every type of damper, which is quite time demanding and expensive.

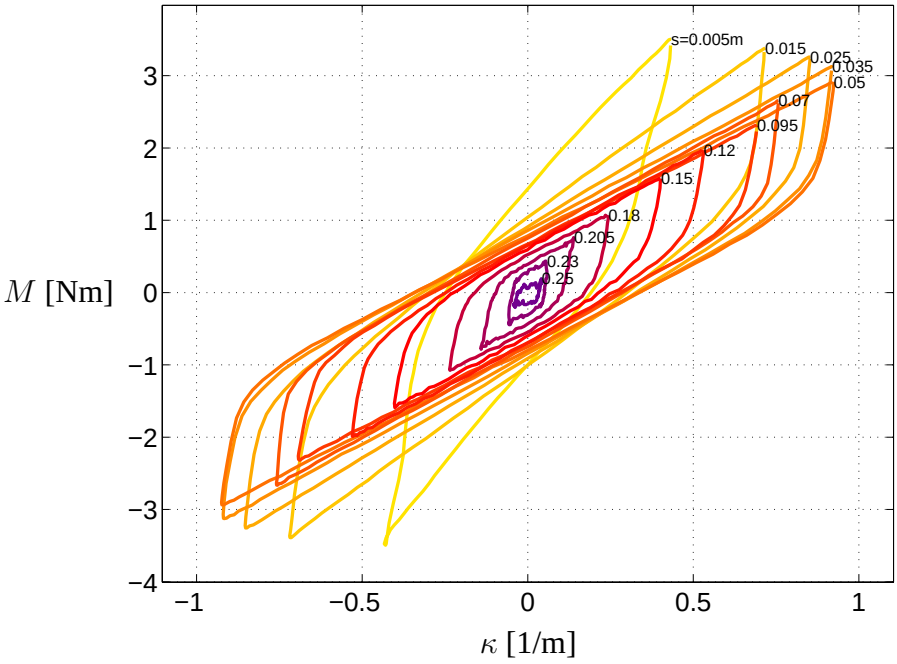

Figure 2.15: Local hysteresis cycles at different locations s for a fixed end displacement amplitude $\hat{x}$ (Experiment a)

Thus, first of all it has to be checked if the (bending) properties of the cable are the same at every location in the roll. To this end, additional quasi-statical experiments were performed using again the experimental setup of experiment (a) as shown in Figure 2.16 a. From Figure 2.17 it can be seen that hysteresis cycles for different cable pieces (same length and same clamps) taken from different positions of the cable roll are nearly identical. This holds for an arbitrary piece of cable taken from the same roll. Thus, it is reasonable to assume that the bending properties are constant throughout the whole cable roll.

In the manufacturing process both the clamp as well as the 'inertial masses' are fixed via compression (clamped) to the damper cables. One can imagine that this clamping may influence the mechanical properties of the STOCKBRIDGE damper. It must therefore be checked if the influence of the clamping is always the same. The previous experiment was therefore repeated, but now with the cable mounted in a STOCKBRIDGE damper as depicted in Figure 2.16 b. Again two arbitrary damper cables from the same roll are compared and the hysteresis cycles are shown in Figure 2.18. It was found that in also this case too the hysteresis cycles are almost identical. From these two experiments we can conclude that for practical purposes it is reasonable to investigate the mechanical behavior of the damper

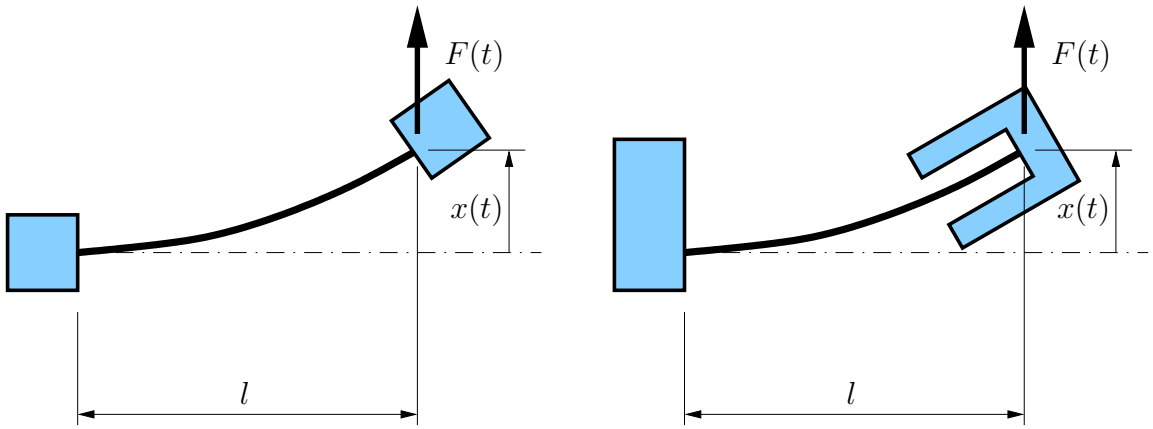

(a) Cable clamped by test clamps

(b) Cable in a STOCKBRIDGE damper

Figure 2.16: Additional experiments

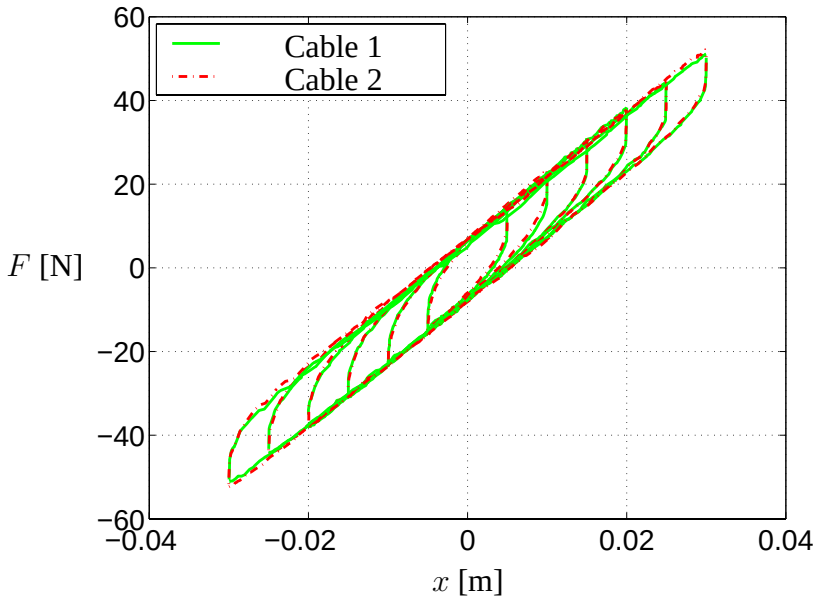

Figure 2.17: Hysteresis cycles for two damper cables of the same length taken from the same cable roll

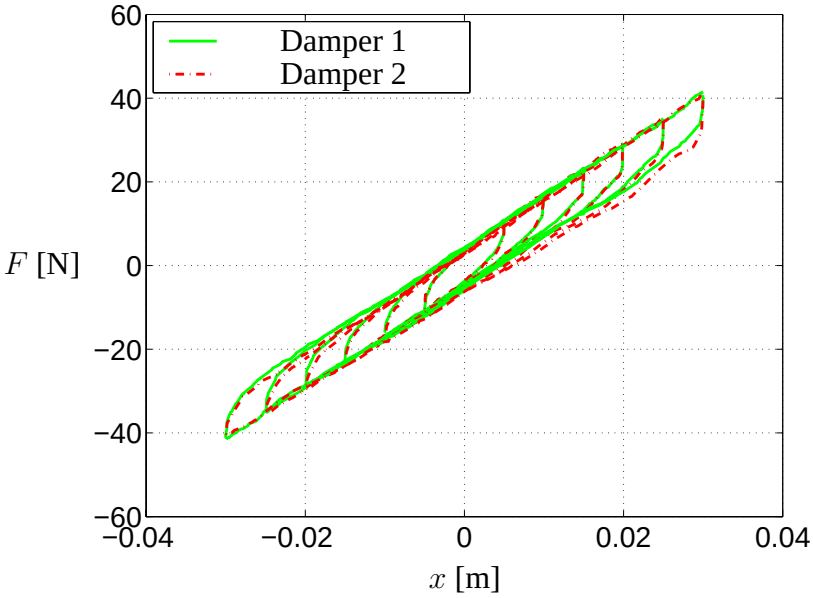

Figure 2.18: Hysteresis cycles for two damper cables of the same length taken from the same cable roll applied to a Stockbridge damper

cable as done here in more detail with view to modeling a STOCKBRIDGE damper.

In addition we compare the hysteresis loops from the latter two experiments (Figure 2.19). This diagram shows the influence of the clamping. For a given displacement amplitude $\hat{x}$ different force amplitudes $\hat{F}$ are obtained. In case of the STOCKBRIDGE damper clamps, smaller force values were found. Furthermore there is a remarkable difference in the area enclosed by the hysteresis loops. This area represents the dissipated energy and is important in the design of dampers. The clamps were therefore examined more closely. It was found that STOCKBRIDGE damper clamps have a tapered ending and do not work up to the edges (Figure 2.20). This means that the active length $l^* = l + \Delta l$ of the cable between the clamps is longer than originally assumed. This may also explain, why a smaller bending stiffness was found in case (b). Special attention must therefore be given to the clamping in the design of dampers and in the further investigations.

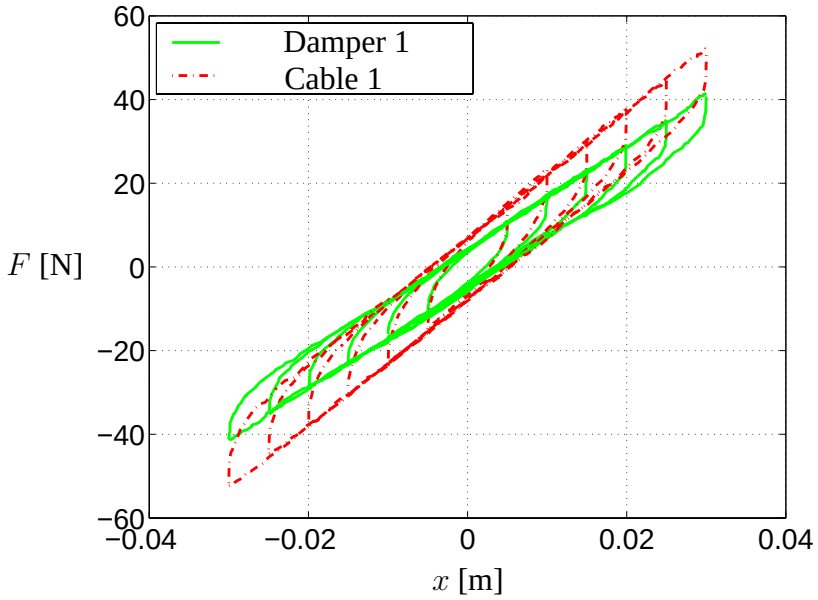

Figure 2.19: Hysteresis cycles for a single damper cable using test clamps and applied to a STOCKBRIDGE damper

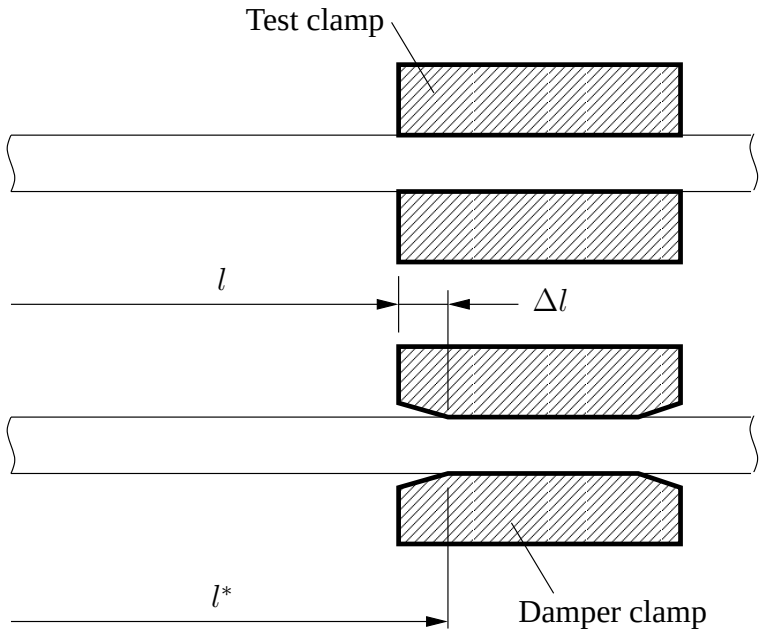

Figure 2.20: Cross section through the clamps

Chapter 3

Bending Model for Slack Wire Cables

3.1 Describing Systems with Statical Hysteresis

It is well known (e.g. [17]) that wire cables subjected to a bending moment represent a system with *statical hysteresis*, i.e. velocity-independent hysteresis. Consider the mechanical system acted on by a force F shown in Figure 3.1. For a *statical hysteretic* system the relation between the displacement x and the restoring force F cannot be described simply by a function $f(x)$, but depends on the history of the displacement x and the sign of $\dot{x}$, where the dot denotes the time derivative. This is because the state of the system is not completely described by the variable x.

If we want to model a hysteretic system, more state variables have to be considered. These additional variables are *internal variables* and for many hysteretic systems they have a physical or geometrical meaning. Introducing the internal variables we get rid of the multivaluedness of the force. The *evolution equations* of hysteretic systems can often

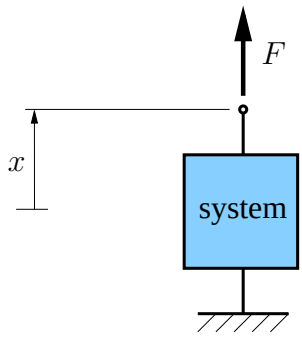

Figure 3.1: Force acting on a hysteretic system

be described by

$$\dot{F}(t) = \mathrm{h}\left(F(t),\ \dot{x}(t),\ \mathrm{sign}\left(\dot{x}(t)\right), \mathbf{k}(t)\right) , \tag{3.1}$$

$$\dot{\mathbf{k}}(t) = \mathbf{K}\left(F(t),\ \dot{x}(t),\ \mathrm{sign}\left(\dot{x}(t)\right), \mathbf{k}(t)\right) , \tag{3.2}$$

where $\mathbf{k}$ is the vector of the internal variables (e.g. [4]). Internal variables are often used in *phenomenological models*.

Instead of internal variables the restoring force can also be described by functionals with so-called *memory functions*. Using such a formulation, the state of a system is represented as a *functional* over the history of the motion. This formulation is equivalent to the description by internal variables, but for the study of vibrations internal variables are more suitable. A detailed description of the modeling of hysteretic mechanical systems was given by KOLSCH [17] and more general literature about hysteresis can also be found e.g. in [2, 18, 25].

3.2 Wire Cable as a One-Dimensional Continuum

In a STOCKBRIDGE damper, the damper cable experiences forces and torques simultaneously at the point of connection to the "inertial mass". The bending shape of the cable then depends on the frequency and amplitude of the clamp motion and is not known a priori. A general model for the hysteretic damper cable is therefore needed for the simulation of STOCKBRIDGE dampers.

A multitude of models for wire cables can be found in literature. Most of these papers deal with the stresses in the wires due to tensile forces and/or bending with a constant bending radius for the whole cable (e.g. [5]). Few models only can be found in the literature to explain the dynamical or quasi-statical behavior of wire cables. In most of these models the wire structure of the cable is reproduced in order to derive the mechanical properties from the known geometry. Depending on the modeling depth, difficult mathematical expressions may appear. Even for the very simple case of a single wire (with finite bending stiffness), wound helically around a rigid cylinder [31] (see Figure 3.4) the analytical solution requires the solution of LOVEs equations for the tridimensionally curved rod [21]. Complicated phenomena such as the appearance of multiple regions in which the wire looses contact with the cylinder are found [31]. It is obvious that the description of the interaction of multiple wires requires remarkable simplifications. An approach for the case

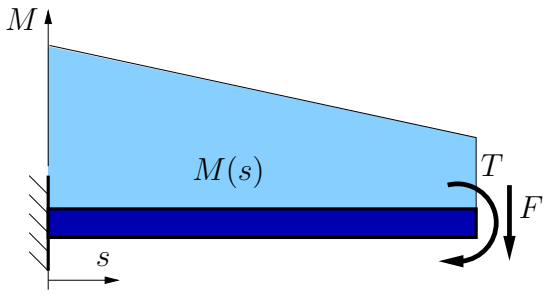

Figure 3.2: Bending moment acting on a damper cable.

of small tension forces as well as a detailed literature survey can be found in [28].

Besides the mentioned computational problems, there is still the problem of estimating parameters such as e.g. stick and slip coefficients of friction between the wires and this can only be done experimentally. Another difficulty is the internal initial state of the cable structure which is unknown in general and complicates the experimental reproducibility.

Due to these difficulties and with the view to the practical application in a damper, the detailed behavior of the individual wires will not be considered here. Instead, we restrict ourselves to macroscopic overall quantities such as the bending moment and curvature of the cable. Thus, the complicated structure is reduced to a *one-dimensional continuum* describing the bending characteristics of the cable. The *moment-curvature-relation* of the cable is considered at each location s along the cable (see Figure 3.2). Such a model is known as a *distributed model*. Furthermore, the properties of the cable can be assumed to be the same at every location along its length except in the vicinity of the clamped ends. The parameters of this model will be determined from experiments (Section 2.3). This approach has already been used successfully for taut cables by GUTZER [7].

The curvature $\kappa(s,\, t)$ at position s is a function of the bending moment $M(s,\, t)$ at the same position and of several *internal variables* $\mathbf{k}(s,\, t)$. Our distributed model is *local* in the sense that *at the same location only*. According to (3.1), (3.2) the relations

$$\dot{M}(s,\, t) \;=\; \mathrm{h}\left(M(s,\, t),\; \dot{\kappa}(s,\, t),\; \mathrm{sign}\left(\dot{\kappa}(s,\, t)\right),\; \mathbf{k}(s,\, t)\right)\,, \tag{3.3}$$

$$\dot{\mathbf{k}}(s,\, t) \;=\; \mathbf{K}\left(M(s,\, t),\; \dot{\kappa}(s,\, t),\; \mathrm{sign}\left(\dot{\kappa}(s,\, t)\right),\; \mathbf{k}(s,\, t)\right) \tag{3.4}$$

are used to describe the cables behavior. This approach implies that the state at any location s of the cable has no direct influence on the the state at other locations of the cable. In real-

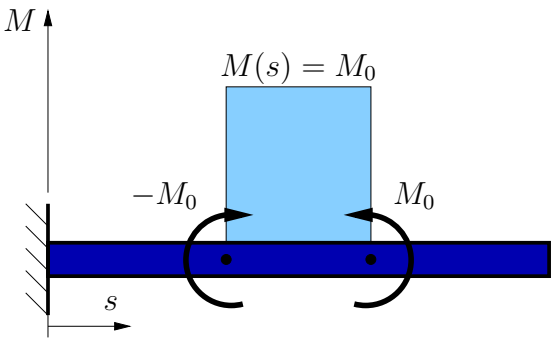

Figure 3.3: Bending moment acting only on part of a damper cable

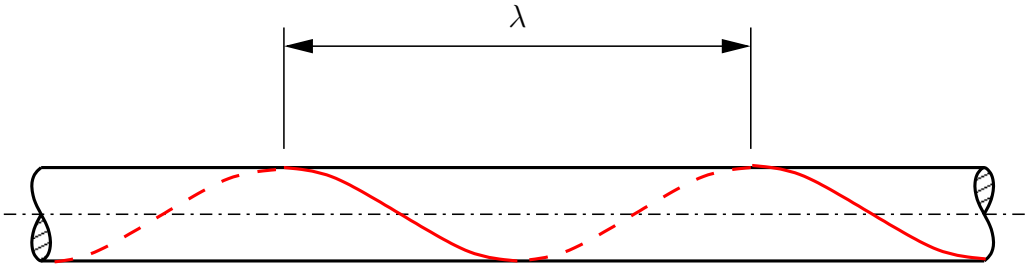

Figure 3.4: Wire (beam) wound around a rigid cylinder

ity of course a wire cable may behave quite differently from a BERNOULLI-EULER beam. For example, if a bending moment is applied only over a small section of a BERNOULLI-EULER beam (Figure 3.3), the curvature outside this region will be zero. In the case of a wire cable however a certain transition zone will appear where the curvature is non-zero, even though there is no bending moment acting. The subject will not be examined more closely at this point, but one can easily imagine that various geometrical parameters, like the lay length λ (see Figure 3.4), influence the bending behavior of a wire cable.

GUTZER [7] found that a distributed local model can be used for taut wire cables. He considered sinusoidal deformation of cables with large lay lengths and ascribed the validity of the distributed local model to an averaging effect, appearing if the curvature changes only very slowly with location, i.e. if the curvature gradient $\partial\kappa(s)/\partial s$ is small. For a damper cable of a STOCKBRIDGE damper $\partial\kappa(s)/\partial s$ may however be relatively large. We will however use the distributed local model, at least as a first step for the problem at hand and potential problems will be discussed later.

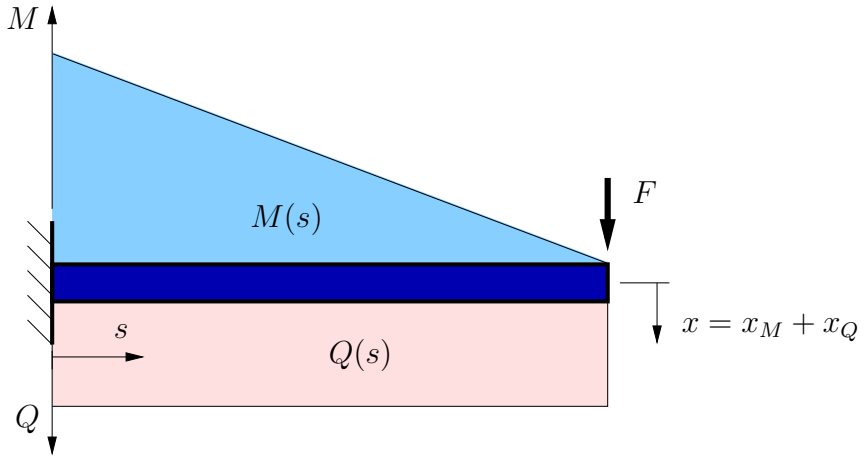

Figure 3.5: Shear force acting on a wire cable

3.3 Shear Force

It was already stated in section 3.2 that the curvature gradient $\partial\kappa(s)/\partial s$ may influence the bending behavior of a wire cable. Since the curvature is connected to the bending moment, the gradient of the bending moment $\partial M(s)/\partial s$ should also be taken into account. It is known from elementary strength of materials that this is the shear force $Q(s)$ in the damper cable.

In case of cantilever damper cables (Figure 3.5), a bending moment $M(s)$ as well as a share force $Q(s)$ distributed throughout the whole length of the cable due to a force F appear. Most previous papers on the bending behavior of wire cables however considered only the bending moment. Regardless of slip appearing or not between the strands, in both cases the displacement x_M due to the bending moment alone will be larger than the displacement x_Q due to the shear force $Q(s)$:

$$x_M \gg x_Q \ , \tag{3.5}$$

if a wire cable is treated as a slender beam. Thus one could be tempted to assume that the shear force is negligible. It may nevertheless be quite important since it can be considered as a trigger for the slipping.

We will however first consider the moment-curvature relation only and we postpone the study of the influence of the shear force and the shear stresses until later.

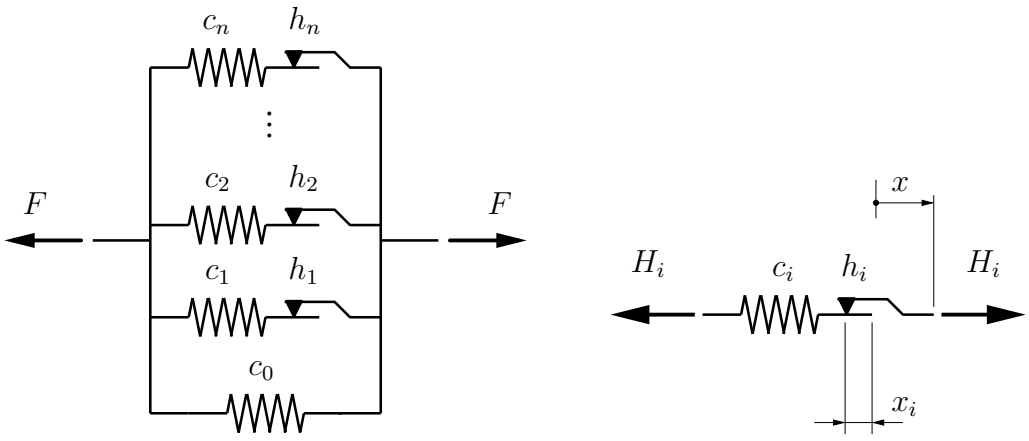

(a) MASING model

(b) Force H_i acting on a JENKIN element

Figure 3.6: MASING model for a mechanical system with statical hysteresis

3.4 MASING Model

The statical hysteresis in a damper cable is due to 'dry' friction which is usually described by COULOMB's friction model. The MASING *model* [23] is therefore chosen here as a phenomenological model for the model. A detailed discussion of the MASING model and of related models can be found in [17] and in literature about plasticity [16, 13].

In general, a MASING model (Figure 3.6a) for a concentrated hysteretic element comprises JENKIN *elements* (Figure 3.6b) connected in parallel. A JENKIN element consists of a linear spring (stiffness c_i) and a COULOMB friction element (max. stiction force h_i). The difference between the stick and slip force is neglected. It is well known that elastic springs in conjunction with dry friction lead to static hysteresis.

A JENKIN element comprises only one internal variable, needed to describe its state. For example the displacement x_i of the COULOMB friction element could be used as an internal variable (Figure 3.6 b). Instead of the displacement x_i one can also take the force H_i at the JENKIN element as an internal variable, since for a given external displacement x the force depends uniquely on x_i.

The force F acting on a MASING model (Figure 3.6 a) is given by

$$F = c_0 x + \sum_{i=1}^{n} H_i \; . \tag{3.6}$$

The evolution equation for the time derivative of the *hysteretic force* H_i of every JENKIN element is

$$\dot{H}_i = c_i \, \dot{x} \, \frac{1}{2} \left[1 - \text{sign}(H_i^2 - h_i^2) - \text{sign}(\dot{x} \, H_i) \left(1 + \text{sign}(H_i^2 - h_i^2) \right) \right] \ . \tag{3.7}$$

Differential equations obtained for hysteretic systems are usually to be solved numerically. Since it yields numerical difficulties, the function $\text{sign}(H_i^2 - h_i^2)$ is approximated:

$$\text{sign}(H_i^2 - h_i^2) \approx \left| \frac{H_i}{h_i} \right|^m - 1 \qquad \text{for} \quad H_i^2 \leq h_i^2, \quad m \in \mathbf{R}^+ \quad \wedge \quad m > 1 \ . \tag{3.8}$$

Thus (3.7) can be written as

$$\dot{H}_i = c_i \dot{x} \left[1 - \frac{1}{2} \left(1 + \text{sign}(\dot{x} \, H_i) \right) \left| \frac{H_i}{h_i} \right|^m \right] \ . \tag{3.9}$$

A hysteretic system described by (3.9) represents a *decomposable* system [4]. Such systems can be expressed as the sum of a hysteretic and an elastic component:

$$F = g(x) + H \ . \tag{3.10}$$

Here the force $g(x)$ is in general a nonlinear, single-valued function and H is the hysteretic force given by an evolution equation. In case of the MASING model the elastic component is linear: $g(x) = c_0 x$.

Figure 3.7 shows an example of the behavior of a JENKIN element for given displacement changes. The MASING model is obviously heavily nonlinear. If the previous history of the system is not known, no unique relation between displacement and force exists.

Generalizing these ideas for a one-dimensional continuous system such as a wire cable leads to the *distributed local* MASING *model* [8] describing the relation between the curvature of the cable $\kappa(s) = \partial^2 w(s)/\partial s^2$ and the bending moment $M(s)$. The characteristics of the model are given by position dependent parameters $ei(s)$, $c_i(s)$, and $h_i(s)$. In Table 3.1 the relation between the discrete and the distributed MASING model is shown. In this model, the hysteresis is taken into account by the additional bending moment $H(s)$ of the distributed JENKIN elements acting on the linear elastic EULER-BERNOULLI beam with bending stiffness $ei(s)$ (see Figure 3.9), where $ei(s)$ is the minimum bending stiffness of the model, appearing when all Jenkin elements are slipping. It should not be confused with the "classical" bending stiffness EI. The maximum bending stiffness $ei(s) + \sum c_i$ appears

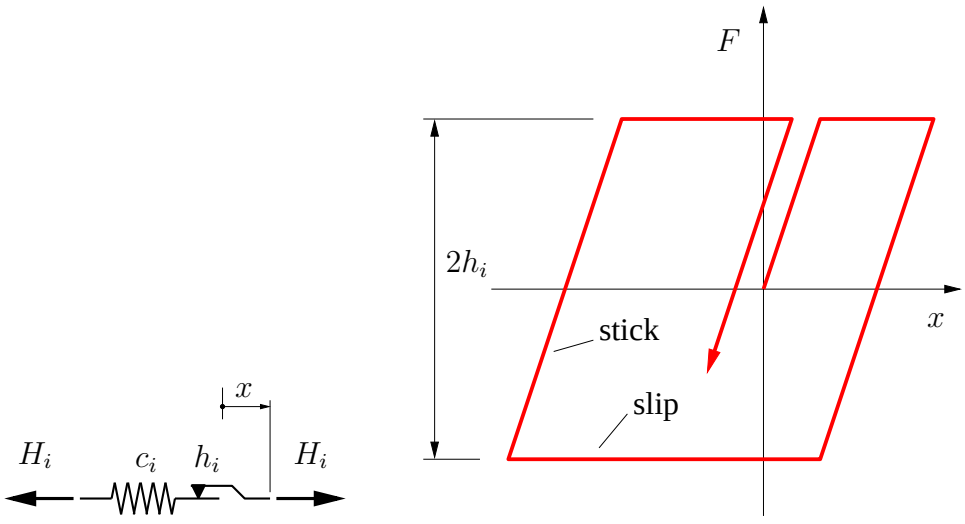

(a) Single JENKIN element (b) Hysteresis cycle

Figure 3.7: Hysteresis cycle for a single JENKIN element

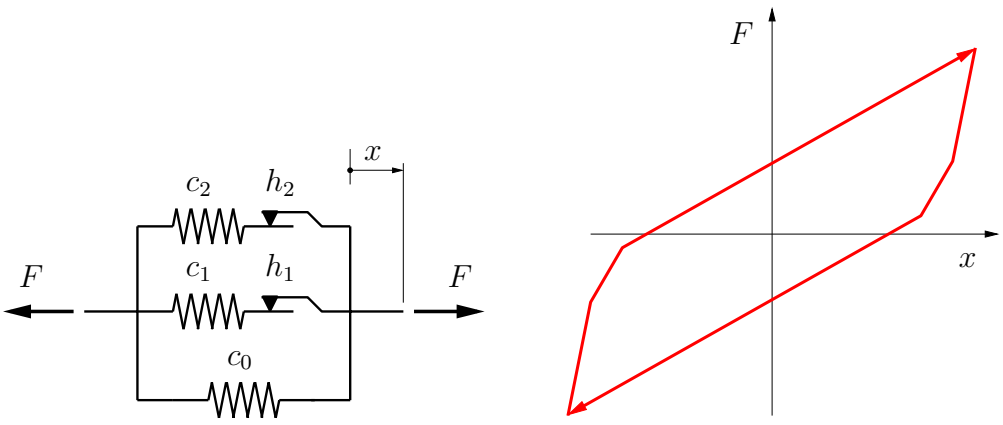

(a) MASING model (2 JENKIN elements) (b) Hysteresis cycle

Figure 3.8: Hysteresis cycle for a Masing model comprising two JENKIN elements and linear spring (periodic displacement)

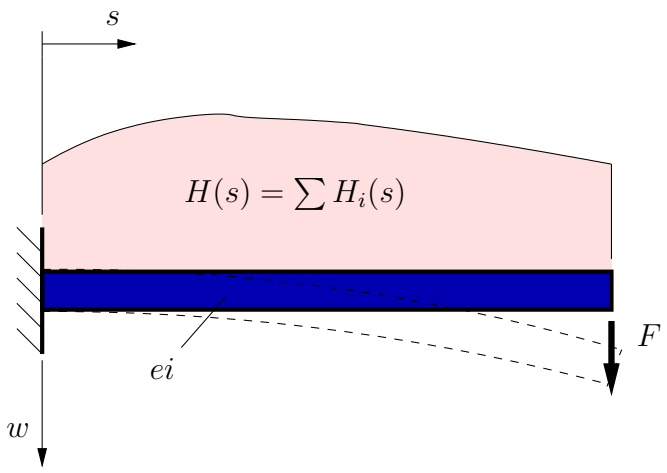

Figure 3.9: Distributed MASING model for a wire cable: EULER-BERNOULLI beam with an additional hysteretic moment $H(s)$ acting on it

when all JENKIN elements stick.

The total bending moment $M(s)$ according to (3.6) is

$$M(s) = ei(s)\,\kappa(s) + \sum_{j=1}^{m} H_j(s)\;, \tag{3.11}$$

with the so-called the *hysteretic moment*

$$H(s) := \sum_{j=1}^{m} H_j(s)\;. \tag{3.12}$$

In general the curvature $\kappa(s)$ of a damper cable is unknown a priori, but the bending moment $M(s)$ follows from the forces or torques acting at the ends (e.g. Figure 3.9). It is therefore convenient to solve for the curvature:

$$\kappa(s) = \frac{1}{ei(s)} \left(M(s) - \sum_{j=1}^{m} H_j(s) \right)\;. \tag{3.13}$$

The evolution equation for the time derivative of the *hysteretic moment* H_i of each distributed JENKIN element is

$$\dot{H}_i(s,t) = c_i(s)\,\dot{\kappa}(s,t)\,\frac{1}{2}\left[1 - \operatorname{sign}(H_i^2(s,t) - h_i(s)^2) - \operatorname{sign}(\dot{\kappa}\,H_i)\left(1 + \operatorname{sign}(H_i^2 - {h_i}^2)\right)\right]\;, \tag{3.14}$$

Discrete MASING model	**Distributed MASING model of cable**
Displacement x	Curvature $\kappa(s)$
External force F	External bending moment $M(s)$
Minimum stiffness c_0	Minimum bending stiffness $ei(s)$
Stiffness of the i-th J. element c_i	Bending stiffness of the i-th J. element $c_i(s)$
Max. force of the i-th J. element h_i	Max. moment of the i-th J. element $h_i(s)$
Hyst. force of the i-th J. element H_i	Hyst. moment of the i-th J. element $H_i(s)$

Table 3.1: Relation between the discrete Masing model and distributed MASING model of a cable

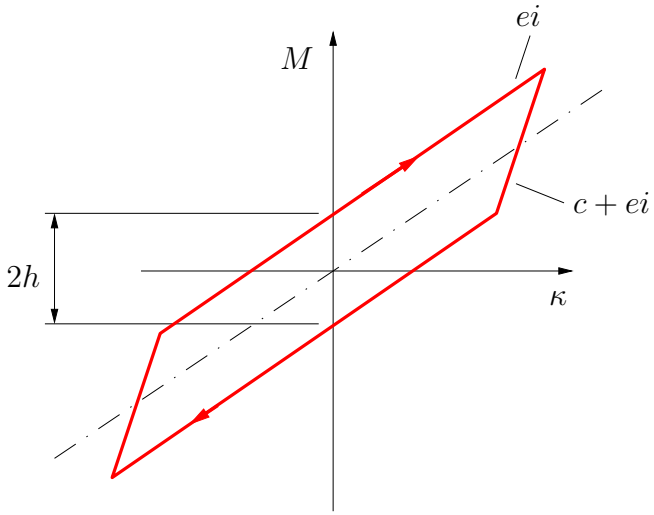

Figure 3.10: Moment-curvature relation (hysteresis cycle) for an EULER-BERNOULLI beam with a single distributed JENKIN element

where the dot denotes the time derivative [17]. On account of numerical reasons again we approximate the sign function:

$$\dot{H}_i(s,t) = c_i(s)\,\dot{\kappa}(s,t)\left[1 - \frac{1}{2}\left(1 + \operatorname{sign}(\dot{\kappa}\,H_i)\right)\left|\frac{H_i}{h_i(s)}\right|^m\right] . \tag{3.15}$$

3.5 Local Parameter Identification

3.5.1 Identification Procedure

In this subsection we will identify the parameters of a wire cable modeled by the local distributed MASING model from the experimental data described in Chapter 2. The identification of the model parameters was done numerically in the time domain using the MATLAB software package [24]. We begin using only a single distributed JENKIN element, which considerably simplifies the procedure.

The parameters $ei(s)$, $h(s)$, and $c(s)$ of the model were identified locally at the same positions $s_1,\ s_2,\ ....,\ s_n$ where the curvature had been measured. To this end the experimentally measured moment-curvature relationship $M_{exp}(\kappa_{exp})$ was approximated by that of the model, $M_{model}(\kappa_{model})$ (see Figure 3.11). The time derivative of the curvature $\dot{\kappa}_{model}(s,t) := \dot{\kappa}_{exp}(s,t)$ was specified and the bending moment $M_{model}(s,t)$ was computed via numerical integration of (3.13) and (3.15) using the MATLAB command `ode23`. This is an implementation of an explicit RUNGE-KUTTA (2,3) pair of BOGACKI and SHAMPINE [1]. `ode23` uses an adaptive step control method so that, instead of the step size, one specifies the desired tolerance for the problem.

The identification was done by fitting the parameters of the model minimizing the error

$$e := \int_0^T |M_{model}(s,t) - M_{exp}(s,t)|\,\mathrm{d}t\,, \tag{3.16}$$

T being the period, via the MATLAB command `fminsearch`, which uses the simplex search method of [19].

3.5.2 Analysis of Identified Parameters

The bending stiffness EI of slack wire cables undergoing bending varies considerably with the curvature. In fact it is difficult to describe the change of the bending stiffness of the cable during a bending cycle, but two limiting cases can be analyzed easily. In the first case we assume that there is no slip in between the wires. Thus the the cable behaves as an elastic beam. In this case we obtain the maximum value for the bending stiffness EI_{max}. In the second case we assume that there is no friction between the wires, which leads to the minimum bending stiffness EI_{min}. In Appendix A.1 these two bending stiffnesses were calculated for the wire cable under consideration:

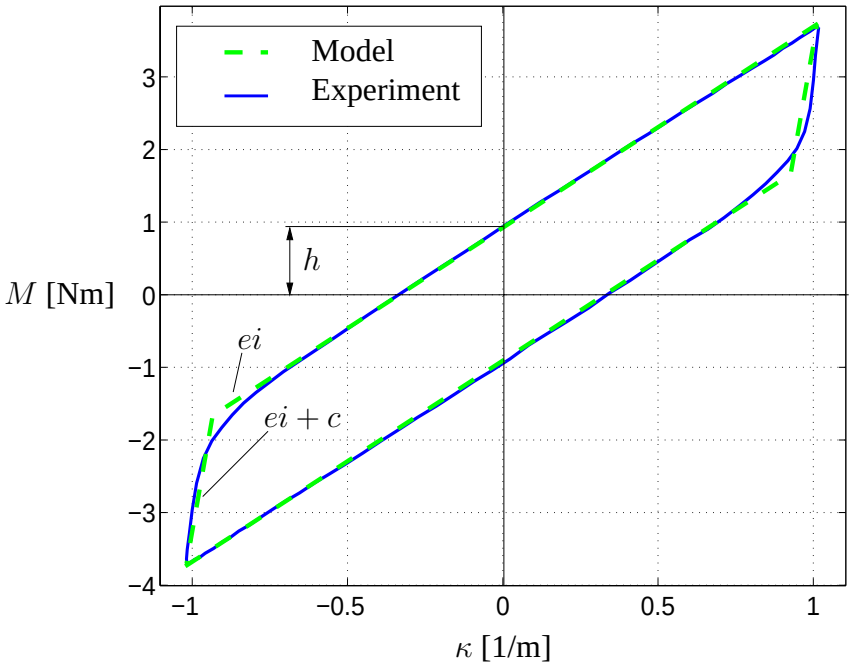

Figure 3.11: Local identification via curve fitting

- $EI_{min} < 3.19\,\mathrm{N/m^2}$,
- $EI_{max} = 66.28\,\mathrm{N/m^2}$.

For actual wire cables the value of the bending stiffness will always lie between these two extreme values. For a wire cable modeled by the MASING model with a single distributed JENKIN element, the minimum bending stiffness EI_{min} corresponds to the parameter ei and the maximum bending stiffness EI_{max} to $ei + c$.

The values of the parameters identified for different amplitudes and for different positions will now be examined. From Figure 3.12 it can be easily seen that for a given position and bending shape the parameters do not depend on the amplitude of the curvature. This was found to hold for all positions at the wire cables and for both bending shapes under consideration.

In contrast to the above, the situation is more complicated if hysteresis cycles at different locations s obtained with the same amplitude $\hat{x}$ are considered (Figure 3.13). Since it is difficult to analyze the hysteresis cycles directly, the resulting values obtained from the identification are shown in Figure 3.14 as functions of the position s. The plots contain the experimental data from both experiments. At some locations the values are missing because the parameters could not be determined due to small amplitudes. For very small

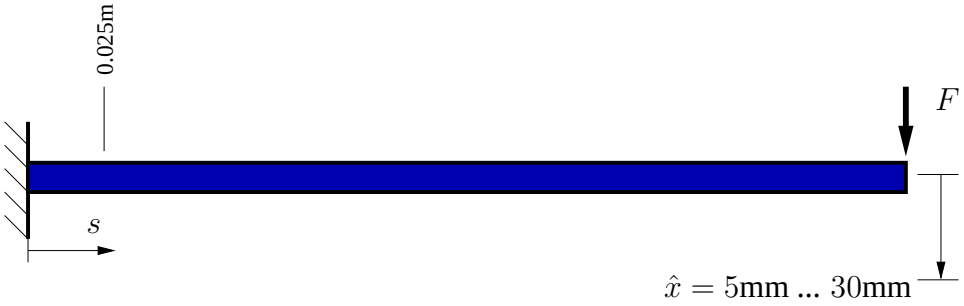

(a) Location

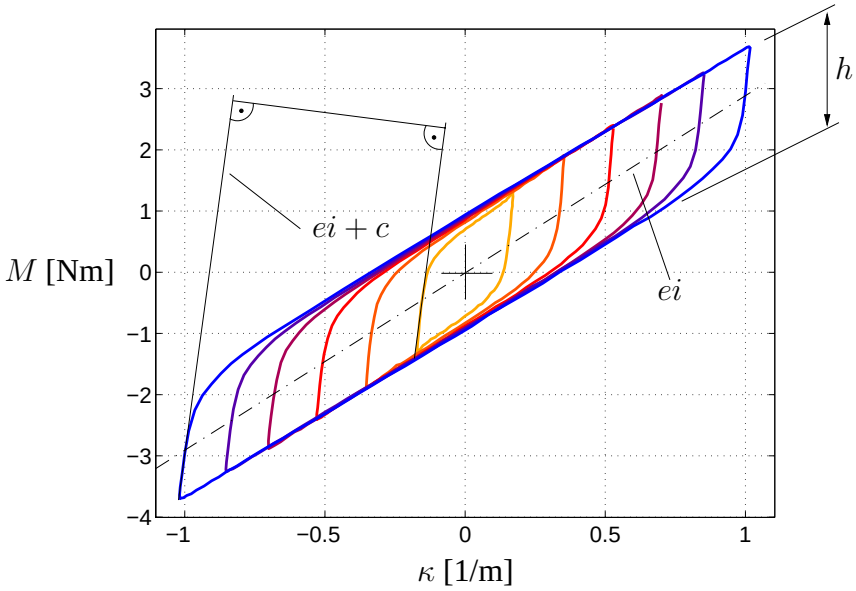

(b) Local hysteresis cycles

Figure 3.12: Local hysteresis cycles for different end displacement amplitudes $\hat{x}$ at the same location $s = 0.025$m

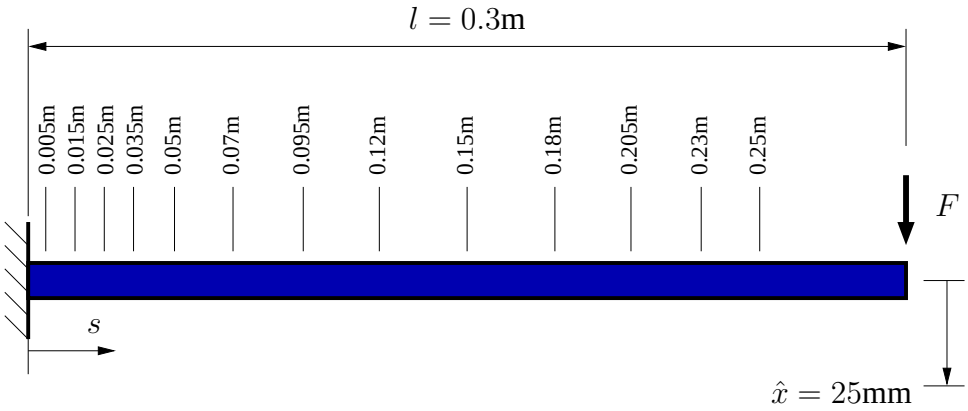

(a) Locations

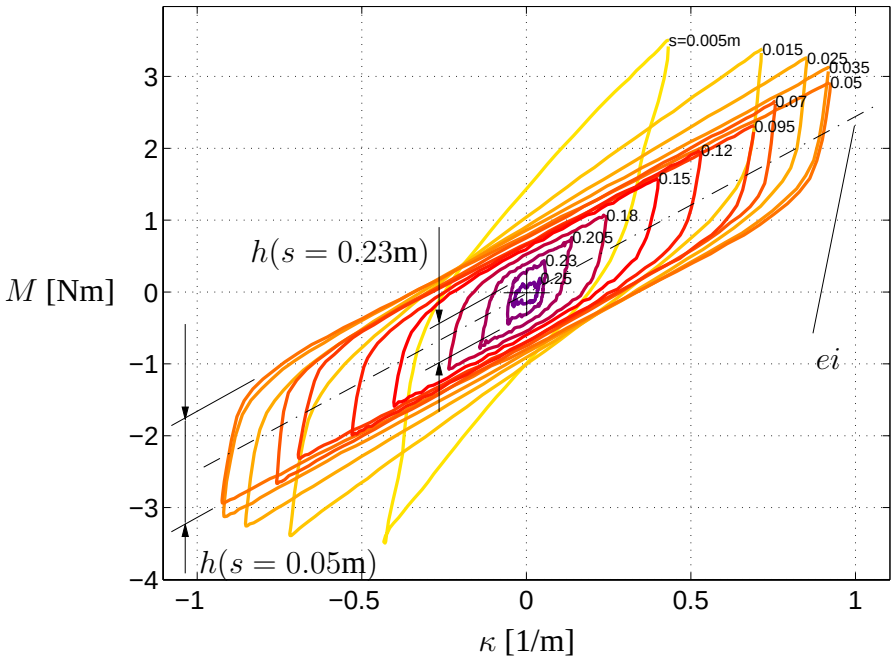

(b) Local hysteresis cycles

Figure 3.13: Local hysteresis cycles at different locations s for a fixed end displacement amplitude $\hat{x} = 0.025$m

displacement amplitudes the hysteresis cycles degenerated into lines and the error e increased.

Different trends were observed in the end regions compared to other locations along the cable. For example, the minimum bending stiffness $ei(s)$ increases near the fixed ends since the strands are pressed together by the clamp. This region can easily be determined directly from the plot (see Figure 3.15).

The minimum bending stiffness $ei(s)$ appears to be constant at a sufficient distance distance from the fixed end. For both experiments nearly the same values are obtained. Thus it can be assumed that this characteristic is a function of the cable only and is independent of the applied load or bending mode. The value of ei is nearly the same as EI_{min}. Therefore it can be assumed in this case, that all the strands are slipping.

Outside of the boundary regions, also $c(s)$ seems have a constant value. Inside the boundary regions the behavior of $c(s)$ is not clear. This may be due to an error in the identification.

In Figure 3.16 the sum $c(s) + ei(s)$ is shown, representing the maximum bending stiffness. As expected, the values are nearly of the same order throughout the cable, different values are obtained only near to the the clamps. However, all the identified values are smaller than EI_{max} of the real cable. This may have two different reasons. On the one hand, the identified values of $c(s)$ may be too small, leading to the differences in the case of sticking as shown in Figure 3.11. In order to identify $c(s) + ei(s)$ more exactly more JENKIN elements may be useful. On the other hand, not all wires may be in contact even in the case of an unbent wire cable.

In contrast to the findings so far obtained, $h(s)$ depends on the position s along the beam and on the bending mode. This can also be seen directly from Figure 3.13 (experiment a). The distance h between the upper and the lower branch decreases with the position s. It contradicts the assumption that the damper cable can be described by a unique distributed local model, where it was assumed that the cable parameters ei, c, and h are independent of the amplitude, position along the cable, and bending mode. The distributed local Masing model in the present form is therefore not sufficiently detailed for a precise description of the local behavior of slack wire cables. In contrast to our findings PLAGGE [29] stated the applicability of the MASING model to slack wire cables. Since no local measurements were made and one bending shape only was studied the invalidity of the model was not noticed.

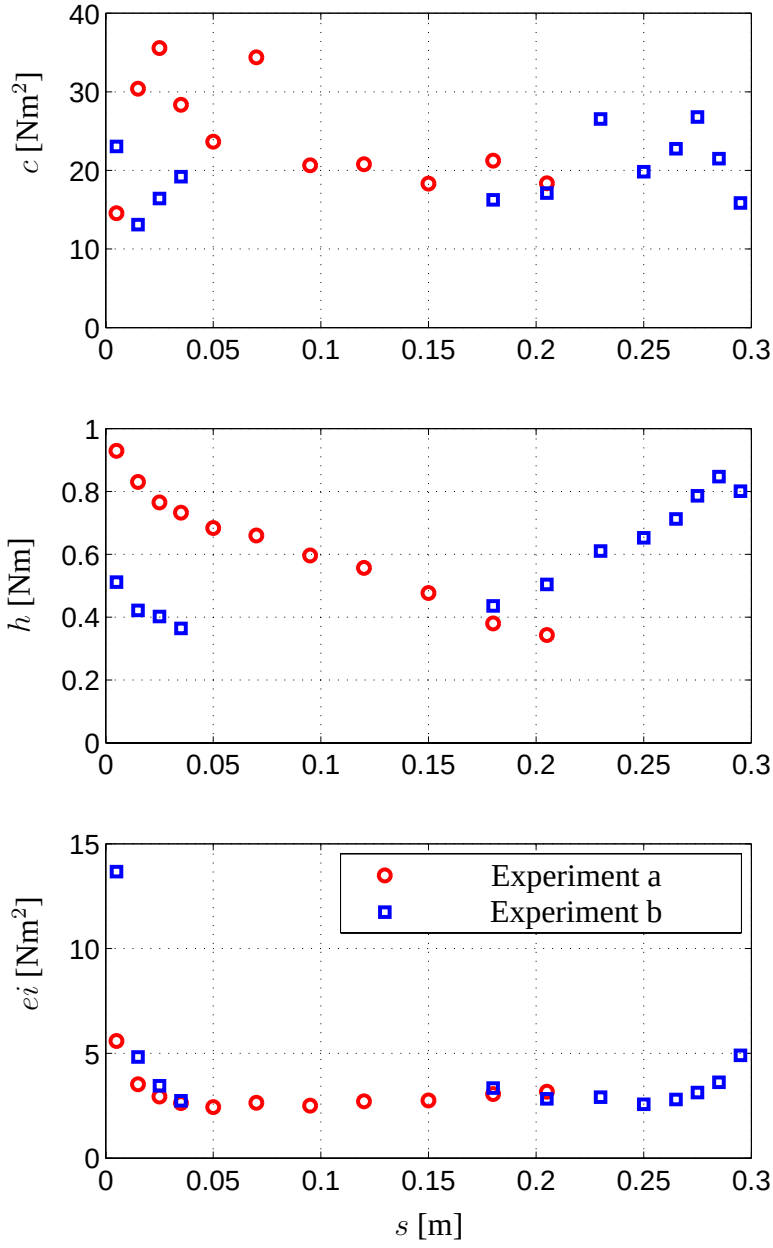

Figure 3.14: Identified parameters $ei(s)$, $h(s)$, $c(s)$ as functions of the location s.

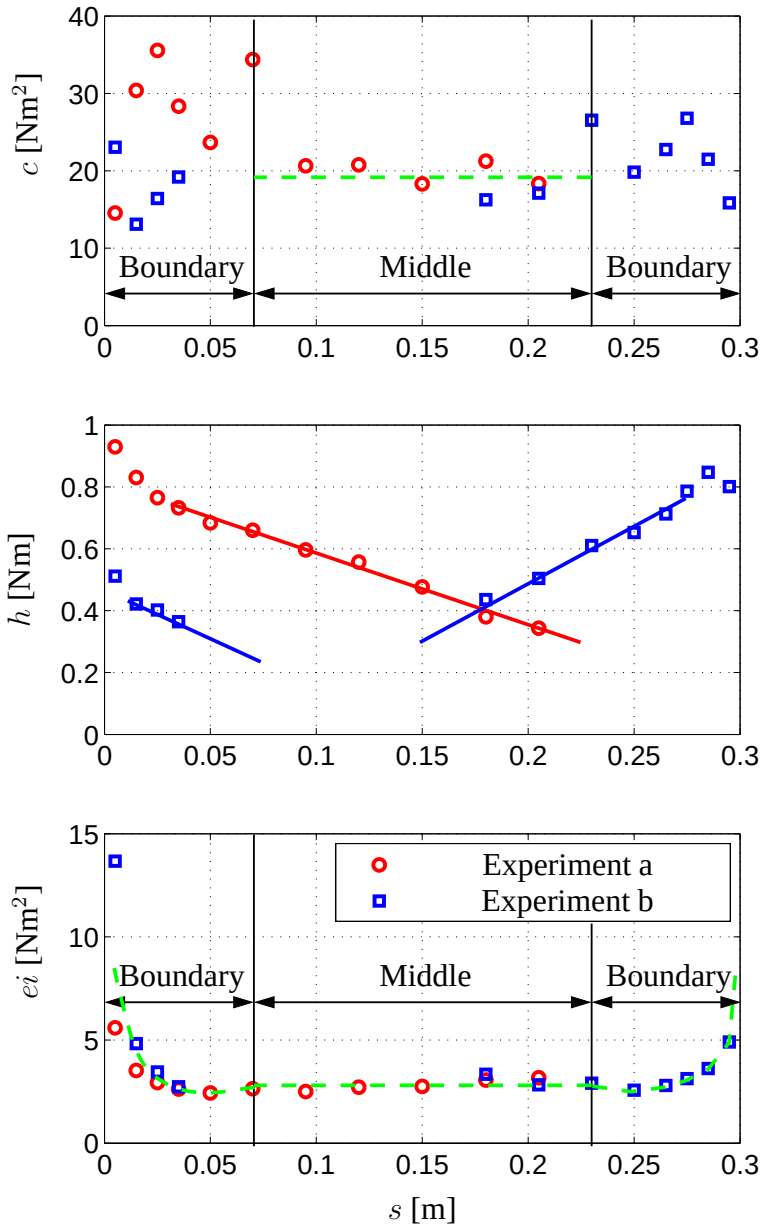

Figure 3.15: Identified parameters (analysis)

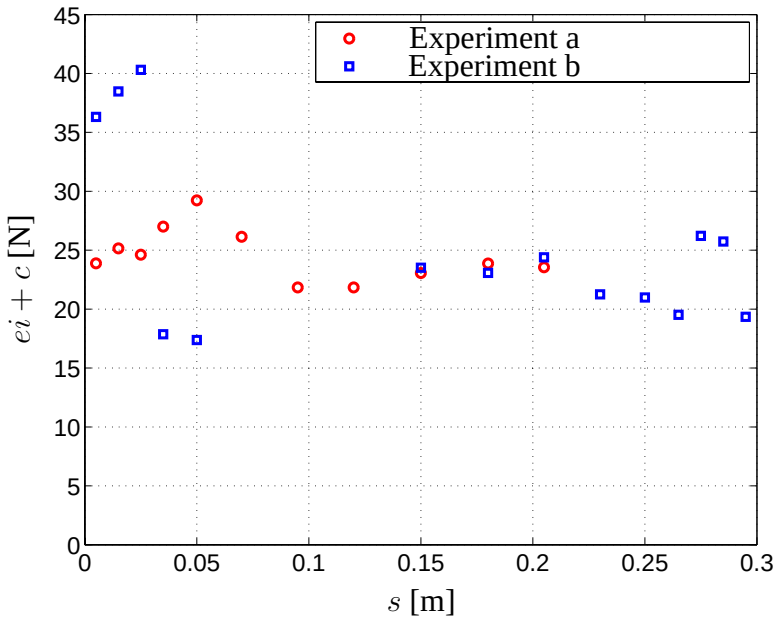

Figure 3.16: Maximum stiffness $ei(s) + c(s)$

3.5.3 Number of JENKIN elements

Still one important issue has to be addressed: How many distributed JENKIN elements should be used? In the previous identification we confined ourselves to only one distributed JENKIN element for modeling the wire cable. Of course, the more elements we use the better we can approximate any individual hysteresis cycle by the MASING model. The computational cost and the error in the identified parameters however increase with more elements. To solve this dilemma, consider 3.17, where hysteresis cycles obtained from experiment as well as simulated by the distributed MASING model are shown. In Figure 3.17 (a) only a single distributed JENKIN element was used. It can be seen that even in this case the hysteresis cycles can be approximated quite well. Only if we want to approximate large and small amplitudes at the same time it may be advantageous to postulate two distributed elements. This is shown in Figure 3.17 (b).

3.6 Mirror Method

As shown before, the Masing model is not completely suitable for the description of the bending characteristics of slack wire cables, which is due to the slipping moment h depending on both the position s and the bending shape. The object of the modeling is the

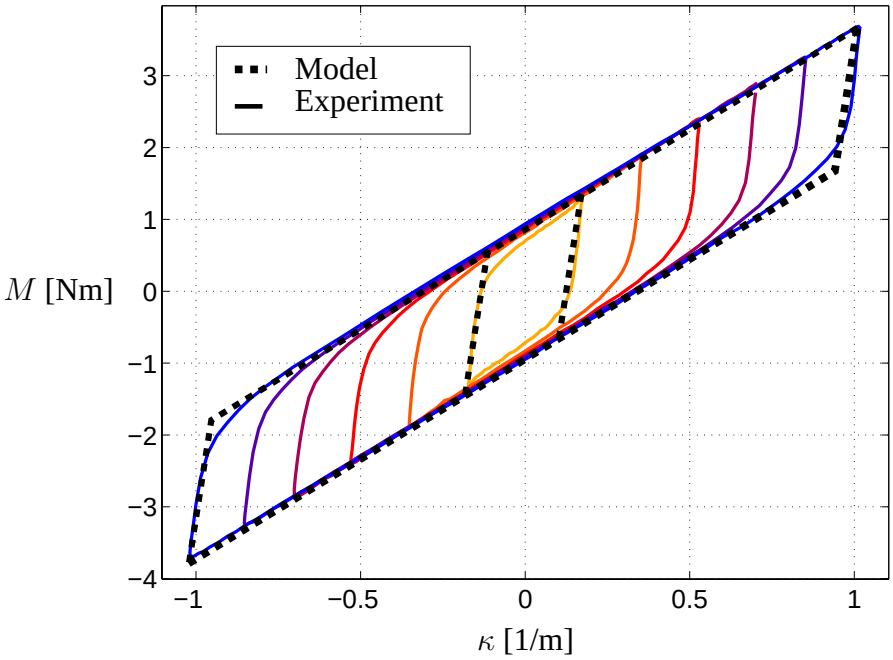

(a) 1 JENKIN element

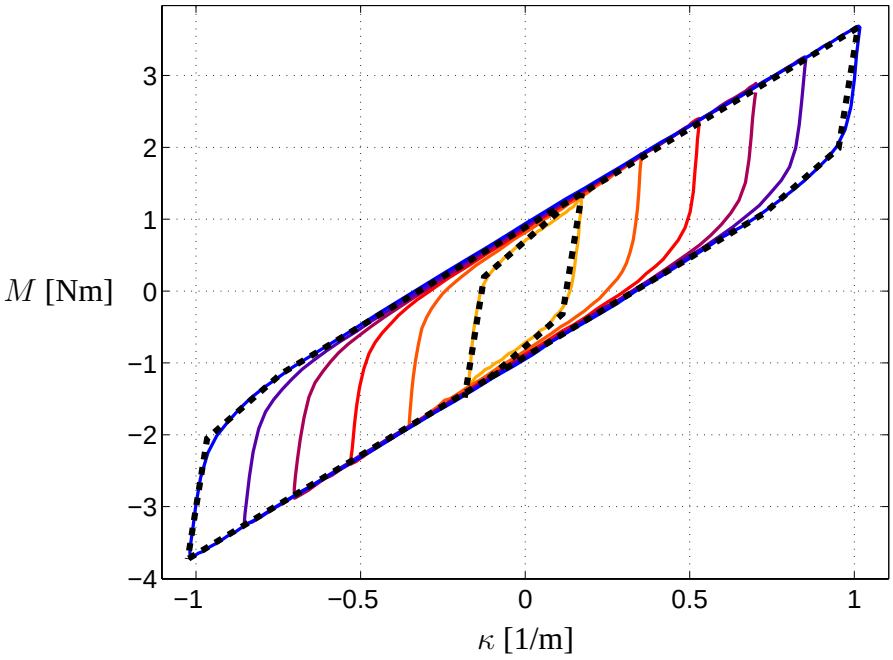

(b) 2 JENKIN elements

Figure 3.17: Local hysteresis cycles for different end displacement amplitudes $\hat{x}$ at the same location $s = 0.025$m (Experiment a)

parameter identification from local measurements taken in a single experiment with specified bending shape and cable length. Using the parameters identified from one bending shape for another bending shape will therefore lead to an error.

In case of a STOCKBRIDGE damper meanly two bending shapes are of interest. Thus it is self-evident to fit the parameters in such a way so that the over-all error of both bending shapes is reduced. Therefore the following method, described in terms of steps, is proposed:

1. Identification of the parameters $h(s)$, $c(s)$, and $ei(s)$ from experiment (a) (see Figure 3.14). The length of the wire cable is l.

2. The parameters identified in step 1 are applied to the cable model of length L in the range $s = [0 \,...\, L/2]$.

3. The model parameters for the range $s = [L/2 \,...\, L]$ are obtained via *mirroring* the parameters from range $s = [0 \,...\, L/2]$ (see Figure 3.18).

Due to symmetry and homogeneity of the wire cable it is reasonable to apply such a procedure further on called *mirror method*. But since the symmetry does not hold for the slipping moment $h(s)$ an error appears. A comparison between the slipping moments h of the mirror method and the actual parameters is shown for each experiment in Figures 3.19 and 3.20. In case of experiment (a) an error appears for h in the range $s > L/2$ (see Figure 3.19) which will only have a small influence on the global behavior of the cable because the bending moment is quite small. In case of experiment (b), astonishingly[1], nearly no error appears in the range $s > L/2$, whereas an error appears in the range $s < L/2$ having a small influence only on the global behavior due to the relative small bending moment (see Figure 3.20). Because the the over-all error of both bending shapes is smaller than in case of using the parameters of experiment (a) only it is advisable to use this method. Therefore we will use it in Chapter 4 for the determination of the global cable behavior.

Finally we have a look at the local hysteresis cycles. Good agreement exists between the hysteretic response predicted by the model with a single distributed JENKIN element and that obtained experimentally (see Figures 3.21 to 3.24). Both curves show the significant change in bending stiffness. The physical model has two different bending stiffnesses, EI and $EI + c$, which correspond to the cases of total wire stick and slip, respectively. The *stiction moment,* h, of the JENKIN element corresponds to the hysteretic moment at which

[1] This fact seems to be worth to be examined more closely in further examinations of the damper cable.

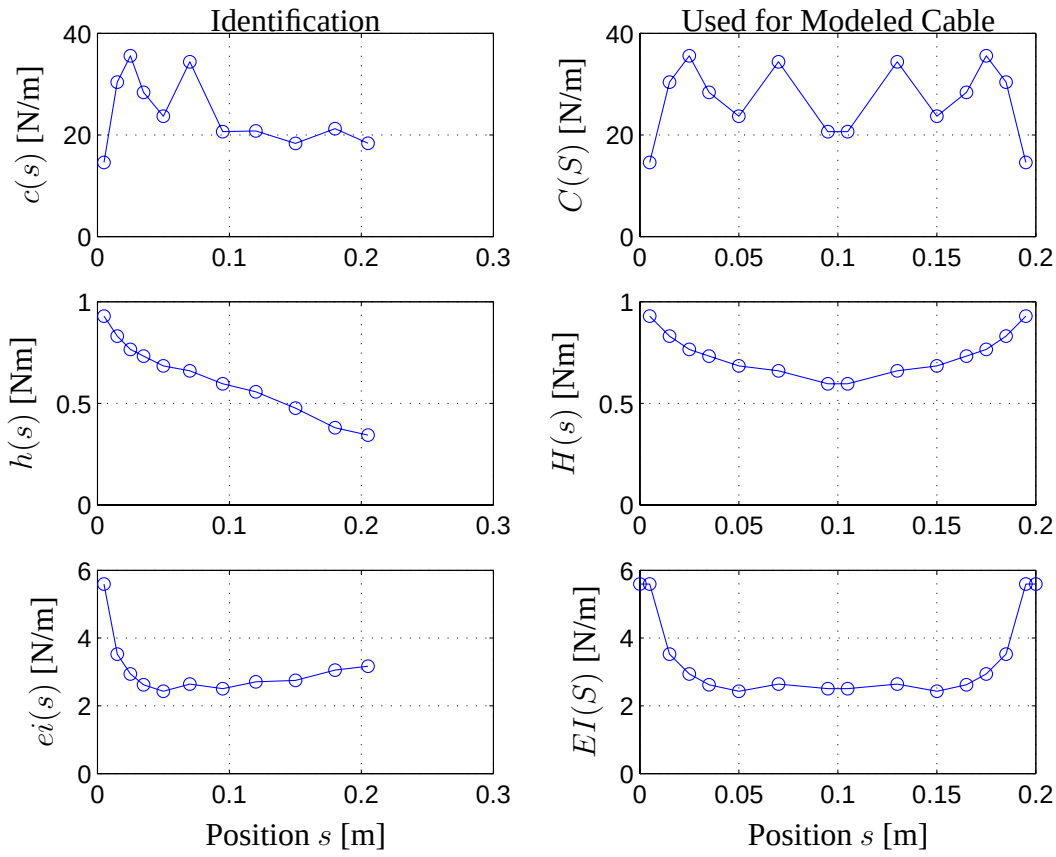

Figure 3.18: Mirror method

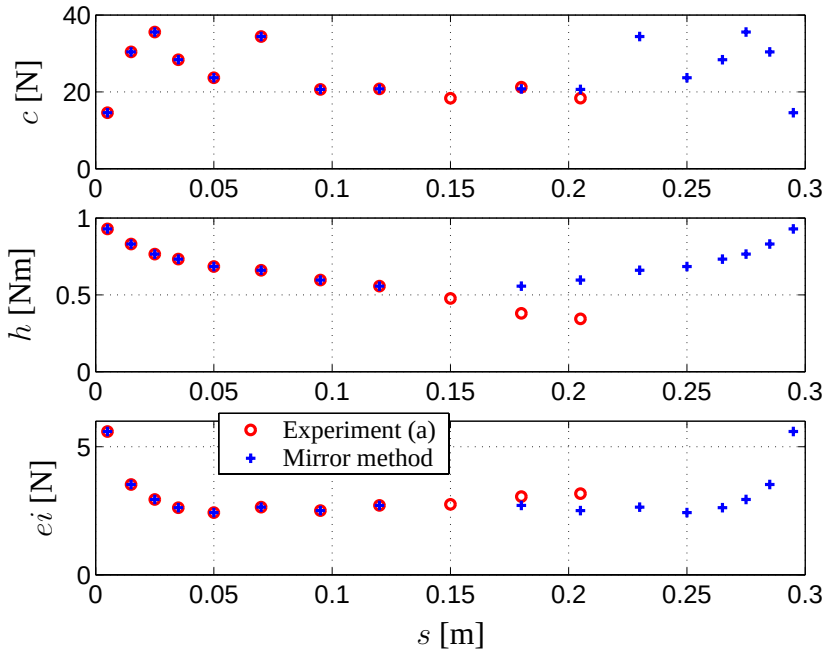

Figure 3.19: Mirror method (experiment a)

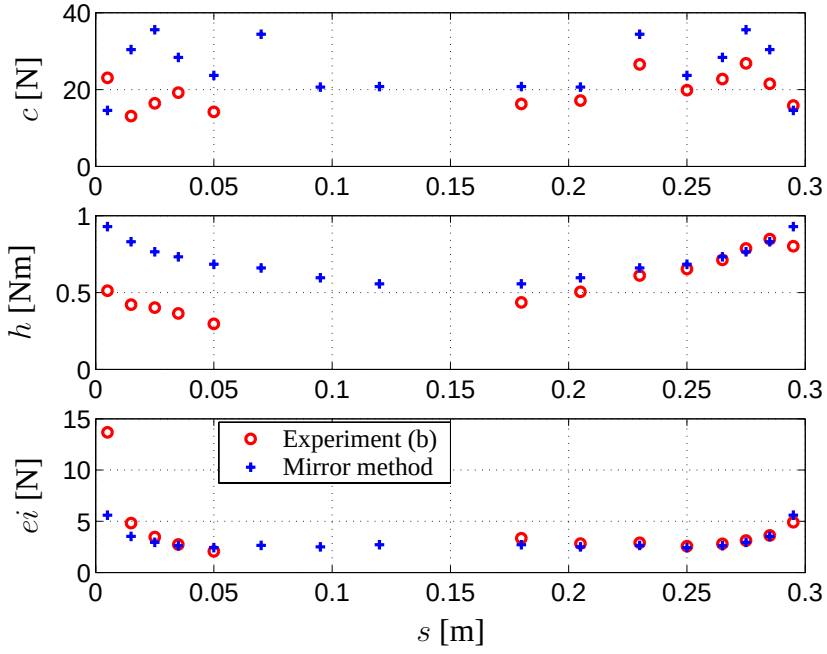

Figure 3.20: Mirror method (experiment b)

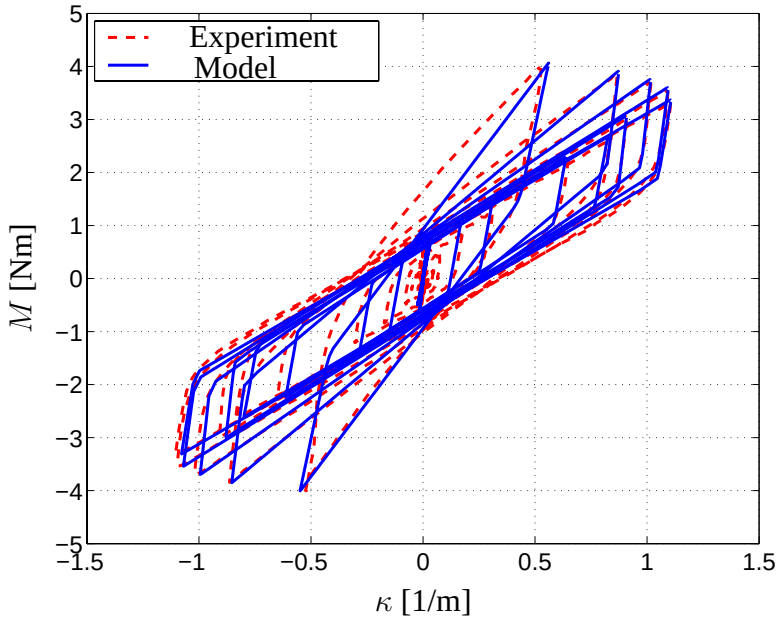

Figure 3.21: Hysteresis cycles of the local Jenkin elements compared to the experimental results for experiment (a)

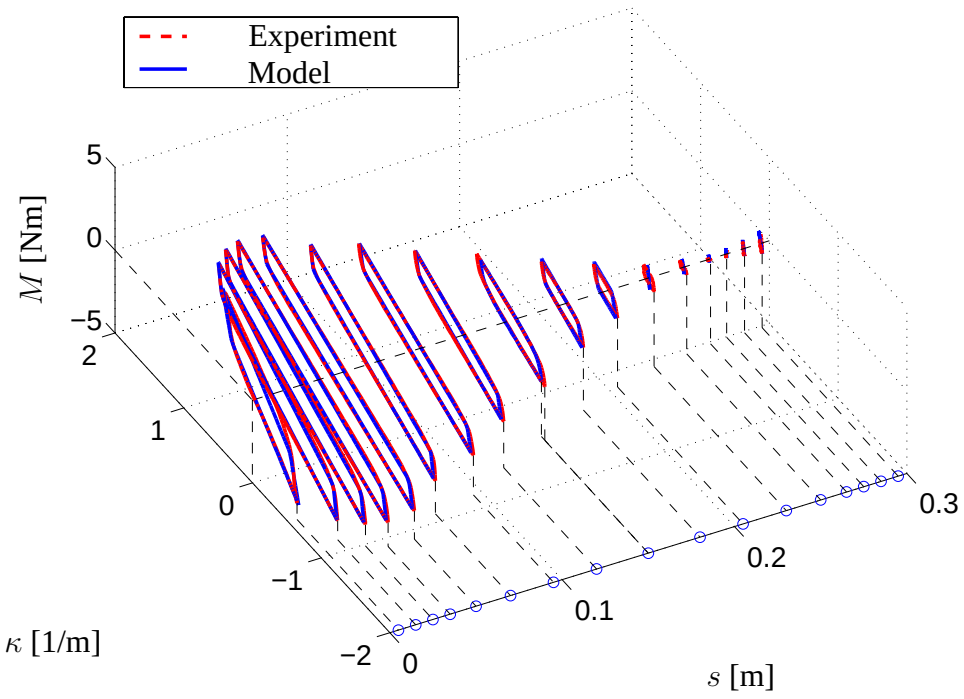

Figure 3.22: Hysteresis cycles of the local Jenkin elements compared to the experimental results for experiment (a)

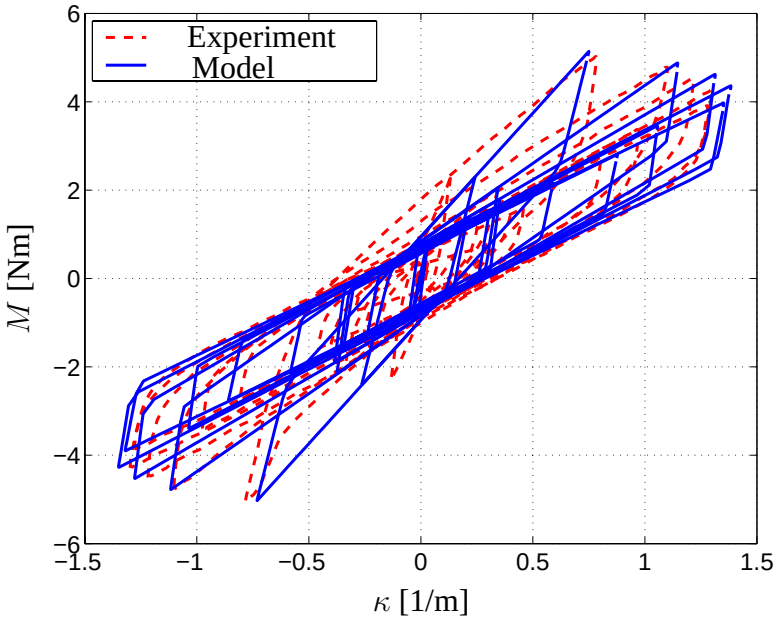

Figure 3.23: Hysteresis cycles of the local Jenkin elements compared to the experimental results for experiment (b)

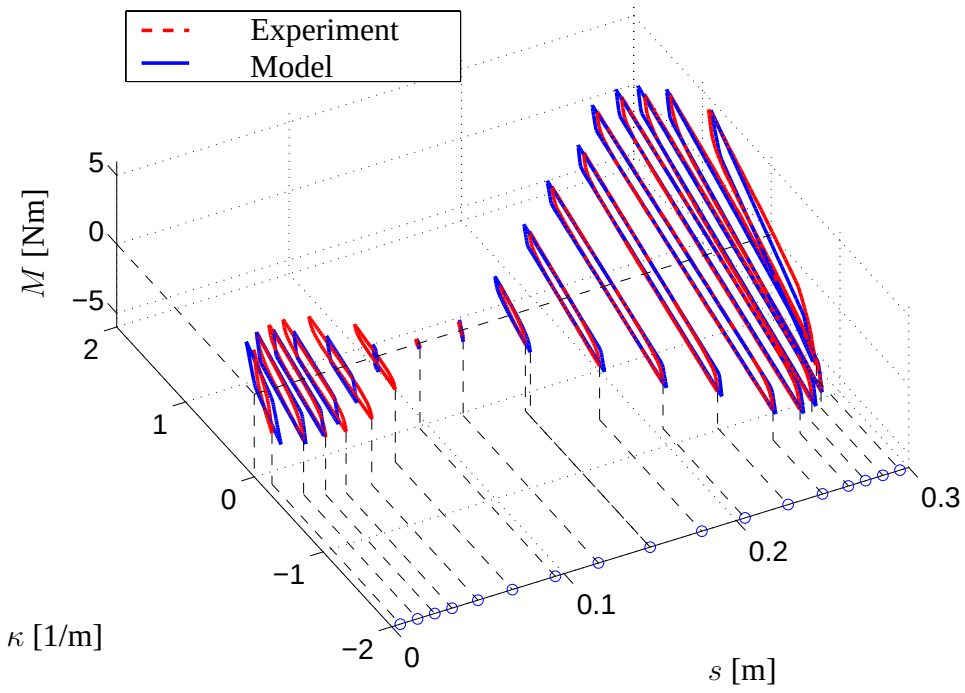

Figure 3.24: Hysteresis cycles of the local Jenkin elements compared to the experimental results for experiment (b)

the wires start slipping. In the case of a real damper cable, the transition between sticking and slipping is a continuous process.

3.7 Modified MASING Model

In the section 3.5 we found that the local MASING model leads to a slipping moment $h(s)$ depending on the bending shape as well as on the position s. In the local moment-curvature relationship via (3.14) the term $\operatorname{sign}(H^2 - h^2)$ represents the slip condition:

$$\dot{H}(s,t) = c(s)\,\dot{\kappa}(s,t)\,\frac{1}{2}\left[1 - \underbrace{\operatorname{sign}(H^2 - h(s)^2)}_{\text{slip condition}} - \operatorname{sign}(\dot{\kappa}\,H)\left(1 + \underbrace{\operatorname{sign}(H^2 - h^2)}_{\text{slip condition}}\right)\right] . \tag{3.17}$$

This equation describes a *bilinear* model with two bending stiffnesses. From the experiments we found that the cable still behaves approximately as such a bilinear model described by (3.17), but the slip condition can no longer be described by COULOMB's friction law.[2] Thus, a generalization of equation (3.17) could possibly be of the type

$$\dot{H}(s,t) = c(s)\,\dot{\kappa}(s,t)\,\frac{1}{2}\left[1 - \text{sign}(?) - \operatorname{sign}(\dot{\kappa}\,H)\,(1 + \text{sign}(?))\right] , \tag{3.18}$$

where the slip condition

$$\text{slip=sign}(?) \tag{3.19}$$

may depend on several quantities. For the MASING model with $H = M - ei\,\kappa$ the slip condition is a function of bending moment M and curvature κ, i.e.:

$$\text{slip} = \text{sign}(M, \kappa) . \tag{3.20}$$

Until now we assumed that slip in the cable was solely due to the bending moment. However, the influence of the shear stresses on slip, due to a shear force, is evident. Thus, in a more general model similar to a TIMOSHENKO beam, both the bending moment $M(s,t)$ and the curvature $\kappa(s,t)$ as well as the shear force $Q(s,t)$ and the slope $w(s,t)' = \partial w/\partial s$ could be taken into consideration, i.e.:

$$\text{slip} = \text{sign}(M, \kappa, Q, w') . \tag{3.21}$$

[2] In between the single wires COULOMB's law is still valid.

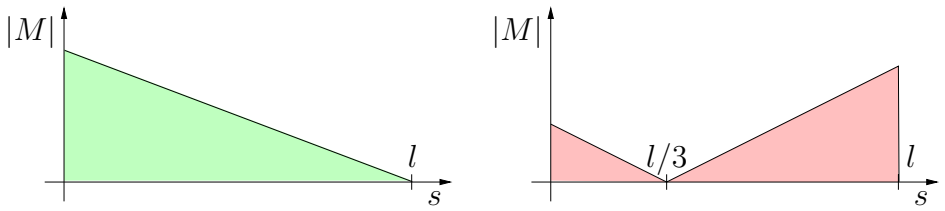

(a) Experiment a (b) Experiment b

Figure 3.25: Absolute values of the bending moments.

Unfortunately, this function is unknown, but the experimental data can be used as a first step towards finding the relation. As stated before, the slipping moment $h(s)$ depends on the shape of the deformation via $Q(s,t)$ and $M(s,t)$ and thus we write

$$h(s,t) = h(M(s,t), Q(s,t)) \; . \tag{3.22}$$

Substituting into equation (3.17) gives

$$\begin{aligned} \dot{H}(s,t) &= c(s)\,\dot{\kappa}(s,t)\,\frac{1}{2}\left[1 - \mathrm{sign}(H^2 - h(M(s,t),Q(s,t))^2) - \right. && (3.23) \\ &\quad \left. -\mathrm{sign}(\dot{\kappa}\,H)\left(1 + \mathrm{sign}(H^2 - h(M,Q)^2)\right)\right] \; . && (3.24) \end{aligned}$$

This equation should hold for both, different displacement amplitudes as well as for different locations along the cable.

First the location dependency for a constant displacement amplitude is considered. Comparing $h(s,t)$ from Figure 3.15 with absolute values of the bending moment $|M(s,t)|$ in Figure 3.25 it can be assumed that the stiction moment $h(s,t)$ is a piecewise linear function of $|M(s,t)|$. In this case the shear force $Q(s,t)$ does not result in a change in the value of h since it is constant throughout the whole cable, thus $h(s,t) = h_0 + k\;|M(s,t)|$. In order to determine the validity of the proposed formula for various lateral displacement amplitudes (respectively bending moment amplitudes) Figure 3.12 (a) is considered. It must be noted that for this case (various displacements), the bending moment $M(s,t)$ at a given location varies while $h(s,t)$ is constant (with respect to s). This is no contradiction since we still have to take $Q(s,t)$ into account. For a given setup, a or b, $|M(s,t)|\,/Q(s,t)$ is constant for all hysteresis cycles. Thus, $k = k_0/Q(s,t)$ must hold and finally

$$h(s,t) = h_0 + k_0\,\frac{|M(s,t)|}{Q(s,t)} \tag{3.25}$$

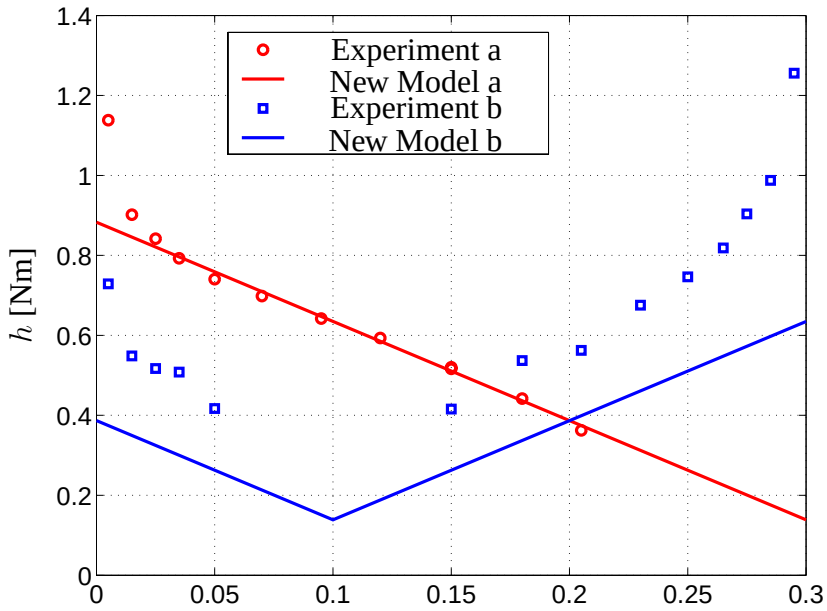

Figure 3.26: Application of the new model

is obtained.

In order to test the validity of the modified model the parameters h_0 and k_0 were identified from experiment (a) and applied to the bending shape of experiment (b) described by $Q(s,t)$ and $M(s,t)$. For the identification the region near to the clamp was excluded. It can be seen from Figure 3.26 that also in case of experiment (b) the slope of the lines is nearly the same, but the values of the model are too small. Thus, using such such approach does not make sense at the moment, since the error arising will be to large. Therefore we will not use it in Chapter 4 for the determination of the global cable behavior. Anyway, this model may be a useful pre-stage in describing the bending characteristics of a slack wire cable completely, which will not be possible without taking the shear force into account.

Chapter 4

Global Behavior of the Cable

4.1 Relation between Loads and Deformation

In Chapter 3 the "local" relation between bending moment and curvature at a given position of the cable was considered but the final object is the accurate description of the "global" behavior of the wire cable for all bending shapes. Here "global" means the relation between the displacement or rotation at any position of the wire cable due to forces or torques torques acting on the cable. In Figure 4.1 the problem is illustrated for the case of a wire cable attached to a STOCKBRIDGE damper. The goal is to determine the displacement $x(t) := w(l,t)$ and the rotation $\varphi(t) := \partial w(l,t)/\partial s$ at the right end of the wire cable ($s = l$) due to the torque $T(t)$ and force $F(t)$ measured at the left end of the cable ($s = 0$). The cable is clamped at the left end, i.e. $w(0,t) = 0,\ \partial w(0,t)/\partial s = 0,\ \forall t$.

Locally the problem is described by equations (3.13) and (3.14) or (3.15). Since we do not know the curvature $\kappa(s,t)$ we insert (3.13) into (3.14) or (3.15) and obtain

$$\begin{aligned} \dot{H}_i(s,t) \;=\; & \frac{c_i(s)}{ei(s)} \left(\dot{M}(s,t) - \sum_{j=1}^{m} \dot{H}_j \right) \frac{1}{2} \left[1 - \operatorname{sign}(H_i^2 - h_i(s)^2) - \right. \\ & \left. - \operatorname{sign}\left(\frac{1}{ei} \left(\dot{M} - \sum_{j=1}^{m} \dot{H}_j \right) H_i \right) \left(1 + \operatorname{sign}(H_i^2 - {h_i}^2) \right) \right] , \end{aligned} \tag{4.1}$$

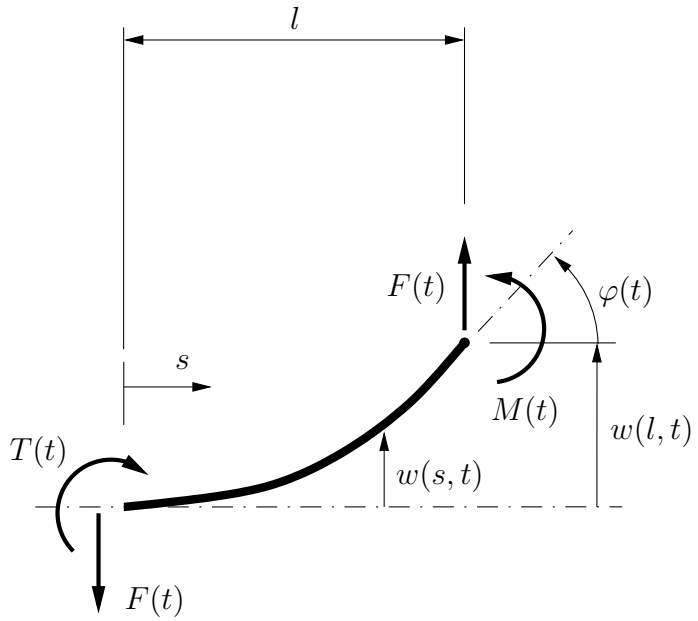

Figure 4.1: Loads and displacements at the deformed damper cable

or

$$\dot{H}_i(s,t) = \frac{c_i(s)}{ei(s)} \left(\dot{M}(s,t) - \sum_{j=1}^{m} \dot{H}_j \right) \left[1 - \frac{1}{2} \left(1 + \operatorname{sign}(\frac{1}{ei} \left(\dot{M} - \sum_{j=1}^{m} \dot{H}_j \right) H_i) \right) \left| \frac{H_i}{h_i(s)} \right|^m \right] , \tag{4.2}$$

respectively.

The displacement $w(l,t)$ and the rotation $w'(l,t)$ are obtained from the curvature via integration of (3.13) . With $w'' = \kappa$ one has

$$w''(s,t) = \frac{1}{ei(s)} \left(M(s,t) - \sum_{j=1}^{m} H_j(s,t) \right) . \tag{4.3}$$

Integration gives the rotation

$$w'(s,t) = \int \frac{1}{ei(s)} \left(M(s,t) - \sum_{j=1}^{m} H_j(s,t) \right) \mathrm{d}s + C_1 , \tag{4.4}$$

and the displacement

$$w(s,t) = \int\int \frac{1}{ei(s)} \left(M(s,t) - \sum_{j=1}^{m} H_j(s,t) \right) \mathrm{d}s \, \mathrm{d}s + C_1 \, s + C_2 \tag{4.5}$$

of the beam. The boundary conditions yield

$$w'(0,t) = 0 \implies C_1 = 0 \, , \tag{4.6}$$

$$w(0,t) = 0 \implies C_2 = 0 \, . \tag{4.7}$$

Thus the displacement and the rotation at $s = l$ can be written as

$$w'(l,t) = \int_0^l \frac{1}{ei(s)} \, M(s,t) \, \mathrm{d}s - \int_0^l \frac{1}{ei(s)} \sum_{j=1}^{m} H_j(s,t) \, \mathrm{d}s \, , \tag{4.8}$$

$$w(l,t) = \int_0^l \int_0^s \frac{1}{ei(\overline{s})} \, M(\overline{s},t) \, \mathrm{d}\overline{s} \, \mathrm{d}s - \int_0^l \int_0^s \frac{1}{ei(\overline{s})} \sum_{j=1}^{m} H_j(\overline{s},t) \, \mathrm{d}\overline{s} \, \mathrm{d}s \, . \tag{4.9}$$

The bending moment $M(s,t)$ for the given loads (Figure 4.1) is

$$M(s,t) = T(t) - F(t) \, s \, . \tag{4.10}$$

This yields

$$\varphi(t) = \int_0^l \frac{1}{ei(s)} \, [T(t) - F(t) \, s] \, \mathrm{d}s - \int_0^l \frac{1}{ei(s)} \sum_{j=1}^{m} H_j(s,t) \, \mathrm{d}s \, , \tag{4.11}$$

$$x(t) = \int_0^l \int_0^s \frac{1}{ei(\overline{s})} \, [T(t) - F(t) \, \overline{s}] \, \mathrm{d}\overline{s} \, \mathrm{d}s - \int_0^l \int_0^s \frac{1}{ei(\overline{s})} \sum_{j=1}^{m} H_j(\overline{s},t) \, \mathrm{d}\overline{s} \, \mathrm{d}s \tag{4.12}$$

or

$$\varphi(t) = T(t) \int_0^l \frac{1}{ei(s)} \, \mathrm{d}s - F(t) \int_0^l \frac{1}{ei(s)} \, s \, \mathrm{d}s - \int_0^l \frac{1}{ei(s)} \sum_{j=1}^{m} H_j(s,t) \, \mathrm{d}s \, , \tag{4.13}$$

$$\begin{aligned} x(t) = {} & T(t) \int_0^l \int_0^s \frac{1}{ei(\overline{s})} \, \mathrm{d}\overline{s} \, \mathrm{d}s - F(t) \int_0^l \int_0^s \frac{1}{ei(\overline{s})} \, \overline{s} \, \mathrm{d}\overline{s} \, \mathrm{d}s - \\ & - \int_0^l \int_0^s \frac{1}{ei(\overline{s})} \sum_{j=1}^{m} H_j(\overline{s},t) \, \mathrm{d}\overline{s} \, \mathrm{d}s \, . \end{aligned} \tag{4.14}$$

with $\varphi(t) = w'(l,t)$ and $x = w(l,t)$. With the abbreviations

$$a = \int_0^l \frac{1}{ei(s)}\,\mathrm{d}s\,, \quad b = -\int_0^l \frac{1}{ei(s)}\,s\,\mathrm{d}s\,, \quad c = -\int_0^l \frac{1}{ei(s)}\sum_{j=1}^{m} H_j(s,t)\,\mathrm{d}s\,,$$

$$d = \int_0^l\int_0^s \frac{1}{ei(\overline{s})}\,\mathrm{d}\overline{s}\,\mathrm{d}\overline{s}\,, \quad e = -\int_0^l\int_0^s \frac{1}{ei(\overline{s})}\,\overline{s}\,\mathrm{d}\overline{s}\,\mathrm{d}s\,, \quad f = -\int_0^l\int_0^s \frac{1}{ei(\overline{s})}\sum_{j=1}^{m} H_j(\overline{s},t)\,\mathrm{d}\overline{s}\,\mathrm{d}s$$

the above equations yield

$$\varphi = T\,a + F\,b + c \tag{4.15}$$

$$x = T\,d + F\,e + f \tag{4.16}$$

or in matrix form

$$\begin{bmatrix} \varphi \\ x \end{bmatrix} = \begin{bmatrix} a & b \\ d & e \end{bmatrix} \begin{bmatrix} T \\ F \end{bmatrix} + \begin{bmatrix} c \\ f \end{bmatrix}\,. \tag{4.17}$$

Solving this linear system for the load vector $\mathbf{f} = [T, F]^T$ we find

$$\begin{bmatrix} T \\ F \end{bmatrix} = \frac{1}{-d\,b + a\,e} \begin{bmatrix} e & -b \\ -d & a \end{bmatrix} \left(\begin{bmatrix} \varphi \\ x \end{bmatrix} - \begin{bmatrix} c \\ f \end{bmatrix} \right)\,. \tag{4.18}$$

From this general general relation the results will be given for the two special cases corresponding to the two experiments (a) and (b) in the next section.

4.1.1 Experiment (a)

In experiment (a) only a force is applied at the right end of the wire cable. $M = 0$ yields $T = F\,l$ and (4.17) gives

$$x(t) = (d\,l + e)\;F(t) + f\,, \tag{4.19}$$

$$x(t) = \int_0^l\int_0^s \frac{1}{ei(\overline{s})}\,F(t)\;(l - \overline{s})\;\mathrm{d}\overline{s}\,\mathrm{d}s - \int_0^l\int_0^s \frac{1}{ei(\overline{s})}\sum_{j=1}^{m} H_j(\overline{s},t)\,\mathrm{d}\overline{s}\,\mathrm{d}s\,. \tag{4.20}$$

Solving for the force gives

$$F(t) = \frac{1}{d\,l+e}\,(x(t)-f)\,, \tag{4.21}$$

$$F(t) = \left(\int_0^l\int_0^s \frac{l-\overline{s}}{ei(\overline{s})}\,\mathrm{d}\overline{s}\,\mathrm{d}s\right)^{-1}\left(x(t)+\int_0^l\int_0^s \frac{1}{ei(\overline{s})}\sum_{j=1}^{m} H_j(\overline{s},t)\,\mathrm{d}\overline{s}\,\mathrm{d}s\right) \tag{4.22}$$

4.1.2 Experiment (b)

In experiment (b) only a rotation is possible at the right end of the cable. With $x = 0$ we obtain from 4.18

$$F(t) = \frac{-d}{-d\,b+a\,e}\,\varphi(t) + \frac{c\,d-a\,f}{-d\,b+a\,e}\,, \tag{4.23}$$

$$T(t) = \frac{e}{-d\,b+a\,e}\,\varphi(t) + \frac{c\,e+b\,f}{-d\,b+a\,e}\,, \tag{4.24}$$

and finally with $M = T - Fl$

$$M(t) = \frac{e+d\,l}{-d\,b+a\,e}\,\varphi(t) + \frac{c\,e+b\,f+(a\,f-c\,d)\,l}{-d\,b+a\,e}\,. \tag{4.25}$$

4.1.3 Numerical Determination of the Global Hysteresis Cycles

Given $x(t)$ and $\varphi(t)$ and the initial conditions for the $H_i(s,t)$ and $w''(s,t)$, $\dot{w}''(s,t)$, the determination of $w(s,t)$ is a nontrivial problem, which can only be solved numerically. For this purpose we utilize the time derivatives of (4.18)

$$\begin{bmatrix} \dot{T} \\ \dot{F} \end{bmatrix} = \frac{1}{-d\,b+a\,e}\begin{bmatrix} e & -b \\ -d & a \end{bmatrix}\left(\begin{bmatrix} \dot{\varphi} \\ \dot{x} \end{bmatrix} - \begin{bmatrix} \dot{c} \\ \dot{f} \end{bmatrix}\right)\,. \tag{4.26}$$

and (4.2):

$$\dot{H}_i(s,t) = \frac{c_i(s)}{ei(s)}\left(\dot{M}(s,t) - \sum_{j=1}^{m}\dot{H}_j(s,t)\right) \left[1-\frac{1}{2}\left(1+\mathrm{sign}(\frac{1}{ei(s)}\left(\dot{M}(s,t)-\sum_{j=1}^{m}\dot{H}_j(s,t)\right)\,H_i(s,t))\right)\left|\frac{H_i(s,t)}{h_i(s)}\right|^m\right]\,. \tag{4.27}$$

Numerical solutions have been obtained by discretizing the damper cable with respect to s. For this purpose we divide the cable length l into n segments:

$$H_{ip}(t) = H_i(s_p, t), \qquad p = 1, \ldots, n \; . \tag{4.28}$$

The hysteretic moment at the JENKIN element (i, p) is given by

$$\begin{aligned} \dot{H}_{ip} &= \frac{c_{ip}}{ei_p} \left(\dot{M}_p - \sum_{j=1}^{m} \dot{H}_{jp} \right) \\ &\quad \left[1 - \frac{1}{2} \left(1 + \text{sign}(\frac{1}{ei_p} \left(\dot{M}_p - \sum_{j=1}^{m} \dot{H}_{jp} \right) H_{ip}) \right) \left| \frac{H_{ip}}{h_{ip}} \right|^m \right] \end{aligned} \tag{4.29}$$

instead of (4.27), with the discretized parameters ei_p, c_{ip}, h_{ip}, and the external bending moment,

$$\dot{M}_p = \dot{T} - \dot{F}\, s_p \; . \tag{4.30}$$

The fact that $\dot{H}_{ip}$ occurs at both sides of (4.29) leads to numerical problems which will be discussed in Section 4.2.5.1. PLAGGE [29] solved the problem using a variational method (applying the principle of virtual work), a different method will be used here.

4.1.4 Comparing the Model to the Experiments

In this section, numerically obtained global hysteresis cycles of the model are compared to those obtained from the experiments. The parameters were identified from experiment (a) with a displacement amplitude of $\hat{w}(l) = 0.03$m applying the mirror method (Section 3.6). In Figure 4.2 the response displacement x is shown for a given load. The model works quite well, except for small amplitudes, where the model is too stiff. From Figure 4.3 it can be seen that our approach also gives good results for experiment (b) (with data identified from experiment (a)), but the stiffness increases too strongly in the model for small amplitudes.

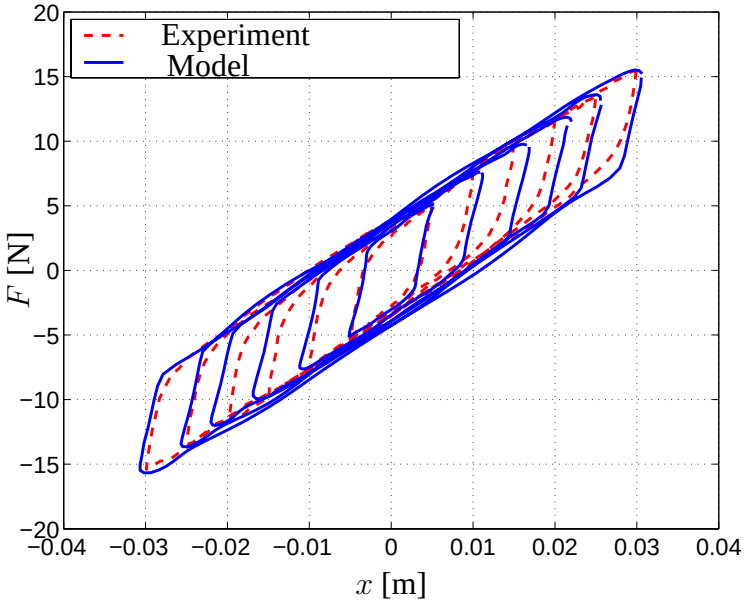

Figure 4.2: Global hysteresis cycles for experiment (a)

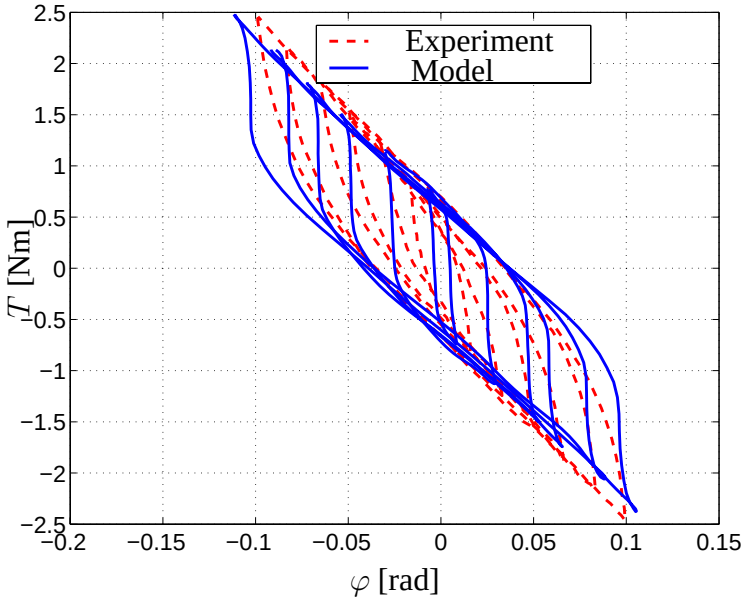

Figure 4.3: Global hysteresis cycles for experiment (b)

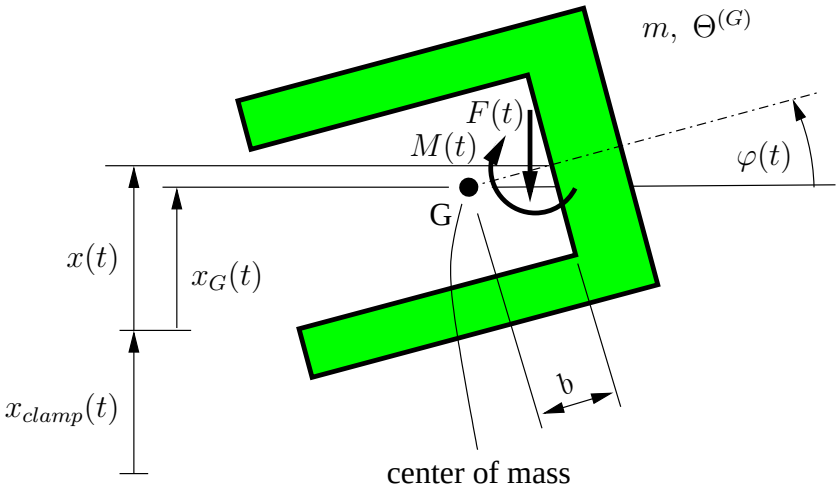

Figure 4.4: "Inertial mass" of a STOCKBRIDGE damper

4.2 STOCKBRIDGE Damper

4.2.1 Modeling the STOCKBRIDGE Damper

The damper cable model will now be applied to a STOCKBRIDGE damper. To this end the equations of motion of the "inertial masses" are needed. The equations of motion for each of the inertial masses (Figure 4.4) can be written as

$$\mathbf{M}\,\ddot{\mathbf{q}} + \mathbf{F}\,\mathbf{f} = -\mathbf{M}\,\ddot{\mathbf{q}}_{clamp} \tag{4.31}$$

if the kinematics is linearized, where

$$\mathbf{q} = \begin{bmatrix} x_G \\ \varphi \end{bmatrix}, \quad \mathbf{q}_{clamp} = \begin{bmatrix} x_{clamp} \\ 0 \end{bmatrix}, \quad \mathbf{f} = \begin{bmatrix} F \\ M \end{bmatrix}, \quad \mathbf{M} = \begin{bmatrix} m & 0 \\ 0 & \Theta^{(G)} \end{bmatrix}, \quad \mathbf{F} = \begin{bmatrix} 1 & 0 \\ b & 1 \end{bmatrix}.$$

The relation between $x_G(t)$, the clamp motion $x_{clamp}(t)$ and the deformation of the damper cable is

$$x_G(t) = x_{clamp}(t) + x(l,t) - b\,x'(l,t)\,. \tag{4.32}$$

A complete simulation model for the STOCKBRIDGE damper can now be obtained using equations (4.31), (4.2), and (4.18). The differential equations can be written as a first order system of the form

$$\dot{\mathbf{z}} = \mathbf{f}(\mathbf{z}, \dot{\mathbf{z}}, t)\,, \tag{4.33}$$

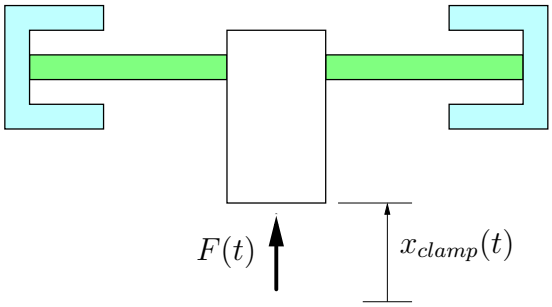

Figure 4.5: Force and displacement at a STOCKBRIDGE damper.

where $\dot{\mathbf{z}}$ stands on both sides of the equation.

Usually the motion of conductor cables is computed by using an energy balancing method [10, 11]. In order to describe the influence of the STOCKBRIDGE damper to a tensioned conductor cable, the mechanical impedance at the clamp is commonly used. For a linear system the impedance is given by

$$\underline{Z} = \frac{\hat{\underline{F}}}{\dot{\underline{x}}} \,, \tag{4.34}$$

where $\underline{\dot{x}}(t) = \dot{\underline{x}}\, e^{j\Omega t}$ is the harmonic velocity and $\underline{F}(t) = \hat{\underline{F}}\, e^{j\Omega t}$ is the harmonic force at the clamp, both harmonic where all quantities being complex (see Figure 4.5). In a somewhat more general way the impedance can be defined by the quotient of the FOURIER transforms of the two signals $F(t)$ and $\dot{x}(t)$. The damper impedance is routinely obtained from experiments in vibration laboratories in industry.

4.2.2 Impedance of a Nonlinear System

Strictly speaking, the impedance is defined for linear systems only. The STOCKBRIDGE damper being a nonlinear system, a harmonic velocity input will lead to a periodic force output which can be decomposed into the following FOURIER series

$$\underline{F}(t) = \hat{\underline{F}}_0 + \hat{\underline{F}}_1 e^{j\Omega t} + \hat{\underline{F}}_2 e^{j2\Omega t} + \dots \,, \tag{4.35}$$

where

$$\hat{\underline{F}}_k = \frac{1}{T} \int_0^T \underline{F}\,(t)\;\; e^{-jk\Omega t} dt \,.$$

We terminate the series after the first harmonic and further we assume $\underline{\hat{F}}_0 = 0$. Thus we write

$$\underline{F}(t) = \underline{\hat{F}}_1 e^{j\Omega t} \ . \tag{4.36}$$

The velocity is given as

$$\underline{\dot{x}}(t) = \underline{\dot{x}}\, e^{j\Omega t} \ , \tag{4.37}$$

where $\underline{\dot{x}} = \dot{x}$ is assumed to be real. We can now define the impedance by

$$\underline{Z} = \frac{\underline{\hat{F}}_1}{\underline{\dot{x}}} \ . \tag{4.38}$$

The real part is given by

$$\mathrm{Re}(\underline{Z}) = \mathrm{Re}\left(\frac{\underline{\hat{F}}_1}{\dot{x}}\right) = \frac{1}{\dot{x}}\,\mathrm{Re}(\underline{\hat{F}}_1) = \frac{1}{\dot{x}}\,\mathrm{Re}\left(\frac{1}{T}\int_0^T \underline{F}\,(t)\ e^{-j\Omega t} dt\right) \tag{4.39}$$

and the imaginary part by

$$\mathrm{Im}(\underline{Z}) = \mathrm{Im}\left(\frac{\underline{\hat{F}}_1}{\dot{x}}\right) = \frac{1}{\dot{x}}\,\mathrm{Im}(\underline{\hat{F}}_1) = \frac{1}{\dot{x}}\,\mathrm{Im}\left(\frac{1}{T}\int_0^T \underline{F}\,(t)\ e^{-j\Omega t} dt\right) \ . \tag{4.40}$$

The phase difference γ_1 between the velocity and the force is

$$\gamma_1 = \arg(\underline{Z}) = \arctan\left(-\frac{\mathrm{Im}(\underline{Z})}{\mathrm{Re}(\underline{Z})}\right) = \arctan\left(-\frac{\mathrm{Im}(\underline{\hat{F}}_1)}{\mathrm{Re}(\underline{\hat{F}}_1)}\right) \ . \tag{4.41}$$

In contrast to linear systems the impedance of a nonlinear system depends not only on the frequency but also on the amplitude of the harmonic input signal.

4.2.3 Considerations about the Excitation

STOCKBRIDGE dampers are applied to overhead transmission lines (see Figure 4.6) in order to damp wind-excited vibrations forced by the vortices shedding from the conductor. The stability of a vortex street shed by a fixed cylinder in steady transverse was studied by VON KÁRMÁN [15]. The phenomenon in an oscillating conductor is more complicated. The alternating shedding of the vortices in first approximation induces a harmonic force

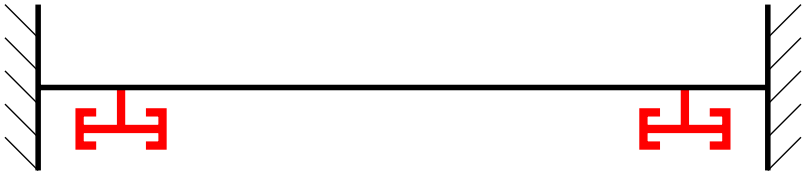

Figure 4.6: Tensioned Cable with STOCKBRIDGE dampers (schematic)

perpendicular to the wind direction with frequency

$$f = \frac{St}{d}\, v_{wind}\,,$$

where d is the diameter of the conductor, St the STROUHAL *number* [33], and v_{wind} the wind speed. For the REYNOLDS numbers of the wind under consideration, the STROUHAL number is approximately constant:

$$St \approx 0.22\,.$$

The vortex excited conductor performs harmonic oscillations of the same frequency, perpendicular to the direction of wind. Since the span lengths may be large (up to a several hundred meters) the conductor's eigenfrequencies are closely spaced. Thus, it may be assumed that for any excitation frequency the cable is always in resonance and damping is needed. A more detailed description of the conductor motions and the underlying mechanisms inducing *lock-in* can be found e.g. in [6].

As it is usually done in studying the conductor vibrations only harmonic oscillations of the conductor and of damper clamp with constant frequency and amplitude

$$\underline{x}(t) = \underline{x}\, e^{j\Omega t} \tag{4.42}$$

will be considered, where $\Omega = 2\pi\, f$ is the circular frequency, transient phenomena being neglected.

4.2.4 Solving the System of Differential Equations

The system of differential equations obtained for a damper is strongly nonlinear. It is not possible to linearize the equations for small amplitudes due to their hysteretic character. Numerical methods are therefore used for the solution. Due to the nonlinearity of the

system it is also not possible to find solutions in the frequency domain using e.g. FOURIER transforms.

Although an extensive literature is devoted to the dynamic analysis of the response of non-linear holonomic systems under sinusoidal excitation (a survey can be found in [9, 26]). Only few papers deal with the solution technique for hysteretic oscillators. CAPECCHI studied the periodic response and stability of single degree of freedom hysteretic oscillators [3]. In [4] also a 2DOF-system was considered. In the present case the system has many degrees of freedom and is described by a system of differential equation of the form

$$\begin{aligned} \dot{f} &= \mathrm{h}\left(f,\ \dot{x},\ \mathrm{sign}\left(\dot{x}\right), \mathbf{k}\right) , \\ \dot{\mathbf{k}} &= \mathbf{K}\left(f,\ \dot{x},\ \mathrm{sign}\left(\dot{x}\right), \mathbf{k}\right) , \end{aligned}$$

where $\mathbf{k}$ is the vector of the internal variables. For such a model (e.g. MASING model) KOLSCH gave an extensive discussion of possible solution methods [17]. Here we primarily will utilize the methods proposed by him.

4.2.5 Periodic Solutions for the Non-Homogeneous System

Here we want to find periodic solutions for the non-homogeneous system. We assume that the displacement of the clamp of the STOCKBRIDGE damper is harmonic [1] with circular frequency Ω:

$$\mathbf{q}_{clamp}(t) = \begin{bmatrix} x_{clamp}(t) \\ 0 \end{bmatrix} = \begin{bmatrix} x_{clamp}\sin(\Omega\, t) \\ 0 \end{bmatrix} . \tag{4.43}$$

Since the STOCKBRIDGE damper is a nonlinear system, we can not be sure that there is a steady state response of the same frequency in general. For example there may be sub-harmonic, super-harmonic or chaotic motions of the system. Investigations on real dampers have however shown the existence of responses with the frequency of the excitation. These responses will not be harmonic but periodic. Thus we want to search for periodic responses with the same period as the excitation.

The problem of finding periodic solutions can be formulated as a boundary value problem in time with the constraints

$$\mathbf{z}(t) = \mathbf{z}(t+T) , \tag{4.44}$$

[1] This assumption is not necessary to solve the system.

where **z(t)** is the state vector. Several methods can be applied for solving such problems, e.g.:

- Numerical Integration of the initial value problem for $t \rightarrow \infty$ (until equation (4.44) is fulfilled approximately)
- Shooting method
- GALERKIN's method (see also [3])
- Collocation method

4.2.5.1 Numerical Integration of the Initial Value Problem

One possibility for solving the system of differential equations is the numerical integration of the initial value problem until equation (4.44) is fulfilled with sufficient accuracy. Here we have to take into account the fact that the equations can not be solved for $\dot{H}_{ip}$. Thus $\dot{H}_{ip}$ appears on both sides of the equations and $\dot{H}_{ip}$ can be obtained by iteration only. As the initial value one can take the $\dot{H}_{ip}$ from the preceding time step. Thus at every time step we need not only $\dot{H}_{ip}$ from the preceding time step but also $\dot{H}_{ip}$.

Increasing the number of iterations we might get better solutions. Unfortunately the iteration does not converge for all parameters or converges very slowly only. Difficulties arise in particular for certain ranges of parameters of c (all the other parameters given). This seems to be the result of the properties of equation (4.29). This equation can be interpreted as a mapping, which does not contract for all ranges of the parameters.

Some of the difficulties can be eliminated by rearranging the equation. By doing this one can achieve that the mapping contracts in a different parameter range. Sometimes convergence seems to occur, but then due to the switching of the sign functions suddenly disappears. Convergence is however needed for all positions of the switches. It seems to be useful to rearrange the equation, as we did for the STOCKBRIDGE damper examined in

the laboratory. Here we succeeded by rearranging equation (4.29) as:

$$\dot{H}_{ip} = \tag{4.45}$$
$$\frac{c_{ip}}{e\dot{i}_p}\left\{\dot{M}_p - \sum_{j=1,\,j\neq i}^{m}\dot{H}_{jp}\right\}$$
$$\left[1-\frac{1}{2}\left(1+\text{sign}(\frac{1}{e\dot{i}_p}\left\{\dot{M}_p-\sum_{j=1}^{m}\dot{H}_{jp}\right\}H_{ip})\right)\left|\frac{H_{ip}}{h_{ip}}\right|^k\right]\Bigg/$$
$$\left\{1+\frac{c_{ip}}{e\dot{i}_p}\left[1-\frac{1}{2}\left(1+\text{sign}(\frac{1}{e\dot{i}_p}\left\{\dot{M}_p-\sum_{j=1}^{m}\dot{H}_{jp}\right\}H_{ip})\right)\left|\frac{H_{ip}}{h_{ip}}\right|^k\right]\right\}\ .$$

On account of clearness we rewrite this as

$$\dot{H}_{ip} = \frac{c_{ip}}{e\dot{i}_p}\left\{\dot{M}_p - \sum_{j=1,\,j\neq i}^{m}\dot{H}_{jp}\right\} Switch \Bigg/ \left\{1+\frac{c_{ip}}{e\dot{i}_p}\,Switch\right\} \tag{4.46}$$

where

$$Switch = \left[1-\frac{1}{2}\left(1+\text{sign}(\frac{1}{e\dot{i}_p}\left\{\dot{M}_p-\sum_{j=1}^{m}\dot{H}_{jp}\right\}H_{ip})\right)\left|\frac{H_{ip}}{h_{ip}}\right|^k\right]\ , \tag{4.47}$$
$$\dot{M}_p = \dot{T} + \dot{F}\,s_p\ . \tag{4.48}$$

Another problem occurring for large amplitudes is the oscillation of the hysteretic moment, $H_{ip}(t)$, around the maximum value, h_{ip}. This effect can be reduced by setting

$$H_{ip} = \text{sign}(H_{ip})\,\min(|H_{ip}|\,, h_{ip}) \tag{4.49}$$

at every step of the numerical integration.

4.2.5.2 Shooting Method

The shooting method transforms the boundary value problem into an initial value problem, which has to be solved repeatedly. One tries to choose the initial conditions in such a way that after numerical integration the end conditions are the same as the initial conditions. Mathematically we can formulate this problem as a nonlinear algebraic system of equations for the initial conditions $\mathbf{z}_0$:

$$\mathbf{z}_0 - \mathbf{z}(t+T, \mathbf{z}_0) = 0\ , \tag{4.50}$$

where $\mathbf{z}_0$ is the state vector at the time t. The solution of the algebraic system is done iteratively, for example by a NEWTON method. Several difficulties appeared when we applied this method. On one hand, for certain initial values the numerical integration is possible only with very small step sizes. On the other hand, the iteration often seems to converge very slowly or not at all, so that this method requires much time. Using a multiple shooting method, where the cycle is divided into smaller intervals, for which also the transition conditions have to be satisfied, was not more successful.

4.2.5.3 GALERKIN's Method

Using a shooting method we can theoretically obtain exact solutions within the bounds of the computing precision. This may however require a high computational cost, so that approximate methods were also tested. First we we used GALERKIN's method.

Since we expect periodic solutions, we search for an approximate solution in form of a FOURIER series:

$$\mathbf{z}(t) = \frac{\mathbf{z}_0}{2} + \sum_{m=1}^{M} \mathbf{z}_{cm} \cos(m\Omega t) + \sum_{m=1}^{M} \mathbf{z}_{sm} \sin(m\Omega t) \;, \qquad \mathbf{z}(t) \in \mathbf{R}^N \;. \tag{4.51}$$

In general it will not be possible to find the exact solution of (4.33) with this approach. The projection of the error

$$\mathbf{e} = \mathbf{f}(\mathbf{z}, \dot{\mathbf{z}}, t) - \dot{\mathbf{z}}$$

on the functions $\mathbf{w}(t) = [1, \cos(\Omega t), \ldots, \cos(M\Omega t), \sin(\Omega t), \ldots, \sin(M\Omega t)]^T$ is now set equal to zero:

$$\int_0^T \mathbf{e}\, w_l(t)\, \mathrm{d}t = 0 \qquad \text{for} \quad l = 1, \ldots, 2M+1 \;. \tag{4.52}$$

Taking the orthogonality properties into account, a nonlinear system of algebraic equations is obtained as

$$\begin{aligned} \mathbf{Z}_{cm}(\mathbf{z}_c, \mathbf{z}_s) - m\Omega \frac{T}{2} \mathbf{z}_{sm} &= 0 \qquad \text{for} \quad m = 0, \ldots, M \\ \mathbf{Z}_{sm}(\mathbf{z}_c, \mathbf{z}_s) + m\Omega \frac{T}{2} \mathbf{z}_{cm} &= 0 \qquad \text{for} \quad m = 1, \ldots, M \;, \end{aligned} \tag{4.53}$$

where

$$\begin{aligned} \mathbf{Z}_{cm}(z_c, \mathbf{z}_s) &= \int_0^T \mathbf{f}(\mathbf{z}, \dot{\mathbf{z}}, t) \cos m\Omega t \, \mathrm{d}t \, , \\ \mathbf{Z}_{sm}(\mathbf{z}_c, \mathbf{z}_s) &= \int_0^T \mathbf{f}(\mathbf{z}, \dot{\mathbf{z}}, t) \sin m\Omega t \, \mathrm{d}t \, . \end{aligned} \tag{4.54}$$

The integrals (4.54) can be computed by the means of a fast Fourier transformation. KOLSCH [17] suggested rearranging the nonlinear system of equations (4.53) to a self mapping and to solve it iteratively. In the present case this was not successful and the system was solved by a NEWTON method instead. The algorithm works well, but in the vicinity of the resonance points the convergence decreases. In finding the frequency response step by step for all frequencies, it is convenient to use the preceding solution of the neighboring frequency as an initial value for the new frequency. Reducing the differences between the frequencies also improves the convergence and multiplication of the equations by weight factors also leads to better results. In the present case the number M of higher harmonics was chosen from 5 to 9.

4.2.5.4 Modified Collocation Method

Another method for the computation of approximate solutions is the modified collocation method. Using this method the solution is also sought in form of a of FOURIER series. We compute the error appearing at K points and minimize the sum of the squares of these errors. Using this method, more collocation points than variables are necessary to ensure the convergence of the method. The problems occurring were the same as for the GALERKIN method and a faster convergence could not be observed.

4.2.6 Comparing the Model and the Experiment

As previously discussed, the mechanical behavior of a STOCKBRIDGE damper is described via its mechanical impedance. A special damper with a well defined cable length and a simple geometry was constructed for verification purposes, in order to avoid problems related to the effective clamp length of the damper cable (see Chapter 2.4).

For the experimental determination of its impedance the STOCKBRIDGE damper was displaced harmonically at its clamp and the resulting force was measured (see Figure 4.5). The experimental setup is shown in Figure 4.7 and the properties of the Stockbridge damper in Table 4.1. The impedance was obtained both in the model as in the experiment using the

Figure 4.7: Measuring the mechanical impedance of a STOCKBRIDGE damper (RIBE Electrical Fittings GmbH & Co. KG)

Mass m	0.856 kg
Moment of inertia $\Theta^{(G)}$	0.001814 kg m^2
Distance to center of mass b	0.0325 m
Cable length l	0.1875 m

Table 4.1: Damper data (see Figure 4.4)

fundamental harmonic of the force. The real part of the impedance is related to the power dissipated by the damper. For the calculation of the real part it is not necessary to know the mass of the clamp and the load cell.

The parameters used for the model where identified from experiment (a) applying the mirror method. Note that the cables used in the experiments and in the actual damper were of different lengths ($l_{ident} = 0.3$m, $l_{damper} = 0.1875$m). Simulation results are shown in Figure 4.8 together with the experimentally measured impedance (real part only) of a STOCKBRIDGE damper for a clamp velocity amplitude $\hat{v}_{clamp} = 0.2$m/s. The clamp displacement amplitude for such a curve is of course not constant but given by

$$\hat{x}_{clamp} = \frac{1}{2\pi f}\,\hat{v}_{clamp}\,.$$

In the neighborhood of the resonance peaks the behavior of the real damper is predicted quite well. The shapes of the curves in between the resonances are quite similar.

Impedance curves have also been determined for a different amplitudes. In Figure 4.9 the impedance is shown for a relative small amplitudes$\hat{v}_{clamp} = 0.05$m/s. Near to the resonance frequencies the model worked quite but in-between them it failed. This is due

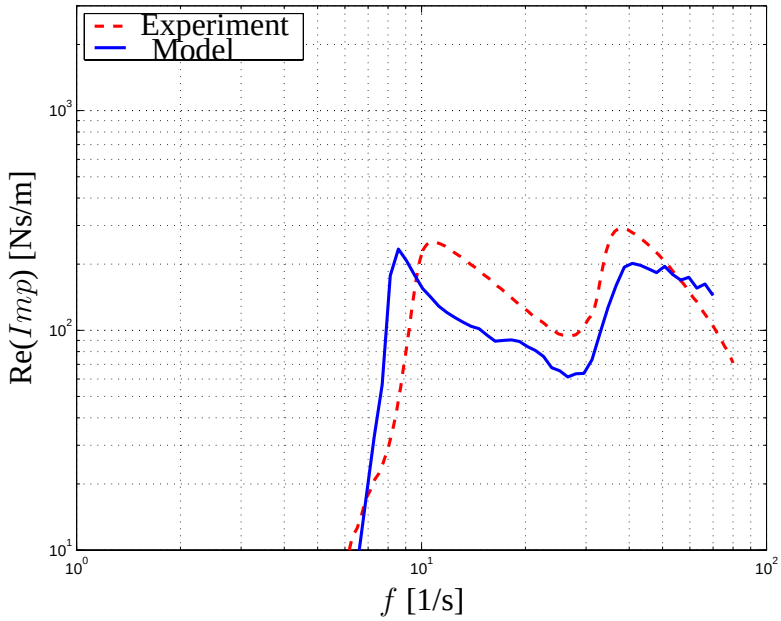

Figure 4.8: Impedance curves for the experiment and the model ($\hat{v}_{clamp} = 0.2$m/s)

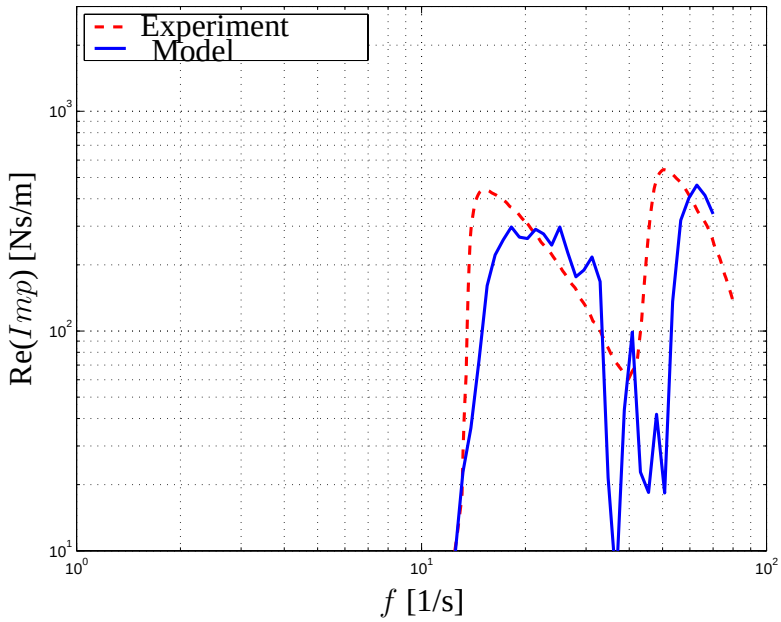

Figure 4.9: Impedance curves for the experiment and the model ($\hat{v}_{clamp} = 0.05$m/s)

to fact that here only very small curvature amplitudes appear at the damper cable. For modeling very small amplitudes it may be necessary to implement a second distributed JENKIN element. In any case, using our approach the damper impedances can now be be computed in advance for different cable lengths and amplitudes. This will be very useful in the optimization of dampers as well in the design of new damper.

4.3 Global Parameter Identification

4.3.1 Current Practice and Objective

It is current industrial practice to describe the properties of a STOCKBRIDGE damper by its frequency response experimentally determined in the lab for different velocities of the clamp. This procedure has several disadvantages. Every new design of a STOCKBRIDGE damper has to be tested even if the same damper cable is used, which is quite time demanding. For industrial applications it would be very useful to have a fast identification of the cable properties.

In the previous chapters it was shown that for the model under consideration it is possible to obtain the parameters from quasi-statical experiments via parameter estimation in the time domain. The properties of the damper cable were obtained from local moment-curvature-measurements. Describing the properties of the damper cable enables us to simulate the behavior of every STOCKBRIDGE damper with the same type of damper cable. This procedure seems to be easier than the experimental determination of the frequency response of each damper and only a few experiments are needed to do this. It would be even more convenient to identify the local parameters of the cable from a global experiment without having to apply the instrumented measurement strip.

4.3.2 General Approach

The quasi-statical global behavior of the damper cable was described by equation (4.18)

$$\begin{bmatrix} T \\ F \end{bmatrix} = \frac{1}{-d\,b + a\,e} \begin{bmatrix} e & -b \\ -d & a \end{bmatrix} \left(\begin{bmatrix} \varphi \\ x \end{bmatrix} - \begin{bmatrix} c \\ f \end{bmatrix} \right) \tag{4.55}$$

resp. the time derivative (4.26)

$$\begin{bmatrix} \dot{T} \\ \dot{F} \end{bmatrix} = \frac{1}{-d\,b + a\,e} \begin{bmatrix} e & -b \\ -d & a \end{bmatrix} \left(\begin{bmatrix} \dot{\varphi} \\ \dot{x} \end{bmatrix} - \begin{bmatrix} \dot{c} \\ \dot{f} \end{bmatrix} \right) , \tag{4.56}$$

where

$$\begin{aligned} a &= \int_0^l \frac{1}{ei(s)}\,\mathrm{d}s\,, \quad b = -\int_0^l \frac{1}{ei(s)}\,s\,\mathrm{d}s\,, \quad c = -\int_0^l \frac{1}{ei(s)} \sum_{j=1}^{m} H_j(s,t)\,\mathrm{d}s\,, \\ d &= \int_0^l \int_0^s \frac{1}{ei(\overline{s})}\,\mathrm{d}\overline{s}\,\mathrm{d}s\,, \quad e = -\int_0^l \int_0^s \frac{1}{ei(\overline{s})}\,\overline{s}\,\mathrm{d}\overline{s}\,\mathrm{d}s\,, \quad f = -\int_0^l \int_0^s \frac{1}{ei(\overline{s})} \sum_{j=1}^{m} H_j(\overline{s},t)\,\mathrm{d}\overline{s}\,\mathrm{d}s\,. \end{aligned} \tag{4.57}$$

The hysteretic moments are given by (4.27) which is reproduced below:

$$\begin{aligned} \dot{H}_i(s,t) &= \frac{c_i(s)}{ei(s)} \left(\dot{M}(s,t) - \sum_{j=1}^{m} \dot{H}_j(s,t) \right) \\ &\quad \left[1 - \frac{1}{2} \left(1 + \mathrm{sign}\left(\frac{1}{ei(s)} \left(\dot{M}(s,t) - \sum_{j=1}^{m} \dot{H}_j(s,t) \right) H_i(s,t) \right) \right) \left| \frac{H_i(s,t)}{h_i(s)} \right|^m \right] . \end{aligned} \tag{4.58}$$

It is a function of $c_i(s)$ and $h_i(s)$.

The global mechanical behavior of the real damper cable is described by the relation between F, M, x, and φ. If two of these quantities are given we can solve equation (4.55) for the remaining two unknown quantities provided all the coefficients are given. Integrating the system of differential equations given by (4.56) and (4.58) yields the two unknown variables. In order to determine the parameters of the JENKIN elements approximately we have to minimize the difference between the output quantities of the model and the real damper for given input quantities.

The question is if it is possible to determine the distributed parameters $ei(s)$, $c_i(s)$, and $h_i(s)$ from one or two global experiments. Even with a single distributed JENKIN element and the wire cable length l is discretized into 10 elements only, still 30 parameters (ei_p, c_{1p}, h_{1p}, $p = 1...10$) have to be identified. However, if both, experiment (a) and (b) are used for the identification, only the four quantities $x(t)$, $\varphi(t)$, $F(t)$, $M(t)$ are measured. It is clear that the optimization process will be doomed to failure unless additional a priori information is used.

In chapter 3.5.2 the identified parameters were analyzed. It was found that for a single JENKIN element the parameters follow certain trends:

- The minimum bending stiffness seems to be constant outside of the boundary region influenced by the clamp: $ei(s) = ei_{center}$.
- The same holds for the additional bending stiffness: $c(s) = c_{center}$.
- The behavior of the slipping moment $h(s)$ is more complicated but it seems to be possible to describe it via 2 constant parameters namely, $h_0,\ k$ used for a modified MASING model as represented in subsection 3.7.

In the boundary regions near the clamps the behavior of the parameters was not examined in detail yet. It seems reasonable that the parameter can be formulated as follows:

$$ei_{boundary}(s) = f_1(s, ei_{center}) \,,$$

$$c_{boundary}(s) = f_2(s, c_{center}) \,,$$

$$h_{boundary}(s) = f_3(s, h_0, k) \,.$$

The functions f_i may depend on both, the type of cable as well as on the type of clamps. Experiments will be needed for more insight into the boundary effects. With the knowledge of these trends and of the functions f_1, f_2, f_3 it should be possible to reduce the number of parameters remarkably. In the present case only the 4 parameters ei_{center}, c_{center}, h_0, k are left for the identification.

4.3.3 Initial Condition Problem

An important problem is how to get the same initial conditions for the internal variables both in the experiment and in the model for the global identification process. To ensure that the initial conditions are the same, the real damper and model first have to be deformed to the maximum amplitude (all JENKIN elements of the model slip). The identification is only started after this event.

KOLSCH [17] gives the following conditions for the time history of the displacement in the identification:

- the deformations have to cover the complete interval, for which the model shall be valid,
- the absolute values of the differences between successive extrema of the deformation must assume all orders of magnitude occurring at the real object.

The above considerations imply that, assuming quasi-harmonic motions at a certain amplitude only one loading and unloading between the maximum values should be enough. Thus, in the present case, we choose a whole cycle. Since the damper cable may assume different amplitudes the identification also has to be done at different amplitudes.

KOLSCH formulated these conditions for a discrete model, our model however is continuous and we need analogous conditions for it. For this purpose we demand that KOLSCH's conditions must be fulfilled at every point of the continuous system.

In the present case of a damper cable the distributed JENKIN element has to be displaced up to the maximum curvature of the real cable at every point of the cable. Since the maximum curvature depends directly on the maximum bending moment at that location, we must ensure that the bending moment of the identification is larger than that of the damper cable in practice.

The easiest way for ensuring the latter condition would be the application of a couple to the cable end. In our case we used experiment (a) and (b) for the identification, because the bending shapes are similar to the eigenforms of a STOCKBRIDGE damper. This approach is reasonable, since the eigenforms represent the maximal amplitudes. Admittedly in both experiments there are regions of the cable where the bending moment vanishes, but both experiments together fulfill the condition.

4.3.4 Identification Method for a Simplified Model

In some cases it may be sufficient to consider the parameters of the damper cable modeled by a MASING model comprising a single distributed JENKIN element with constant values throughout the whole length l:

$$ei(s) = ei,\ c(s) = c,\ h(s) = h\,.$$

This simplification leads to the model PLAGGE [29] used. Thus, equation (4.55) can be written as

$$\begin{bmatrix} T \\ F \end{bmatrix} = ei \begin{bmatrix} -\frac{2}{l} & \frac{6}{l^2} \\ -\frac{6}{l^2} & \frac{12}{l^3} \end{bmatrix} \left(\begin{bmatrix} \varphi \\ x \end{bmatrix} - \begin{bmatrix} c \\ f \end{bmatrix} \right) \tag{4.59}$$

where

$$c = -\frac{1}{ei} \int_0^l H(s)\,\mathrm{d}s\,,\quad f = -\frac{1}{ei} \int_0^l \int_0^s H(\bar{s}, t)\,\mathrm{d}\bar{s}\,\mathrm{d}s\,. \tag{4.60}$$

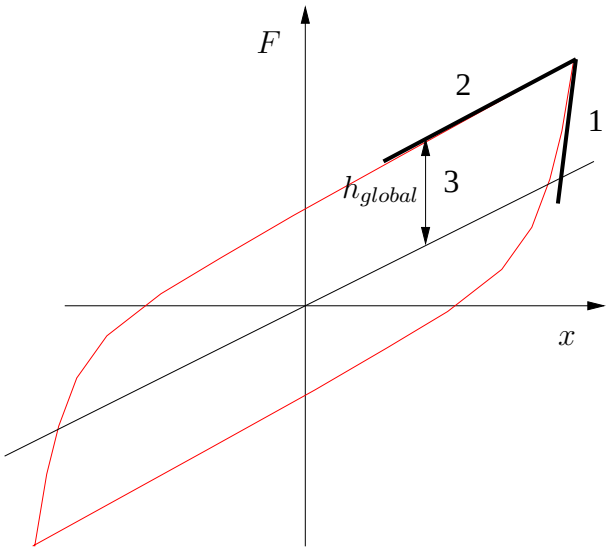

Figure 4.10: Global identification in three steps using a global hysteresis cycle obtained from experiment (a)

Therefore, in case of experiment (a) the force is obtained as

$$F = \frac{3\,ei}{l^3}\,x - \frac{3\,ei}{l^3}\,f \tag{4.61}$$

and for experiment (b) the torque as

$$T = -\frac{2\,ei}{l}\,\varphi + \frac{2\,ei}{l}\,c - \frac{6\,ei}{l^2}\,f\,. \tag{4.62}$$

Here we want to find the parameters of the damper cable, modeled in such a manner. Identifying the parameters all at once may lead to long computation times. Therefore we use step by step identification of the quantities. For this purpose we make use of the facts that for very small amplitudes of deformation the cable behaves almost elastically and on the other hand for large amplitudes all wires slip. Such an approach also has the advantage of giving more insight into the relation.

Step 1: For very small deformation amplitudes Δx, $\Delta\varphi$ as well as at an instant just after a direction reversal, all JENKIN elements stick. Therefore the damper cable behaves as an elastic beam with bending stiffness $ei_{\max} = ei(s) + c(s)$:

$$\begin{bmatrix} \Delta T \\ \Delta F \end{bmatrix} = ei_{\max} \begin{bmatrix} -\frac{2}{l} & \frac{6}{l^2} \\ -\frac{6}{l^2} & \frac{12}{l^3} \end{bmatrix} \begin{bmatrix} \Delta\varphi \\ \Delta x \end{bmatrix}\,. \tag{4.63}$$

For hysteresis curves obtained from experiment (a) $ei_{\max}$ is obtained by

$$ei_{\max} = \frac{l^3}{3} \max(\frac{\Delta F}{\Delta x}) \,, \tag{4.64}$$

where $\max(\Delta F/\Delta x)$ is the maximum slope of the slope (see Figure 4.10 (1)). In case of experiment (b) we obtain

$$ei_{\max} = \frac{l}{2} \max(\frac{-\Delta T}{\Delta \varphi}) \,. \tag{4.65}$$

Step 2: For very large amplitudes nearly all JENKIN elements are slipping.[2] Differentiation of equation (4.59) with respect to the time t yields

$$\begin{bmatrix} \dot{T} \\ \dot{F} \end{bmatrix} = ei_{\min} \begin{bmatrix} -\frac{2}{l} & \frac{6}{l^2} \\ -\frac{6}{l^2} & \frac{12}{l^3} \end{bmatrix} \left(\begin{bmatrix} \dot{\varphi} \\ \dot{x} \end{bmatrix} - \begin{bmatrix} \dot{c} \\ \dot{f} \end{bmatrix} \right) \,, \tag{4.67}$$

where

$$\dot{c} = -\int_0^l \frac{1}{ei(s)} \sum_{j=1}^{m} \dot{H}_j(s,t)\,\mathrm{d}s \,, \quad \dot{f} = -\int_0^l \int_0^s \frac{1}{ei(\bar{s})} \sum_{j=1}^{m} \dot{H}_j(\bar{s},t)\,\mathrm{d}\bar{s}\,\mathrm{d}s \,. \tag{4.68}$$

For a slipping JENKIN element the hysteretic moment is constant in time:

$$H_j(s,t) = h_{\mathrm{j}}(s) \,. \tag{4.69}$$

Therefore the time derivative will be zero and this has to hold along the whole cable. Thus

$$\dot{H}(s,t) = 0 \,, \qquad \forall s \,, \tag{4.70}$$

which leads to $\dot{c} = 0$, $\dot{f} = 0$ in (4.67). Equation (4.67) can then be written as

[2] Slipping occurs at any point s if

$$M_{\max}(s) > \frac{h_j(s)}{1 - \frac{ei(s)}{ei(s) + \sum c_i(s)}} \,, \qquad \forall s \,. \tag{4.66}$$

i.e. the external moment must be large enough. The best way to ensure this would be to apply only a couple at the free end of the cable. If we apply only a force at the free cable end (experiment (a)), not at all locations of the cable slipping will occur. At the free end there will always be a larger or smaller zone where sticking is present, depending on the magnitude of the force. But no matter in which way the cable is loaded; if the load is large enough, nearly the whole cable will slip. However, we must remember that these equations only hold for large amplitudes.

$$\begin{bmatrix} \dot{T} \\ \dot{F} \end{bmatrix} = ei \begin{bmatrix} -\frac{2}{l} & \frac{6}{l^2} \\ -\frac{6}{l^2} & \frac{12}{l^3} \end{bmatrix} \begin{bmatrix} \dot{\varphi} \\ \dot{x} \end{bmatrix} . \tag{4.71}$$

Now this results is applied to the two experiments carried out. Since $\dot{f} = 0$ we can write for experiment (a):

$$\dot{F} = \frac{3\,ei}{l^3}\,\dot{x}\,. \tag{4.72}$$

Rearranging for the minimum bending stiffness yields

$$ei = \frac{l^3}{3}\,\frac{\dot{F}}{\dot{x}}\,. \tag{4.73}$$

With $\dot{F}/\dot{x} = \Delta F/\Delta x$ we find

$$ei = \frac{l^3}{3}\,\frac{\Delta F}{\Delta x}\,. \tag{4.74}$$

This equation holds only for large displacements. Since $\Delta F/\Delta x$ is minimal at the maximum displacement (see Figure 4.10 (2)), we can write:

$$ei = \frac{l^3}{3}\,\min(\frac{\Delta F}{\Delta x})\,. \tag{4.75}$$

In experiment (b), similarly we find with $\dot{c} = 0$, $\dot{f} = 0$

$$\dot{T} = -\frac{2\,ei}{l}\,\dot{\varphi} \tag{4.76}$$

and finally

$$ei = \frac{l}{2}\,\min(\frac{-\Delta T}{\Delta \varphi})\,. \tag{4.77}$$

Step 3: We now identify the slipping moment h. If the distributed JENKIN element is assumed to be slipping at every location it is given as $H(s,t) = h\,\mathrm{sign}(\dot{\kappa}(s,t))$ because it is always acting against the changing curvature.

This yields in case of experiment (a) to

$$f \;=\; -\frac{1}{ei}\int_0^l \int_0^s h\,\mathrm{d}\bar{s}\,\mathrm{d}s = -\frac{l^2}{2\,ei}\,h\,.$$

Thus the force is given as

$$F = \frac{3\,ei}{l^3}\,x + \frac{3}{2\,l}\,h\,.$$

Solving for the slipping moment

$$h = \frac{2\,l}{3}\left(F - \frac{3\,ei}{l^3}\,x\right)\,. \tag{4.78}$$

The term $F - (3\,ei/l^3)\;x$ can be interpreted as the 'global slipping force', h_{global}, which is shown in Figure 4.10 (3).

For experiment (b) the hysteretic moment is given as

$$H(s,t) = \begin{cases} h & for \quad 0 \le s < l/3 \\ -h & for \quad l/3 \le s \le l \end{cases}\,.$$

Thus, c and f are computed as follows:

$$\begin{aligned} c &= -\frac{1}{ei}\int_0^l h\,\mathrm{d}s = -\frac{1}{ei}\left(\int_0^{l/3} h\,\mathrm{d}s + \int_{l/3}^{l}(-h)\;\mathrm{d}s\,\mathrm{d}s\right) = \frac{l}{3\,ei}\,h\,, \\ f &= -\frac{1}{ei}\int_0^l\int_0^s h\,\mathrm{d}\bar{s}\,\mathrm{d}s = -\frac{1}{ei}\left(\int_0^{l/3}\int_0^s h\,\mathrm{d}\bar{s}\,\mathrm{d}s + \int_{l/3}^{l}\int_0^s (-h)\;\mathrm{d}\bar{s}\,\mathrm{d}s\right) = \frac{7\,l^2}{18\,ei}\,h\,. \end{aligned}$$

Thus the torque is given as

$$T = -\frac{2\,ei}{l}\,\varphi - 3\,h\,.$$

Solving for the slipping moment leads to

$$h = \frac{1}{3}\left(-T - \frac{2\,ei}{l}\,\varphi\right)\,. \tag{4.79}$$

The term $-T - (2\,ei/l)\;\varphi$ can be interpreted as the global slipping moment, h_{global}.

Step 4: In the last step, the bending stiffness c can be determined by the difference

$$c = ei_{max} - ei\,. \tag{4.80}$$

Thus all local quantities describing the simplified bending behavior of a wire cable could be obtained from global experiments.

Results: In the present case we used a cable of length $l = 0.3$m to identify the parameters for both experiments, (a) and (b). The parameters obtained are given in Table 4.2 and in Figure 4.11 they are compared to the locally identified parameters. It can be seen that the parameters ei and c fit well to the locally identified parameters and the values are nearly the

	Exp. (a)	Exp. (b)
Minimum bending stiffness ei	2.8 N	2.9 N
Bending stiffness of the J. element c	20 N	21 N
Max. moment of the i-th J. element h	0.7 Nm	0.55 Nm

Table 4.2: Globally identified local parameters ei, h, c for the simplified model.

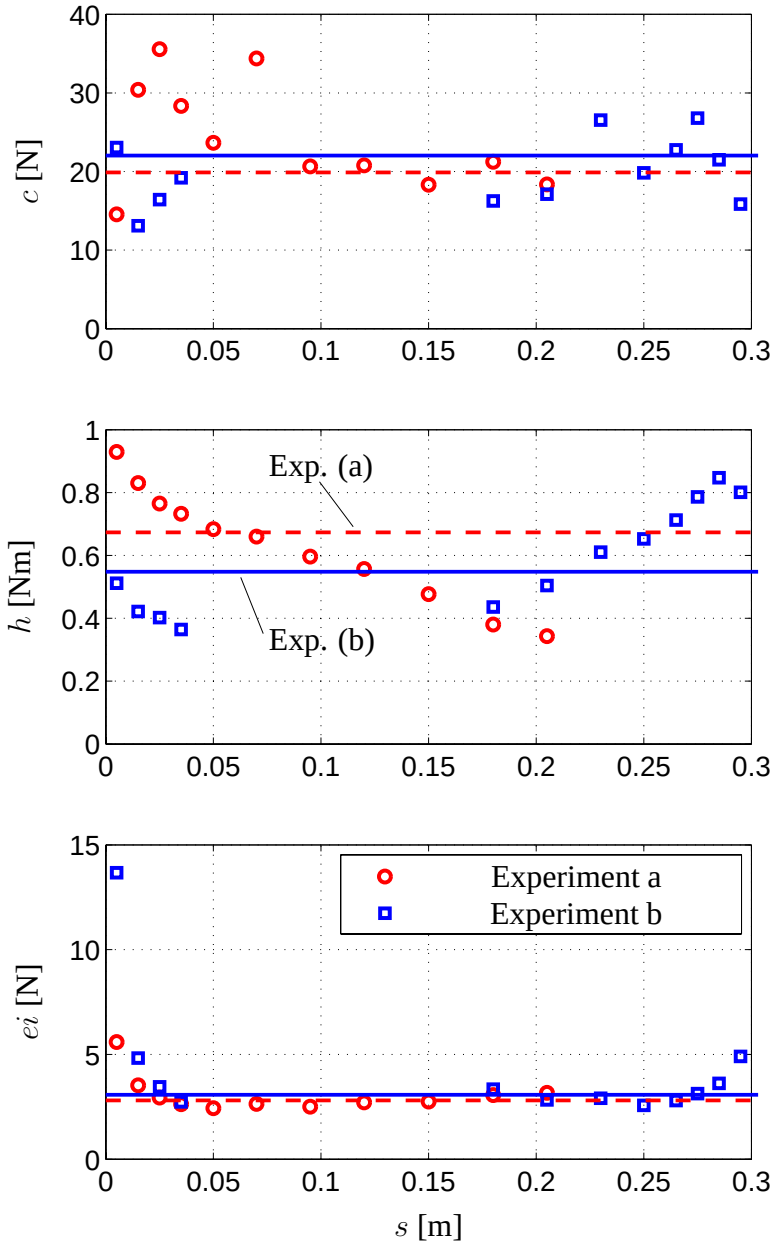

Figure 4.11: Globally identified local parameters ei, h, c of the simplified model (lines) compared to the locally identified parameters $ei(s)$, $h(s)$, $c(s)$ (squares and circles).

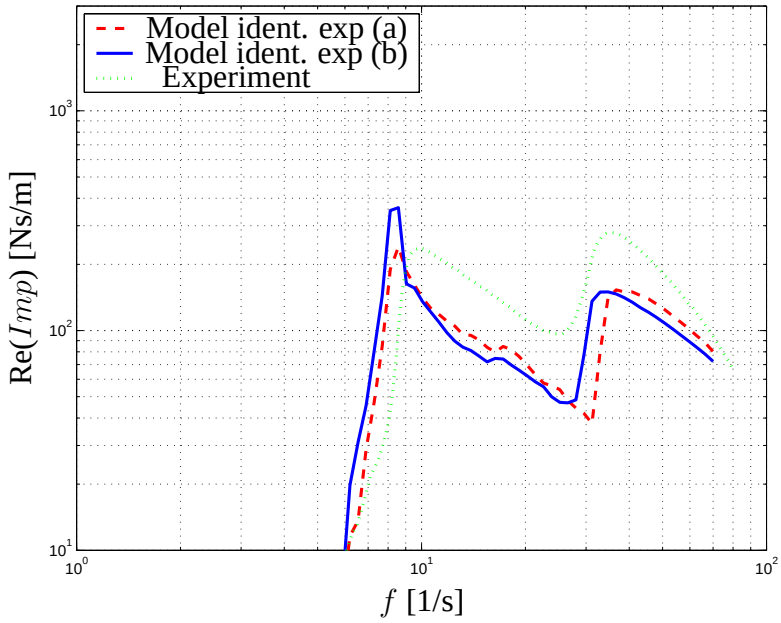

Figure 4.12: Impedance curves for the experiment and the simplified model with the globally identified parameters ($\hat{v}_{clamp} = 0.2$m/s)

same for experiment (a) and (b). In contrast, the slipping moment h depends on the shape of the deformation. Thus the parameters behave as expected. Finally the impedance of the STOCKBRIDGE damper given by Table 4.1 (cable length $l = 0.1875$m) was computed for both sets of cable parameters. In Figure 4.12 the impedance curves of the model are compared with the experiment. It can be seen that the curves do not fit as well as in case of the locally identified parameters (see Figure 4.8) in Section 4.2.6. On the one hand this error is due to the simplification of assuming constant parameters, on the other hand the length of the identification cable was different from the length of the cable used at the Stockbridge damper. Therefore the use of such a simplified model must be well deliberated.

Chapter 5

Summary

Up to now, the dimensioning of the slack wire cables used for the purpose of damping in devices like STOCKBRIDGE dampers is quite elaborate which is also due to the lack of knowledge about their mechanical behavior. Therefore, the main object of this thesis was to find the dynamic behavior of slack wire cables just by measuring their quasi-statical properties. The distributed energy dissipation due to inter-strand friction has been described in detail. Important features, such as changes in the dynamic behavior with varying vibration amplitudes could be described by a simulation model in a satisfying manner. For such a model the design and the optimization of the damper cables is considered which is quite important in the creation of new dampers, which, at the moment, are frequently designed on a trial and error basis.

Since the deformation of the damper cables is mainly due to bending, the local bending behavior of a slack wire cable was examined experimentally. For the experimental determination of the local *moment-curvature relation* in a damper cable a special arrangement was developed. Using such a device local hysteresis cycles have been measured showing the statical hysteretic character of the damping mechanism resulting from COULOMB friction between the individual wires of the cable (*inter-strand friction*) undergoing bending deformation. In the experiments also different bending shapes have been taken into account.

Since the statical hysteresis has its origin in the COULOMB friction between the wires throughout the whole length of the cable, we used the local (distributed) MASING model which is a phenomenological model. The MASING model comprises of several JENKIN elements arranged in parallel, consisting of linear springs and COULOMB friction elements. Using such an approach, the complexity of the model is reduced remarkably and makes the

calculation of dynamical problems possible.

The model under consideration comprised only a single distributed JENKIN element. It has been illustrated that a single Jenkin element is sufficient if the amplitudes of deformation do not differ too much. Using a single distributed JENKIN element simplified the identification process remarkably. Furthermore it was quite simple to describe the phenomena appearing at the wire cable during the bending process by the parameters of the MASING model. In particular the local hysteresis cycles have described in detail using terms like minimum, maximum stiffness, and slipping moment.

The identification of the model parameters from the experimentally obtained data was done numerically in the time domain for different bending shapes. Apart from the regions near to the clamps, it should be assumed due to the homogeneity of a wire cable that the model parameters are independent of the position along the cable as well as of the bending mode. Admittedly the local MASING model in the present form is not sufficiently detailed for a precise description of the local behavior of slack cables since the slipping moment changes with position and the bending shape. For taut wire cables (e.g. conductors in overhead transmission lines) such an phenomenon has not observed yet. Due to the large axial pretension in taut cables the basic slipping moment is large too. Therefore a small change of the slipping moment due to a transverse force may be negligible. Likewise, in former considerations of slack wire cables this effect was not noticed because a single bending shape was examined only.

As a consequence a modified model has been proposed in which the transverse force acting on the wire cable is also included. In such a way the changing slipping force is described more accurately but still not perfectly. This may be due to the minimum slipping moment which is difficult to determine. In addition an alternative method has been shown describing the model parameters for the different eigenforms of a (STOCKBRIDGE) damper cable approximately. This *mirror method* worked quite well and was used in the subsequent examination.

The validity of the model was shown by testing the global quasi-statical behavior of the cable. This was done by identifying the parameters of the model for one shape of deformation and applying them to another using the mirror method. Approximate correspondence was found between the real damper cable and the model. After testing the global behavior of the cable the equations of motion have been formulated for a STOCKBRIDGE damper, and discretization of the damper cable leads to a system of nonlinear ordinary differential equations. For the solution of the problem several methods have been examined. In or-

der to test the dynamical model of a STOCKBRIDGE damper impedance curves have been computed and compared with experimental results. In particular for large amplitudes of the damper clamp displacement good agreement was found. Only for for small amplitudes the model failed. This was because only a single JENKIN element, identified at large amplitudes, was used. It can be expected that by the use of more Jenkin elements also amplitudes of different size can be modeled.

Up to now for every type of damper frequency response experiments have to be executed in order to determine the the length of the damper cable which is quite circuitous. With the local MASING model described before it is possible to design different dampers (e.g. with different cables length) after identifying the properties of a cable roll. By the introduction of the MASING model a 'language' is given to the manufacturer for the description of the dynamical properties of slack wire cables.

Because the application of the strain gages strip for the local measurement is quite elaborate a method was shown in order to gain the local parameters from a global quasistatical experiment in the time domain. This was done for a simplified model assuming the parameters of the local MASING model to be the same throughout the whole wire cable. Before the same method can be applied for a more sophisticated model the behavior of the parameters near to the clamps has to be examined in more detail.

Appendix

A.1 Approximate Determination of the Bending Stiffness of a Wire Cable

The bending stiffness, EI, of slack wire cables undergoing bending changes considerably depending on the extent of the curvature. Here, the bending stiffness will be computed analytically for two limiting cases. In the first case it is assumed that there is no slip in-between the wires. Thus the cable behaves like an elastic beam. In this case the maximum value for the bending stiffness, EI_{max}, is obtained. In the second case it is assumed that there is no friction between the wires, which leads to the minimum bending stiffness, EI_{min}. For actual wire cables the value of the bending stiffness will always lie between these two limits. Thus EI_{min} and EI_{max} will be be determined approximately analytically for the two-layered wire cable under consideration (see Figure A.1).

LANTEIGNE [20] gave an equation for the computation of the maximum bending stiffness, EI_{max}, of the wire cable. For derivation of the formula the helical shape of the strands was taken into account. The equation is given as

$$EI_{\text{max}} = E\left[\sum_{j=1}^{L}\frac{1}{2}\left\{N_j r_j^2 \pi\left(\frac{r_j^2}{2}+R_j^2\right)\cos^3(\alpha_j)\right\} + I_c + \sum_{j=1}^{L}\sum_{i=1}^{N_j} r_j^2 \pi B_{i,j}\right] \tag{A.1}$$

where

$$B_{i,j} = \frac{R_j^3\cos^3(\alpha_j)}{4l\,\tan(\alpha_j)}\left[\sin\left(\frac{4\,\pi\,i}{N_j}\right) - \sin\left(\frac{4\,\pi\,i}{N_j}+\frac{2\,l\,\tan(\alpha_j)}{R_j}\right)\right] \tag{A.2}$$

and

$$\alpha_j = \frac{2\,\pi\,R_j}{\lambda_j}\,. \tag{A.3}$$

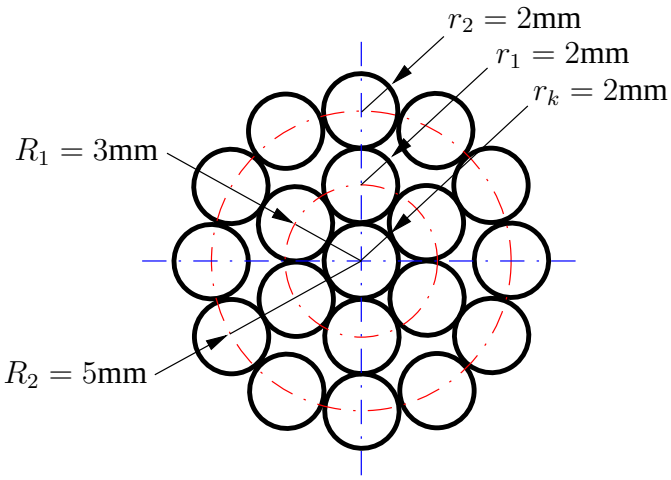

Figure A.1: Cross-section through a two-layered wire cable

λ_j is the length of the j-th layer, α_j is the layer angle of the j-th layer, and R_j stands for the radius of the j-th layer (see Figure A.1). The cable consist of L layers. The number of wires of the j-th layer is N_j. r_j is the wire radius of the j-th layer. For a steel cable the modulus of elasticity is given as E =210.000 N/mm^2. For the damper cable used in the experiments (see Table 2.1) we obtain the maximum bending stiffness: EI_{max} =66.28 Nm^2.

For the minimum bending stiffness no exact analytical expression could be found. WINDSPERGER [34] gave an equation for the bending stiffness of a single-layered cable taking the helix-structure of the strands into consideration. Unfortunately this equation can not be used for the two-layered damper cables under consideration. Thus the bending stiffness will be determined approximately by restraining on freely relocatable parallel strands. Then the minimum bending stiffness is given by

$$EI_{min} = E\left(I_K + \sum_{j=1}^{L} N_j I_j\right) \tag{A.4}$$

where

$$I_k = \frac{\pi r_K^4}{4}, \quad I_j = \frac{\pi r_j^4}{4}\,. \tag{A.5}$$

I_K and I_j denotes the geometrical moment of inertia of the core wire respectively of the j-th layer. For the damper cable used in the experiments (see Table 2.1) we obtain the minimum bending stiffness: EI_{min} =3.19 Nm^2. Due to the helix structure, the actual minimum bending stiffness will be even smaller.

Bibliography

[1] Bogacki, P. and Shampine, L. F. A 3(2) pair of Runge-Kutta formulas. *Appl. Math. Letters*, 2:1–9, 1989.

[2] Brokate, M. and Sprekels, J. *Hysteresis and Phase Transitions*. Springer Verlag, New York, 1996.

[3] Capecchi, D. Periodic response and stability of hysteretic oscillators. *Dynamics and Stability of Systems*, 6(2):89–106, 1991.

[4] Capecchi, D., Masiani, R., and Vestroni, F. Periodic and non-periodic oscillations of a class of hysteretic two-degrees of freedom systems. *Nonlinear Dynamics*, 13:309–325, 1997.

[5] G.A. Costello. *Theory of Wire Rope*. Springer, New York, 1990.

[6] Doocy, E.S., Hard, A.R., Ikegami, R., and Rawlins C.B. *Transmission Line Reference Book*. EPRI, 1979.

[7] Gutzer, U. *Dynamische Identifikation statischer Hysterese am Beispiel eines Leiterseils*. Dissertation, Institut für Mechanik, TU Darmstadt; Normed Verlag, 1998.

[8] Gutzer, U., Seemann, W., and Hagedorn, P. *Nonlinear Structural Damping Described by the MASING Model and the Method of Slowly Varying Amplitude and Phase*. Proceedings (3A) of the 15th Biennial Conference on Vibration and Noise, Boston, USA, September 17-21, 773-779, 1995.

[9] P. Hagedorn. *Non-Linear Oscillations*. Clarendon Press, Oxford, 1988.

[10] Hagedorn P. Ein einfaches Rechenmodell zur Berechnung winderregter Schwingungen an Hochspannungsleitungen mit Dämpfern. *Ingenieur-Archiv*, 49:161–177, 1980.

[11] Hagedorn P. On the computation of damped wind-excited vibrations of overhead transmission lines. *Journal of Sound and Vibration*, 83(2):253–271, 1982.

[12] Hardy, C. and Leblond, A. On the estimation of a 2x2 complex stiffness matrix of symetric stockbridge-type dampers. In *Proceeding of the Third International Symposium on Cable Dynamics*, Trondheim, Norway, 1999.

[13] Hill, R. *The Mathematical Theory of Plasticity*. Oxford University Press, 1998.

[14] Hooker, R.J. and Dulhunty, P.W. Influence of asymmetry on Stockbridge damper performance. In *Proceedings of the International Symposium on Cable Dynamics*, pages 373–383, Liège, Belgium, October 1995.

[15] T. von Kármán. *Über den Mechanismus des Widerstandes, den ein bewegter Körper in einer Flüssigkeit erfährt*. Göttinger Nachrichten, mathematisch-physikalische Klasse, 509-517, 1911; 547-556, 1912.

[16] Khan, A.S. and Huang, S. *Continuum Theory of Plasticity*. John Wiley, 1995.

[17] H. Kolsch. *Schwingungsdämpfung durch statische Hysterese (= Vibration Damping by Static Hysteresis)*. Doctoral Dissertation, Technical University Braunschweig, 1993.

[18] Krasnoselskii, M. and Pokrovskii, A. *Systems with Hysteresis*. Springer Verlag, 1983.

[19] Lagarias, J. C., Reeds, J. A., Wright, M. H., and Wright, P. E. Convergence properties of the nelder-mead simplex method in low dinemsions. *SIAM Journal of Optimization*, 9(1):112–147, 1998.

[20] Lanteigne, J. Theoretical estimation of the response of helically armored cables to tension, torsion, and bending. *Journal of Applied Mechanics*, 52:423–432, 1985.

[21] A.E.H. Love. *A Treatise on the Mathematical Theory of Elasticity*. Cambridge University Press, 1952.

[22] Markiewicz M. Optimum dynamic characteristics of stockbridge dampers for dead-end spans. *Journal of Sound and Vibration*, 188:243–256, 1995.

[23] G. Masing. *Zur Heynschen Theorie der Verfestigung der Metalle durch verborgene elastische Spannungen*. Wissenschaftliche Veröffentlichungen aus dem Siemens-Konzern 3, 1923/24.

[24] MathWorks. *MATLAB: The Language of Technical Computing*. The MathWorks Inc., MA, USA, 1984-2001.

[25] Mayergoyz I.D. *Mathematical Models of Hysteresis*. Springer-Verlag, Berlin, Heidelberg, New York, 1991.

[26] Nayfeh, A.H. and Mook, D.T. *Nonlinear Oscillations*. J. Wiley and Sons, New York, 1979.

[27] K. Papailiou. *Die Seilbiegung mit einer durch innere Reibung, die Zugkraft und die Seilkrümmung veränderlichen Biegesteifigkeit (= The Bending of Cables with a Bending Stiffness Varying with Internal Friction, Normal Force and Curvature)*. Doctoral Dissertation, ETH Zürich, 1995.

[28] F. Plagge. *Nichtlineares, inelastisches Verhalten von Spiralseilen*. Braunschweiger Schriften zur Mechanik Nr. 31-1997, 1997.

[29] Plagge, F. and Ottl, D. Inelastisches Verhalten von Spiralseilen unter Biegung. *Forschung im Ingenieurwesen, Springer-Verlag*, 63(9):281–284, 1997.

[30] Sauter D. Modeling the Stockbridge damper as a continuous hysteretic system. Master's thesis, Technische Hochschule Darmstadt, Fachbereich Mechanik, 1997.

[31] W. Seemann. *Deformation of an Elastic Helix in Contact with a Rigid Cylinder*. Archive of Applied Mechanics 67, 117-139, Springer, 1996.

[32] G.H. Stockbridge. *Overcoming Vibration in Transmission Lines*. Electrical World, 86, 1304-1305, 1925.

[33] V. Strouhal. *Über eine besondere Art der Tonerregung*. Annalen der Physik und Chemie 5, 216-251, 1878.

[34] Windsperger, G. *Zur Biegesteifigkeit der Drahtseile*. PhD thesis, Technische Universität Wien, 1982.

Lebenslauf

Daniel Sauter
Hindenburgstr. 4
78467 Konstanz

09. 07. 1967	Geboren in Donaueschingen
1973 - 1977	Grundschule Riedöschingen
1977 - 1986	Fürstenberg-Gymnasium in Donaueschingen
1987 - 1988	Volkswirtschaftstudium an der Uni Konstanz (abgebrochen)
1989 - 1994	Maschinenbaustudium (FH Darmstadt + FH Konstanz)
1995 - 1997	Mechanikstudium an der TU Darmstadt
1998 - 2001	Wissenschaftlicher Mitarbeiter am Institut für Mechanik, AG Dynamik, der Technischen Universität Darmstadt
seit 2002	Entwicklungsingeneur bei der Burckhardt Compression AG in Winterthur